Australia's National Science Agency

Australian Government

National Water Grid

Floodplain inundation mapping and modelling for the Southern Gulf catchments

A technical report from the CSIRO Southern Gulf Water Resource Assessment for the National Water Grid

Fazlul Karim, Shaun Kim, Catherine Ticehurst, Matt Gibbs, Justin Hughes, Steve Marvanek, Ang Yang, Bill Wang, Cuan Petheram

ISBN 978-1-4863-2057-8 (print)

ISBN 978-1-4863-2058-5 (online)

Citation

Karim F, Kim S, Ticehurst C, Gibbs M, Hughes J, Marvanek S, Yang A, Wang B and Petheram C (2024) Floodplain inundation mapping and modelling for the Southern Gulf catchments. A technical report from the CSIRO Southern Gulf Water Resource Assessment for the National Water Grid. CSIRO, Australia.

Copyright

Important disclaimer

CSIRO Southern Gulf Water Resource Assessment acknowledgements

This report was funded through the National Water Grid's Science Program, which sits within the Australian Government's Department of Climate Change, Energy, the Environment and Water.

Aspects of the Assessment have been undertaken in conjunction with the Northern Territory and Queensland governments.

The Assessment was guided by two committees:

i. The Governance Committee: CRC for Northern Australia/James Cook University; CSIRO; National Water Grid (Department of Climate Change, Energy, the Environment and Water); Northern Land Council; NT Department of Environment, Parks and Water Security; NT Department of Industry, Tourism and Trade; Office of Northern Australia; Queensland Department of Agriculture and Fisheries; Queensland Department of Regional Development, Manufacturing and Water

ii. The Southern Gulf catchments Steering Committee: Amateur Fishermen's Association of the NT; Austral Fisheries; Burketown Shire; Carpentaria Land Council Aboriginal Corporation; Health and Wellbeing Queensland; National Water Grid (Department of Climate Change, Energy, the Environment and Water); Northern Prawn Fisheries; Queensland Department of Agriculture and Fisheries; NT Department of Environment, Parks and Water Security; NT Department of Industry, Tourism and Trade; Office of Northern Australia; Queensland Department of Regional Development, Manufacturing and Water; Southern Gulf NRM

Responsibility for the Assessment's content lies with CSIRO. The Assessment's committees did not have an opportunity to review the Assessment results or outputs prior to their release.

This report was reviewed by Dr Zaved Khan and Mr Mahdi Montazeri of CSIRO.

Acknowledgement of Country

CSIRO acknowledges the Traditional Owners of the lands, seas and waters of the area that we live and work on across Australia. We acknowledge their continuing connection to their culture and pay our respects to their elders past and present.

Photo

Nicholson River. Source: CSIRO

Director's foreword

Sustainable development and regional economic prosperity are priorities for the Australian, Queensland and Northern Territory (NT) governments. However, more comprehensive information on land and water resources across northern Australia is required to complement local information held by Indigenous Peoples and other landholders.

Knowledge of the scale, nature, location and distribution of likely environmental, social, cultural and economic opportunities and the risks of any proposed developments is critical to sustainable development. Especially where resource use is contested, this knowledge informs the consultation and planning that underpin the resource security required to unlock investment, while at the same time protecting the environment and cultural values.

In 2021, the Australian Government commissioned CSIRO to complete the Southern Gulf Water Resource Assessment. In response, CSIRO accessed expertise and collaborations from across Australia to generate data and provide insight to support consideration of the use of land and water resources in the Southern Gulf catchments. The Assessment focuses mainly on the potential for agricultural development, and the opportunities and constraints that development could experience. It also considers climate change impacts and a range of future development pathways without being prescriptive of what they might be. The detailed information provided on land and water resources, their potential uses and the consequences of those uses are carefully designed to be relevant to a wide range of regional-scale planning considerations by Indigenous Peoples, landholders, citizens, investors, local government, and the Australian, Queensland and NT governments. By fostering shared understanding of the opportunities and the risks among this wide array of stakeholders and decision makers, better informed conversations about future options will be possible.

Importantly, the Assessment does not recommend one development over another, nor assume any particular development pathway, nor even assume that water resource development will occur. It provides a range of possibilities and the information required to interpret them (including risks that may attend any opportunities), consistent with regional values and aspirations.

All data and reports produced by the Assessment will be publicly available.

Chris Chilcott

Project Director

The Southern Gulf Water Resource Assessment Team

Project Director	Chris Chilcott
Project Leaders	Cuan Petheram, Ian Watson
Project Support	Caroline Bruce, Seonaid Philip
Communications	Emily Brown, Chanel Koeleman, Jo Ashley, Nathan Dyer

Activities

Agriculture and socio-economics	Tony Webster, Caroline Bruce, Kaylene Camuti[1], Matt Curnock, Jenny Hayward, Simon Irvin, Shokhrukh Jalilov, Diane Jarvis[1], Adam Liedloff, Stephen McFallan, Yvette Oliver, Di Prestwidge[2], Tiemen Rhebergen, Robert Speed[3], Chris Stokes, Thomas Vanderbyl[3], John Virtue[4]
Climate	David McJannet, Lynn Seo
Ecology	Danial Stratford, Rik Buckworth, Pascal Castellazzi, Bayley Costin, Roy Aijun Deng, Ruan Gannon, Steve Gao, Sophie Gilbey, Rob Kenyon, Shelly Lachish, Simon Linke, Heather McGinness, Linda Merrin, Katie Motson[5], Rocio Ponce Reyes, Jodie Pritchard, Nathan Waltham[5]
Groundwater hydrology	Andrew R. Taylor, Karen Barry, Russell Crosbie, Margaux Dupuy, Geoff Hodgson, Anthony Knapton[6], Stacey Priestley, Matthias Raiber
Indigenous water values, rights, interests and development goals	Pethie Lyons, Marcus Barber, Peta Braedon, Petina Pert
Land suitability	Ian Watson, Jenet Austin, Bart Edmeades[7], Linda Gregory, Ben Harms[10], Jason Hill[7], Jeremy Manders[10], Gordon McLachlan, Seonaid Philip, Ross Searle, Uta Stockmann, Evan Thomas[10], Mark Thomas, Francis Wait[7], Peter Zund
Surface water hydrology	Justin Hughes, Matt Gibbs, Fazlul Karim, Julien Lerat, Steve Marvanek, Cherry Mateo, Catherine Ticehurst, Biao Wang
Surface water storage	Cuan Petheram, Giulio Altamura[8], Fred Baynes[9], Jamie Campbell[11], Lachlan Cherry[11], Kev Devlin[4], Nick Hombsch[8], Peter Hyde[8], Lee Rogers, Ang Yang

Note: Assessment team as at September, 2024. All contributors are affiliated with CSIRO unless indicated otherwise. Activity Leaders are underlined.

[1]James Cook University; [2]DBP Consulting; [3]Badu Advisory Pty Ltd; [4]Independent contractor; [5] Centre for Tropical Water and Aquatic Ecosystem Research. James Cook University; [6]CloudGMS; [7]NT Department of Environment, Parks and Water Security; [8]Rider Levett Bucknall; [9]Baynes Geologic; [10]QG Department of Environment, Science and Innovation; [11]Entura

Shortened forms

SHORT FORM	FULL FORM
AEP	annual exceedance probability
AGDC	Australian Geoscience Data Cube
AHD	Australian Height Datum
AMTD	Adopted Middle Thread Distance
AR6	Sixth Assessment Report
AWRA-L	Australian Water Resource Assessment – Landscape model
AWRA-R	Australian Water Resource Assessment – River model
AWRC	Australian Water Resources Council
BRDF	Bidirectional Reflectance Distribution Function
CMIP	Coupled Model Intercomparison Project
CAWCR	Collaboration for Australian Weather and Climate Research
DCFR	diversion commencement flow requirement
DEA	Digital Earth Australia
DEM	digital elevation model
DOI	digital object identifier
ERP	equivalent Riemann problem
ESA	European Space Agency
ETM	Enhanced Thematic Mapper
ETS	Equitable Threat Score
FAR	False Alarm Ratio
FB	Frequency Bias
GCM	global climate model
GCM-PS	global climate model – pattern scaling
GIS	Geographic Information System
GPU	graphics processing unit
HAND	Height Above Nearest Drainage
HDF	hierarchical data format
IDL	Interactive Data Language
IPCC	Intergovernmental Panel on Climate Change
LiDAR	Light Detection and Ranging
LP DAAC	Land Processes Distributed Active Archive Center
MGA	Map Grid of Australia
MODIS	Moderate-Resolution Imaging Spectroradiometer
NBAR	Nadir BRDF-Adjusted Reflectance

SHORT FORM	FULL FORM
NCI	National Computing Infrastructure
NDWI	Normalized Difference Water Index
OLI	Operational Land Imager
OWL	Open Water Likelihood
PE	potential evaporation
POD	Probability Of Detection
PS	pattern scaling
RCP	Representative Concentration Pathway
SAR	Synthetic Aperture Radar
SILO	scientific information for land owners
SRTM	Shuttle Radar Topography Mission
SSP	Shared Socioeconomic Pathway
TM	Thematic Mapper
URBS	Unified River Basin Simulator
USGS	United States Geological Survey

Units

UNIT	DESCRIPTION
cm	centimetre
GL	gigalitre
km	kilometre
m	metre
ML/d	megalitres per day
GL/d	gigalitres per day
mm	millimetre
s	second

Preface

Sustainable development and regional economic prosperity are priorities for the Australian, NT and Queensland governments. In the Queensland Water Strategy, for example, the Queensland Government (2023) looks to enable regional economic prosperity through a vision that states 'Sustainable and secure water resources are central to Queensland's economic transformation and the legacy we pass on to future generations.' Acknowledging the need for continued research, the NT Government (2023) announced a Territory Water Plan priority action to accelerate the existing water science program 'to support best practice water resource management and sustainable development.'

Governments are actively seeking to diversify regional economies, considering a range of factors, including Australia's energy transformation. The Queensland Government's economic diversification strategy for North West Queensland (Department of State Development, Manufacturing, Infrastructure and Planning, 2019) includes mining and mineral processing; beef cattle production, cropping and commercial fishing; tourism with an outback focus; and small business, supply chains and emerging industry sectors. In its 2024–25 Budget, the Australian Government announced large investment in renewable hydrogen, low-carbon liquid fuels, critical minerals processing and clean energy processing (Budget Strategy and Outlook, 2024). This includes investing in regions that have 'traditionally powered Australia' – as the North West Minerals Province, situated mostly within the Southern Gulf catchments, has done.

For very remote areas like the Southern Gulf catchments (Preface Figure 1-1), the land, water and other environmental resources or assets will be key in determining how sustainable regional development might occur. Primary questions in any consideration of sustainable regional development relate to the nature and the scale of opportunities, and their risks.

How people perceive those risks is critical, especially in the context of areas such as the Southern Gulf catchments, where approximately 27% of the population is Indigenous (compared to 3.2% for Australia as a whole) and where many Indigenous Peoples still live on the same lands they have inhabited for tens of thousands of years. About 12% of the Southern Gulf catchments are owned by Indigenous Peoples as inalienable freehold.

Access to reliable information about resources enables informed discussion and good decision making. Such information includes the amount and type of a resource or asset, where it is found (including in relation to complementary resources), what commercial uses it might have, how the resource changes within a year and across years, the underlying socio-economic context and the possible impacts of development.

Most of northern Australia's land and water resources have not been mapped in sufficient detail to provide the level of information required for reliable resource allocation, to mitigate investment or environmental risks, or to build policy settings that can support good judgments. The Southern Gulf Water Resource Assessment aims to partly address this gap by providing data to better inform decisions on private investment and government expenditure, to account for

intersections between existing and potential resource users, and to ensure that net development benefits are maximised.

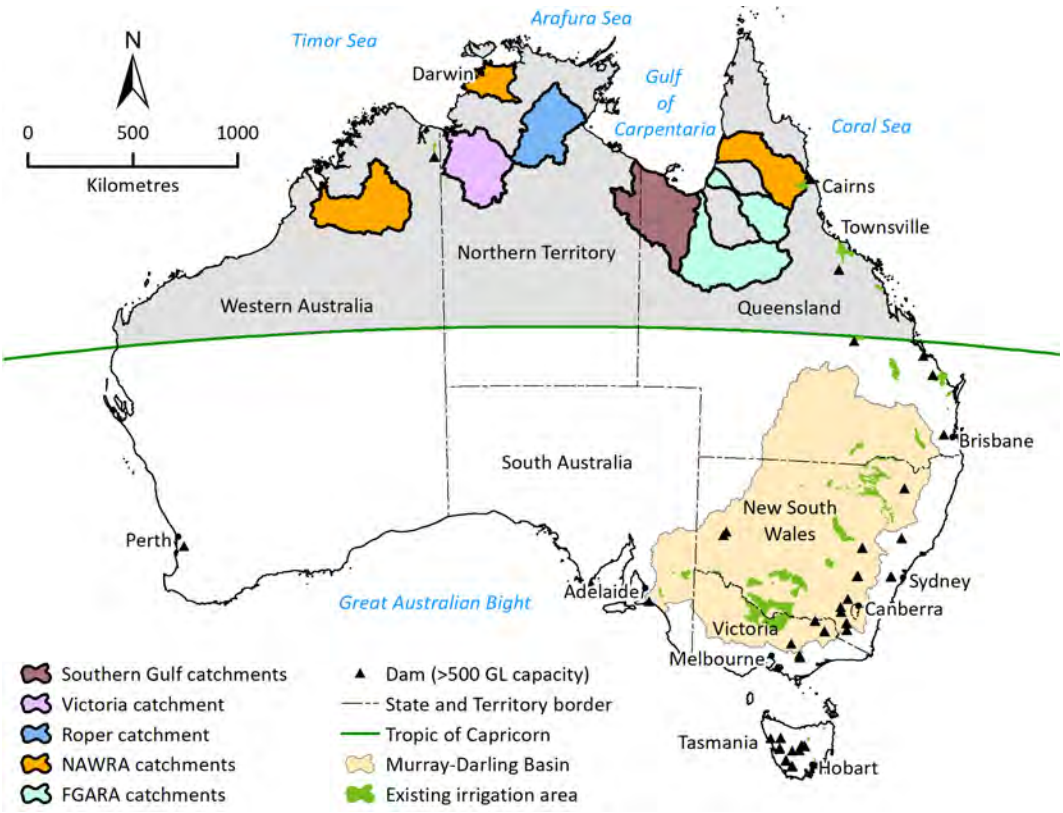

Preface Figure 1-1 Map of Australia showing Assessment area (Southern Gulf catchments) and other recent CSIRO Assessments

FGARA = Flinders and Gilbert Agricultural Resource Assessment; NAWRA = Northern Australia Water Resource Assessment.

The Assessment differs somewhat from many resource assessments in that it considers a wide range of resources or assets, rather than being a single mapping exercises of, say, soils. It provides a lot of contextual information about the socio-economic profile of the catchments, and the economic possibilities and environmental impacts of development. Further, it considers many of the different resource and asset types in an integrated way, rather than separately.

The Assessment has agricultural developments as its primary focus, but it also considers opportunities for and intersections between other types of water-dependent development. For example, the Assessment explores the nature, scale, location and impacts of developments relating to industrial, urban and aquaculture development, in relevant locations. The outcome of no change in land use or water resource development is also valid.

The Assessment was designed to inform consideration of development, not to enable any particular development to occur. As such, the Assessment informs – but does not seek to replace – existing planning, regulatory or approval processes. Importantly, the Assessment does not assume a given policy or regulatory environment. Policy and regulations can change, so this flexibility enables the results to be applied to the widest range of uses for the longest possible time frame.

It was not the intention of – and nor was it possible for – the Assessment to generate new information on all topics related to water and irrigation development in northern Australia. Topics

not directly examined in the Assessment are discussed with reference to and in the context of the existing literature.

CSIRO has strong organisational commitments to Indigenous reconciliation and to conducting ethical research with the free, prior and informed consent of human participants. The Assessment allocated significant time to consulting with Indigenous representative organisations and Traditional Owner groups from the catchments to aid their understanding and potential engagement with its requirements. The Assessment did not conduct significant fieldwork without the consent of Traditional Owners. CSIRO met the requirement to create new scientific knowledge about the catchments (e.g. on land suitability) by synthesising new material from existing information, complemented by remotely sensed data and numerical modelling.

Functionally, the Assessment adopted an activities-based approach (reflected in the content and structure of the outputs and products), comprising activity groups, each contributing its part to create a cohesive picture of regional development opportunities, costs and benefits, but also risks. Preface Figure 1-2 illustrates the high-level links between the activities and the general flow of information in the Assessment.

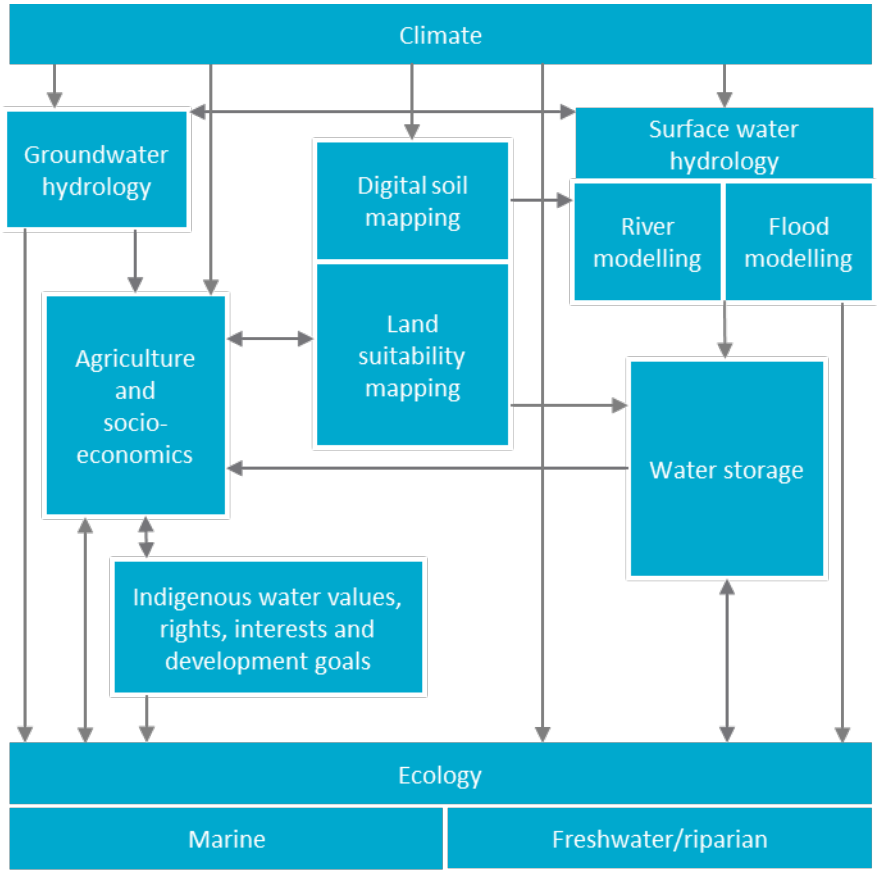

Preface Figure 1-2 Schematic of the high-level linkages between the eight activity groups and the general flow of information in the Assessment

Assessment reporting structure

Development opportunities and their impacts are frequently highly interdependent and, consequently, so is the research undertaken through this Assessment. While each report may be read as a stand-alone document, the suite of reports for each Assessment most reliably informs discussion and decisions concerning regional development when read as a whole.

The Assessment has produced a series of cascading reports and information products:

- Technical reports present scientific work with sufficient detail for technical and scientific experts to reproduce the work. Each of the activities (Preface Figure 1-2) has one or more corresponding technical reports.
- A catchment report, which synthesises key material from the technical reports, providing well-informed (but not necessarily scientifically trained) users with the information required to inform decisions about the opportunities, costs and benefits, but also risks, associated with irrigated agriculture and other development options.
- A summary report provides a shorter summary and narrative for a general public audience in plain English.
- A summary fact sheet provides key findings for a general public audience in the shortest possible format.

The Assessment has also developed online information products to enable users to better access information that is not readily available in print format. All of these reports, information tools and data products are available online at https://www.csiro.au/southerngulf. The webpages give users access to a communications suite including fact sheets, multimedia content, FAQs, reports and links to related sites, particularly about other research in northern Australia.

Executive summary

This report focuses on flooding characteristics of the Southern Gulf catchments in Queensland. The impact of flooding on agricultural production can be significant, potentially leading to the loss of livestock, fodder and topsoil, and damage to crops and infrastructure. However, flooding is generally favourable to floodplain wetlands and coastal ecosystems. For example, flood pulses create opportunities for offstream wetlands to connect with the main river channels, allowing the exchange of water, sediments, organic matter and biota.

This report provides an overview of inundation duration and depth across the floodplains of the major rivers in the Southern Gulf catchments. It also details the hydrodynamic modelling tools utilised to assess flood inundation. This includes information on data acquisition, model configuration, and the evaluation process, and a comparison of the model results with satellite-based flood inundation maps and water levels at gauging sites.

Hydrodynamic models offer several advantages over satellite-based approaches and conceptual node-link river system models when it comes to evaluating flood inundation. Hydrodynamic models enable the assessment of not only the extent of inundation but also water depth and velocity, with the ability to analyse these factors at very fine time intervals, often in the order of seconds. Furthermore, satellite-based approaches primarily focus on analysing historical flood events, whereas hydrodynamic models can be used to assess how flood characteristics might change under future climate and development scenarios.

The outputs derived from the hydrodynamic modelling play a crucial role, including:

- identifying areas prone to flooding under historical climates and the current level of development, commonly known as the baseline scenario
- estimating changes in inundation area under projected future climate and hypothetical development scenarios
- estimating changes in inundation depth and duration across the floodplain under future climate and development scenarios.

Hydrodynamic model configuration and calibration

In the Assessment, a two-dimensional flexible-mesh hydrodynamic model, MIKE 21 Flow Model FM, was used to simulate floodplain hydraulics (e.g. depth, velocity) and inundation dynamics across the floodplains of three large river systems: Nicholson, Gregory and Leichhardt.

The boundary conditions were derived from the daily discharge from a calibrated river system model called the Australian Water Resources Assessment – River model (AWRA-R), the hourly tide gauge information, and Sacramento rainfall-runoff model simulations. A two-dimensional hydrodynamic model (MIKE 21 FM) was configured for the middle and downstream reaches of the Nicholson, Gregory and Leichhardt rivers and their tributaries. The model domain includes areas downstream of Doomadgee on the Nicholson River, Gregory on the Gregory River and Lorraine on the Leichhardt River, and encompasses an area of 17,130 km^2. Flood inundation maps for individual flood events from 2000 to 2023 were created using Terra (EOS AM-1), Aqua (EOS PM-1), Landsat, Sentinel-1 and Sentinel-2 satellite imagery. These maps were used to calibrate the hydrodynamic model.

High-resolution Light Detection and Ranging (LiDAR) data (5 m) was acquired over the floodplains of the Albert, Gregory, Leichhardt and Nicholson rivers and only a small proportion of the Alexandra River, as part of the Assessment. For the remainder of the model domain, where floods are less frequent, a 30 m Forest And Buildings removed Copernicus digital elevation model (DEM) was used for land topography. The highest resolution publicly available topographic data covering the entire Southern Gulf catchments includes 1-second (i.e. ~30 m) Shuttle Radar Topography Mission (SRTM) digital elevation model (DEM) and 1-second FABDEM. These two global DEMs were compared, with the FABDEM being chosen due to its superior vertical accuracy in the Assessment area. The final combined DEM was created by resampling the FABDEM to 5 m, to match the original LiDAR resolution. The area covered by LiDAR is 7490 km^2, which is approximately 43.7% of the hydrodynamic model domain.

The hydrodynamic model was calibrated for the 2005 (annual exceedance probability (AEP) of 1 in 2), 2016 (AEP of 1 in 3), 2018 (AEP of 1 in 5), 2019 (AEP of 1 in 10) and 2023 (AEP of 1 in 38) flood events. The model was calibrated primarily by adjusting the roughness coefficient and the infiltration rate. While a good match was attained for the flood peaks, there were differences in the rising and falling limbs of the flood hydrograph. The model demonstrated reasonable simulation of spatial inundation patterns when compared with the Landsat, MODIS and Sentinel water maps. Overall, the model performed better for large floods, followed by medium-sized events, and then small events. There are some limitations to the model, and a lack of good-quality satellite imagery restricts rigorous calibration of the model results. Moreover, there are uncertainties in river model simulations that were used to specify the inflow boundaries of the hydrodynamic model.

The calibrated hydrodynamic models were utilised to investigate flood characteristics under future climate and development scenarios. Due to the extensive computation time, a limited number of simulation runs were conducted to explore the impact of future climate and hypothetical developments.

Flood characteristics

Intense seasonal rains from monsoonal bursts and tropical cyclones from November to March create flooding in parts of the Southern Gulf catchment and inundate large areas of floodplains, mostly in the downstream reaches between the Nicholson, Gregory and Leichhardt rivers. Floodplains along the Alexandra and Albert rivers are also heavily flooded. Rivers in Southern Gulf regions are unregulated, and its overbank flow is generally governed by the topography of the floodplain.

Flooding is widespread in parts of Lawn Hill Creek and the Gregory, Leichhardt and Albert rivers near Burketown. In the last 40 years (1984 to 2023), there have been 41 floods ranging from small to large in the catchments. This is based on an overbank threshold of 709 m^3/second, which was estimated by obtaining the daily streamflow at Floraville on the Leichhardt River (913007) that corresponded to floodplain inundation in available satellite imagery. While floods can occur in any month between October and May, the majority of the historical floods have occurred between December and March.

Additional observations of flooding under the historical climate are as follows:

- Flood peaks typically take about 2 days to travel from Gregory to Burketown, with a mean speed of 3.2 km/hour.
- For flood events of AEP of 1 in 2, 1 in 5 and 1 in 10, the peak discharge at Floraville on the Leichhardt River is 1220, 3350 and 7140 m^3/second, respectively (i.e. 105.4, 289.4 and 616.9 GL/day, respectively).
- Between 1984 and 2023 (40 years), events with a discharge greater than or equal to AEP of 1 in 1 occurred during all months from October to May, with approximately 90% of historical floods occurring between December and March and the maximum in January (33.3%).
- Of the ten largest flood peak discharges at Floraville, four events occurred during January, four in March, one in February and one in December.

Scenario analysis

A limited number of simulations were conducted to investigate the effects of future climate and development on inundation duration and depth. Three dam sites with the total capacity of 2560 GL at full supply level and five water harvesting sites with a total annual maximum diversion of 150 GL were implemented in the model for impact assessment.

The model results revealed that the impacts of future projected wet (Scenario Cwet) and dry (Scenario Cdry) climates on floodplain inundation were more pronounced than the modelled impacts of water resource development. The decrease in floodplain inundation under Cdry was larger than the increase under Cwet, which is consistent with the changes in modelled streamflow under Cdry and Cwet scenarios.

The inclusion of three hypothetical dams resulted in a 33.8% decrease in the inundated area downstream for an event with an AEP of 1 in 3, and a 5.1% decrease for an event with an AEP of 1 in 38. In general, impacts are higher for smaller flood events, because dams store a substantial proportion of floodwater. The smaller relative impact found for the 1 in 38 AEP event during 2023 was due to a large flood volume (~21,000 GL) compared with the combined dam capacity (2560 GL). The impacts are also influenced by antecedent conditions at the beginning of the flood event and the flow hydrograph (e.g. impacts are less for multipeak floods).

Water harvesting (150 GL) resulted in a 5.4% decrease in inundation area and very minor changes to inundation duration for an event with an AEP of 1 in 3 (2016 flood). For the event with an AEP of 1 in 38, the decrease in inundation area was only 0.8%, and the changes in inundation duration were negligible. As expected, impacts were relatively large for the smaller flood event, given the same amount of water was extracted for both flood events.

Hydrodynamic models are computationally demanding and therefore only a limited number of events can be analysed. This in turn means that the characteristics and timing (particularly antecedent effects) of chosen events can influence the apparent response to various scenarios. To counter this, a flood area emulator was derived using river model daily flows that could predict flooded area across the entire 133-year time series. Using the emulator, the annual maximum flooded area was calculated for various scenarios. The mean annual maximum flooded area across 133 years of simulation was 1132 km^2 under Scenario A. This was reduced to 785 km^2 under the three dams scenario, while the water harvesting scenario with an irrigation target of 150 GL was associated with only a very small reduction in the annual maximum flooded area, to 1086 km^2.

Page deliberately left blank

Contents

Figures

Tables

1 Introduction

The most frequent, and often most damaging type of natural disaster has for many years been floods (Kron, 2015; Wang and Gao, 2022; Yu et al., 2022). The changes in climate and land use (including rapid urbanisation) that have occurred in recent times have caused flood events to become even more frequent and disastrous (Arnell and Gosling, 2016; Dottori et al., 2018; Tabari, 2020). In Australia, floods are one of costliest types of natural disasters (Rice et al., 2022; Ulubasoglu et al., 2019).

While floods are generally perceived as natural disasters, they can provide many environmental and ecological benefits (Opperman et al., 2009; Tockner et al., 2008). Floodplain inundation contributes to species diversity and relative abundance, aquatic biota growth (Phelps et al., 2015), groundwater recharge (Doble et al., 2012) and soil fertility (Ogden and Thoms, 2002). During floods, there is an exchange of water, sediments, chemicals, organic matter, and biota between the main river channels and their floodplains (Bunn et al., 2006; Thoms, 2003; Tockner et al., 2010). Since the Flood Pulse Concept first appeared in the scientific literature (Junk et al., 1989), the importance of floodplain inundation for these exchanges and for the productivity of diverse aquatic biota in river–floodplain systems has been emphasised in many studies (Bayley, 1991; Gallardo et al., 2009; Heiler et al., 1995; Middleton, 2002). However, our knowledge of the frequency and duration of floodplain inundation, of the associated connectivity between water bodies, and of its impact on the ecological functioning of many of the world's largest floodplain systems is very limited. To date, the published knowledge is insufficient to adequately inform water management for biodiversity protection or adaptation to future climates (Arthington et al., 2015; Beighley et al., 2009).

Despite centuries of human activities that altered river floodplains worldwide, remnant permanent water bodies still exist on the floodplains, but they are diminishing at increasing rates (Bayley, 1995; Tockner et al., 2008). An important requirement for the management of floodplain water bodies, including the management of wetlands of historical, cultural, economic and other biodiversity values, is knowledge of the extent, frequency and duration of floodplain inundation and of the hydrological connectivity between them. This is essential in deriving strategies for maintaining, or even enhancing to an optimal level, the biophysical exchanges between rivers and floodplains. The catchments of the Southern Gulf, the Assessment area, has large floodplains in their middle and lower reaches, and they support a larger number of offstream wetlands with high ecological, cultural and biodiversity values. Therefore, it is important to quantify the inundation dynamics (in terms of extent, frequency and duration) and the hydrological connectivity between the offstream wetlands and the main channel (or several channels) under the historical climate, and to assess how the inundation and connectivity could be impacted under future climate and development.

However, the quantification of floodplain inundation dynamics and hydrological connectivity between water bodies remains a great challenge. A number of studies have used a combination of remotely sensed inundated area and concurrent river flow to predict the impact of river flow on flooded area (e.g. Frazier and Page, 2009; Overton, 2005; Peake et al., 2011; Townsend and Walsh,

1998). The same approach has also been used to quantify how river flow affects the number of inundated wetlands (e.g. Frazier et al., 2003; Shaikh et al., 2001). However, this approach is not dynamic. It cannot produce a continuous time series of predicted inundation extent, and it is not possible to cannot predict the duration of wetland connectivity. Inundation extent and the duration of wetland connectivity can have an important influence on wetland ecology. With the development of computational methods and computer technology, hydrodynamic modelling has become popular for the study of floodplain hydraulics and for quantifying the time course of flood inundation with high spatial and temporal resolution (Nicholas and Mitchell, 2003; Schumann et al., 2009). By combining these modelling techniques with high-resolution topography data, the duration, frequency and timing of wetland connectivity can be quantified (Karim et al., 2012, 2015). Previous studies have used a combination of hydrological and hydrodynamic models using simplified one-dimensional (e.g. Beighley et al., 2009; Chormanski et al., 2009) to more complex two-dimensional (Tuteja and Shaikh, 2009) modelling. In this Assessment, a two-dimensional flexible-mesh hydrodynamic module (MIKE 21 Flow Model FM, hereafter referred to as MIKE 21 FM) has been used with advanced model configuring with flexible-mesh modelling tool to simulate floodplain inundation.

1.1 Objectives

The Southern Gulf Water Resource Assessment flood modelling activity seeks to answer the following questions:

- What areas on the floodplains are susceptible to flooding under the historical climate scenario?
- What are the extent, duration and frequency of floodplain inundation under the historical climate scenario?
- What changes could be expected in inundation dynamics under future climate and development scenarios?
- What changes could be expected in hydrological connectivity between floodplain water bodies due to flow regime change under future climate and development scenarios?

This report describes the configuration and calibration of the MIKE 21 FM and scenario modelling for the future climate and water infrastructure development scenarios.

1.2 Previous flood studies in the Southern Gulf catchments

Large-scale flood modelling for the Southern Gulf catchments has been very limited. However, some local-scale flood studies have been conducted by the Queensland Reconstruction Authority as a part of the Queensland Flood Mapping Program 2013. The Queensland Reconstruction Authority (2012) investigated flood extent and depth for the town of Gregory using Geographic Information Systems (GIS)-based methods, by combining topography and flood magnitude. They produced inundation maps for floods of various magnitudes up to an annual exceedance probability (AEP) of 1 in 100. Under the same flood mapping program, the Queensland Reconstruction Authority (2013) investigated flood level, velocity and hazard in the vicinity of Doomadgee township. The Assessment was conducted using a combination of hydrological input and a two-dimensional hydrodynamic model (TUFLOW). Engeny (2020) undertook a flood study

for Burketown, which is located on a remnant of the main channel of the Albert River and represents the most eastward extent of a very flat ridgeline that forms the highest ground (~5 m above sea level) on the western bank of the river. The study was conducted using TUFLOW and produced inundation maps for floods of various magnitudes.

1.3 Overview of flood modelling frameworks used in the Assessment

Hydrodynamic models are considered to be very useful tools for detailed flood inundation modelling, and they have been utilised for several decades (Bulti and Abebe, 2020; Liu et al., 2015; Teng et al., 2017). Based on the complexity of the river–floodplain network and the availability of input data for model configuration, one can select one-dimensional, two-dimensional or coupled one- and two-dimensional models (Horritt and Bates, 2002; Teng et al., 2017). However, it is extremely difficult to represent complex floodplain features using one-dimensional models because of the one-directional representation of river–floodplain system. Two-dimensional models avoid much of the conceptualisation required for building an accurate one-dimensional model by using gridded topography data (Pinos and Timbe, 2019). Nonetheless, the application of traditional fixed-grid two-dimensional models is not always sufficient for reproducing river conveyance. This is because model grids are not aligned with the riverbanks, and in many cases the lowest points in the river are not adequately represented in the model (Bomers et al., 2019; Teng et al., 2017). More recently, flexible-mesh (also called irregular-grid) models have been found to be superior to regular-grid models in terms of accuracy and computational time (Kim et al., 2014; Mackay et al., 2015; Pinos and Timbe, 2019). The use of a flexible-mesh model can overcome many of the limitations of regular-grid models, as they allow complex floodway geometries to be modelled with precision. They do not require the remainder of the floodplain to be modelled at the same spatial resolution, since they allow the computational mesh to be aligned and refined to suit the geometry of the floodplain (Mackay et al., 2015; Symonds et al., 2016).

The hydrodynamic models need to be calibrated against historical streamflow and inundation data before they can be applied with a degree of confidence. Traditionally, flood models are calibrated by comparing instream water heights (commonly gauge records) with floodplain inundation (commonly water marks on trees, buildings and electric poles). However, for relatively remote and sparsely populated catchments, it is often not possible to collect the field data that are necessary to robustly calibrate the model. This serves as a major constraint in the use of hydrodynamic models in remote and data-sparse areas. In recent years, there have been major advances in flood inundation mapping using satellite and airborne remote sensing. While the satellite imagery–based approaches have some limitations, including spatial and temporal resolutions, these techniques provide very useful data for hydrodynamic model calibration. In the Assessment, a combination of field-based observed stage heights and satellite-based inundation maps were used to calibrate the hydrodynamic model. Figure 1-1 shows the general steps in configuring and calibrating the two-dimensional hydrodynamic model (MIKE 21 FM) and scenario modelling for the future climate and dam impact assessment.

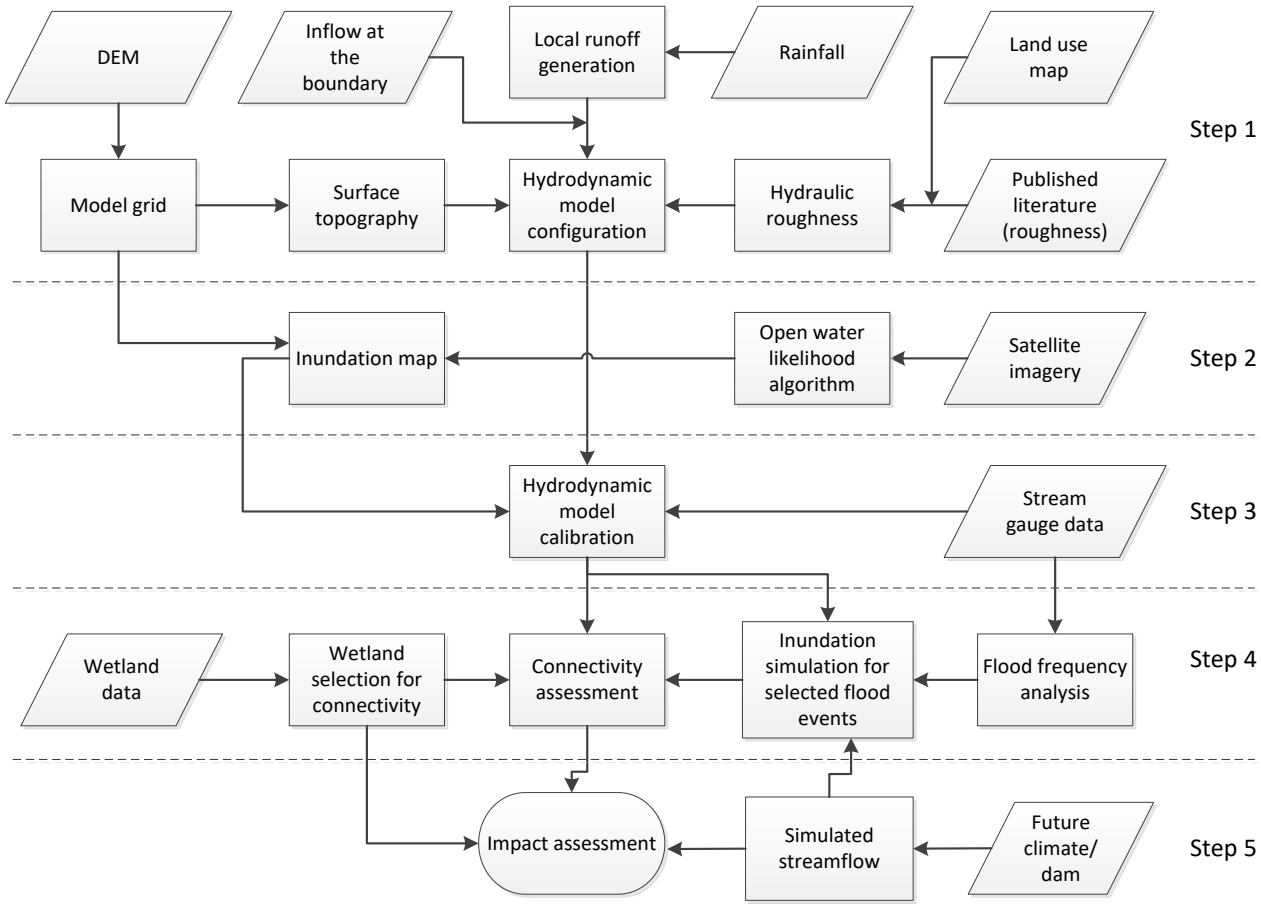

Figure 1-1 Flowchart illustrating the method used to calibrate a hydrodynamic model (MIKE 21 FM) and scenario modelling for future climate and dam impact assessment

DEM = digital elevation model.

1.4 Report overview and structure

This report has been prepared to:

- document the methods that were used to calibrate the MIKE FLOOD hydrodynamic models for the Assessment area
- report on the assessment of hydrodynamic model performance relative to satellite-based flood inundation mapping
- report on potential flood inundation extent under the historical climate and current level of development scenario
- report on potential changes to flood inundation and wetland connectivity under future climate and development scenarios.

This report is structured as follows. Chapter 2 describes the inundation mapping approach using satellite data and provides a summary of long-term inundation extent for the three study areas. Chapter 3 describes the hydrodynamic modelling approach, including the rationale for the selection of the MIKE 21 FM model, its input/output data requirements and the model calibration algorithm. Chapters 4 describes the hydrodynamic model configuration and the calibration of hydrodynamic model parameters for the Southern Gulf catchments. Chapter 5 provides the results

and discussion on impacts of future climate and infrastructure scenarios on floodplain inundation. Chapter 6 summarises the key findings of the Assessment.

1.5 Key terminology and concepts

1.5.1 WATER YEAR AND WET AND DRY SEASONS

Northern Australia has a highly seasonal climate, with most rain falling from December to March. Unless otherwise specified, the Assessment defines the wet season as the 6-month period from 1 November to 30 April, and the dry season as the 6-month period from 1 May to 31 October.

All results in the Assessment are reported over the water year, defined as the period 1 September to 31 August, unless otherwise specified. This allows each individual wet season to be counted in a single 12-month period, rather than being split over two calendar years (i.e. counted as two separate seasons). This is more realistic for reporting climate statistics from a hydrological and agricultural assessment viewpoint.

1.5.2 SCENARIO DEFINITIONS

The Assessment considered four scenarios, reflecting a combination of different levels of development and historical and future climates, much like those used in the Northern Australia Water Resource Assessment projects (Charles et al., 2016) and the Victoria, Roper and Southern Gulf Water Resource Assessment (McJannet et al., 2023):

- Scenario A – historical climate and current development
- Scenario B – historical climate and hypothetical future water resource development
- Scenario C – future climate and current development
- Scenario D – future climate and hypothetical future water resource development.

SCENARIO A

Scenario A is a historical climate and current development scenario. The historical climate series is defined as the observed climate (rainfall, temperature and potential evaporation (PE) for the water years from 1 January 1889 to 1 July 2023). All baseline data presented in this report has been calculated from data for this period unless otherwise specified. Justification for use of this period is provided in the companion technical report on climate (McJannet et al., 2023). The current level of surface water, groundwater and economic development were assumed (as of 1 July 2023). This scenario was referred to as Scenario AE in the river model scenario analysis (Gibbs et al., 2024b), as distinct from Scenario A, which assumed full use of the existing entitlements in that report. Scenario A was used as the baseline against which assessments of relative change were made. Historical tidal data were used to specify downstream boundary conditions for the hydrodynamic modelling.

SCENARIO B

Scenario B is a historical climate and future development scenario, as generated in the Assessment. Scenario B used the same historical climate series as Scenario A and assumed full use of existing entitlements. River inflow, groundwater recharge and flow, and agricultural productivity were modified to reflect future development. Two types of hypothetical future development were considered. The first was an increase in water harvest extraction directly from watercourses, typically assumed to supply water to nearby farm-scale developments. The second hypothetical future development considered was the construction of large instream dams, typically assumed to supply water to large contiguous irrigation districts. The impacts of changes in flow due to this future development were assessed, including impacts on:

- instream, riparian and near-shore ecology
- Indigenous water values
- economic costs and benefits
- opportunity costs of expanding irrigation
- institutional, economic and social considerations that may impede or enable the adoption of irrigated agriculture.

SCENARIO C

Scenario C is a future climate with current levels of surface water and ground development (assuming full use of existing entitlements as under Scenario A) assessed at approximately the year 2060. It is based on the 133-year climate series (as in Scenario A) derived from global climate model (GCM) projections for an approximately 1.6 °C global temperature rise (by ~2060) relative to the 1990 scenario. This climate projection represents Shared Socioeconomic Pathway (SSP) 2-4.5, as defined in the United Nations Intergovernmental Panel on Climate Change (IPCC) Sixth Assessment Report (IPCC, 2022). McJannet et al. (2023) provides further on the definition and selection of SSPs. As in Scenario B, full use of existing surface water entitlements was assumed, along with current level of groundwater and economic development.

SCENARIO D

Scenario D is a future climate and future development scenario. It used the same future climate series as Scenario C, but river inflow was modified to reflect future development, as in Scenario B. Therefore, in this report, the climate data for scenarios A and B were the same (based on historical observations from 1 January 1889 to 1 July 2023), and the climate data for scenarios C and D were the same (the above historical data scaled to reflect a plausible range of future climates).

1.5.3 HYPOTHETICAL DEVELOPMENT TERMINOLOGY

Water harvesting – an operation in which water is pumped or diverted from a river into an offstream storage, assuming no instream structures.

Offstream storages – usually fully enclosed circular or rectangular earthfill embankment structures situated close to major watercourses or rivers to minimise the cost of pumping.

Large engineered instream dam – a barrier across a river for storing water in the created reservoir, usually constructed from earth, rock or concrete materials. In the Southern Gulf catchments, most

hypothetical dams were assumed to be concrete gravity dams with a central spillway (see companion technical report on water storage (Yang et al., 2024)).

Annual diversion commencement flow requirement (DCFR) – the sum of the cumulative flow that must pass the most downstream nodes sum in the Nicholson (node number 9121090), Albert (node number 9129040) and Leichhardt rivers (node number 9130071) during a water year (1 September to 31 August) before pumping can commence. It is usually implemented as a strategy to mitigate the ecological impact of water harvesting.

Pump start threshold – a daily flow rate threshold above which pumping or diversion of water can commence. It is usually implemented as a strategy to mitigate the ecological impact of water harvesting.

Pump capacity – the capacity of the pumps expressed as the number of days it would take to pump the entire node irrigation target.

Reach irrigation volumetric target – the maximum volume of water extracted in a river reach over a water year. Note, the end use is not necessarily limited to irrigation. Users could also be involved in aquaculture, mining, urban or industrial activities.

System irrigation volumetric target – the maximum volume of water extracted across the entire study area over a water year. Note, the end use is not necessarily limited to irrigation. Users could also be involved in aquaculture, mining, urban or industrial activities.

Transparent flow – a strategy to mitigate the ecological impacts of large instream dams by allowing all reservoir inflows below a flow threshold to pass ‘through’ the dam.

2 Floodplain inundation mapping

Spatial maps of water in the landscape were derived from satellite imagery for dates coinciding with flood events. They were useful in calibrating and post-auditing the hydrodynamic models used to simulate floodplain inundation in the Southern Gulf catchments. These maps were produced using satellite imagery from the optical sensors of Moderate Resolution Imaging Spectroradiometer (MODIS), Landsat and Sentinel-2, and from the radar sensor Sentinel-1. However, frequent cloud occurrence across northern Australia during the wet season limits the optical remote-sensing opportunities for capturing inundation extents over the various rivers and floodplains in the hydrodynamic model domain, particularly during flood peaks. Refer to the technical report on Earth observation methods, Sims et al. (2016), for further details on the satellite data, processing methods, and calibration of the inundation maps.

2.1 Satellite imagery acquisition and pre-processing

MODIS satellite data were used for producing daily maps of surface water. The MODIS sensor is an optical/infrared sensor from the National Aeronautics and Space Administration. There are two MODIS sensors currently orbiting the Earth (TERRA since 2000 and AQUA since 2002), although they are approaching their end of life. They acquire daytime images of Australia at around 10 am (TERRA) and 2 pm (AQUA). MODIS surface reflectance data are available from early 2000 until the present from the United States Geological Survey (USGS) Land Processes Distributed Active Archive Center (LP DAAC) (https://lpdaac.usgs.gov/) as gridded tiles, and they are also stored at CSIRO for the whole of Australia. These data are available in hierarchical data format (HDF), in a sinusoidal projection, with a pixel size of 0.004697 degrees (~500 m). Daily images of surface reflectance from the TERRA MODIS sensor (MOD09GA) and an 8-day composite product (based on cloud-free, good-quality images; from TERRA – MOD09A1) were used. (Data from the AQUA sensor were not used, due to a detector failure in Band 6 (Gladkova et al., 2012) that resulted in a striped pattern in the data.)

Landsat data, where available, are also useful for mapping surface water. These data are at a much finer spatial resolution (30-m pixels) than MODIS, which is better suited to identifying narrow or small water features. However, Landsat images are only available every 8 to 16 days at best (depending on the number of operating sensors). This is usually less frequent due to cloud cover and missing data. Landsat 5 data (Thematic Mapper or TM), Landsat 7 data (Enhanced Thematic Mapper or ETM), and Landsat 8 and Landsat 9 data (Operational Land Imager or OLI) are available from Digital Earth Australia (DEA) from 1987 until the present. The DEA provides consistent pre-processing, organisation and analytics of Landsat data for the Australian continent (Dhu et al., 2017). This processing involves corrections for illumination and observation angles, the Bidirectional Reflectance Distribution Function (BRDF, which influences relative pixel brightness across large scene areas) and atmospheric conditions. Refer to the companion technical report on Earth observation methods, Sims et al. (2016), for further details on Landsat data processing.

The European Space Agency (ESA) operates the Sentinel-2 satellites. Sentinel-2 has two operating sensors (2A since 2015 and 2B since 2017), and its data has a spatial resolution of 10 to 20 m and a

temporal frequency of every 5 days. Sentinel-2A and -2B are optical remote-sensing instruments, so cloud cover reduces the amount of useful data for identifying inundation. These data are available from DEA (https://www.ga.gov.au/scientific-topics/dea) in a similar analysis-ready format to the Landsat data.

To help overcome the negative impact of frequent cloud cover during flood events, the ESA's Sentinel-1 Synthetic Aperture Radar (SAR) sensors were also used. Sentinel-1 SAR operates in the microwave wavelength range, so is not affected by cloud cover (although heavy rain can influence its return signal). Sentinel-1A (launched in 2014) and Sentinel-1B (operating from 2016 until 2022) have a pixel size of 10 m and a temporal frequency of (generally) every 12 days within Australia. These data are currently available through the Sentinel Australasia Regional Access (SARA) hub (https://copernicus.nci.org.au/sara.client/#/home) as a level 1 product in their native radar coordinates.

2.2 Inundation mapping using MODIS

The Open Water Likelihood (OWL) algorithm (Guerschman et al., 2011) was used for mapping open surface water with MODIS imagery at a 500 m pixel resolution. The OWL was developed using empirical statistical modelling and calculates the fraction of water within a MODIS pixel. A cloud mask was applied using the MODIS state band associated with each product, which contains information on cloud and cloud-shadow locations. Refer to the technical report on Earth observation methods, Sims et al. (2016), for further details on the MODIS OWL algorithm. Using Python code, the daily MODIS OWL water maps (from TERRA – MOD) and the 8-day MODIS OWL water maps (also from TERRA – MOD) for the Assessment area were extracted from the Australia-wide products.

A limitation of MODIS mapping of surface water is that it is not of sufficient detail for mapping narrow water features of less than 1 pixel in width (~500 m). This problem is even more exaggerated when the narrow river channel is covered by vegetation along the banks or floating vegetation, which effectively obscures the water from the sensor.

2.2.1 EVENT MAPS

The daily MODIS maps were extracted and subset for the Southern Gulf hydrodynamic model domain for flood events used for inundation modelling. The years 2005, 2016, 2018, 2019 and 2023 were considered. The MODIS OWL water maps were converted into a map of water and non-water pixels, and a threshold was used to stratify each MODIS OWL water fraction into water/non-water. Ticehurst et al. (2015) showed that, in the Flinders catchment, a 10% threshold resulted in the best match when comparing MODIS and Landsat inundation maps. Thus, all pixels above the OWL threshold of 10% were mapped as water, and the images reprojected onto the geographic latitude/longitude coordinate system (coordinate system code EPSG:4326), before conversion to a GeoTIFF format for use with the hydrodynamic models. To help reduce the commission errors throughout the Southern Gulf catchments, the Height Above Nearest Drainage (HAND) algorithm (Nobre et al., 2011) was used to identify areas that were unlikely to flood. Pixels for which the HAND value was above 40 were masked as nulls.

2.2.2 SUMMARY MAPS

Summary maps were also produced for the flood events processed for the hydrodynamic modelling (Figure 2-1). These summary maps used composites of the MOD09A1 MODIS OWL water maps to show maximum inundation extent, and the percentage of clear observations (i.e. observations without clouds and/or nulls).

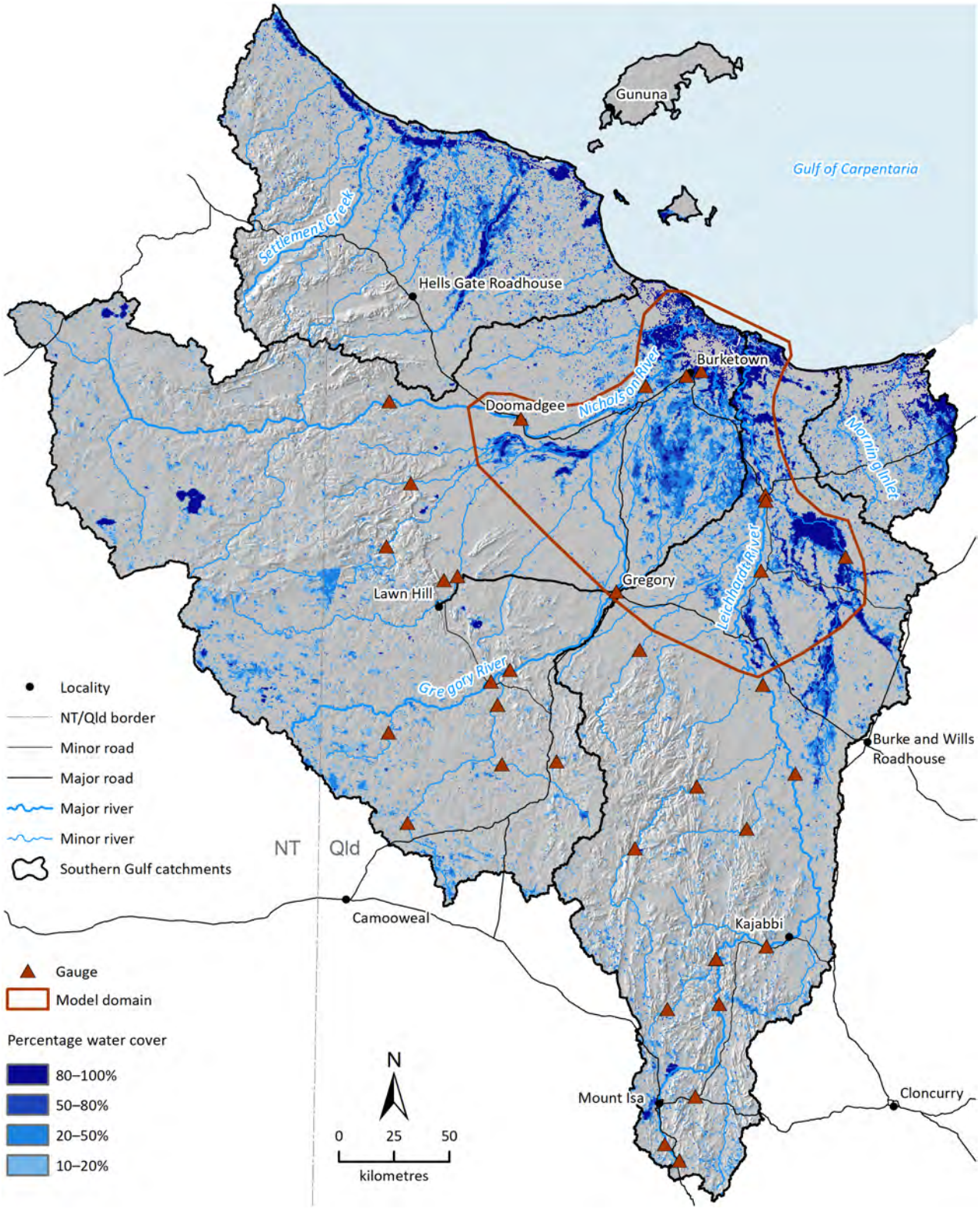

Figure 2-1 MODIS satellite–based flood inundation map of the Southern Gulf catchments
Data captured using MODIS satellite imagery. This figure illustrates the maximum percentage of MODIS pixel inundation between 2000 and 2020.

2.3 Inundation mapping using Landsat

2.3.1 ALGORITHM USED

Landsat 5 TM, 7 ETM, 8 OLI and 9 OLI data were extracted from DEA. For mapping flood inundation, the Normalized Difference Water Index $(NDWI)_{Xu}$ (Xu, 2006) – an index based on the green and mid infrared wavelengths – was used. Water was separated from other features using a threshold of $NDWI_{Xu} \geq -0.3$, which is consistent with Xu (2006) and balances errors of omission and commission in the Southern Gulf catchments. Masking of cloud cover was undertaken by extracting the pixel quality band ('fmask') available with each Nadir BRDF-Adjusted Reflectance (NBAR) product. As for the MODIS water maps, to reduce the commission errors that were detected throughout the catchment, the HAND algorithm (with a threshold of 15) was applied to mask pixels in steep terrain. This threshold worked well for the Landsat spatial resolution along the narrow, steep valleys.

2.3.2 EVENT MAPS

Landsat water maps were selected for the same hydrodynamic model domains and flood events as the MODIS data. These were examined to find those images least affected by cloud cover, which greatly limited the number of available images, given that deep clouds and sustained rain prevail during the wet season across northern Australia, and the infrequent satellite overpass. These images were then converted to the geographic latitude/longitude (EPSG:4326) coordinate system and GeoTIFF format for use with the hydrodynamic models.

2.4 Inundation mapping using Sentinel-2

2.4.1 ALGORITHM USED

All Sentinel-2 imagery available during the flood event dates were extracted from DEA. The $NDWI_{Xu}$ was used to separate water from non-water, and the same threshold as used for Landsat was used for the Sentinel-2 imagery. The 'fmask' band was used to mask pixels affected by cloud or cloud shadow. As for the Landsat data, the HAND algorithm (with a threshold of 15) was applied to mask pixels in steep terrain.

2.4.2 EVENT MAPS

Sentinel-2 water maps were selected for the same hydrodynamic model domains and flood events as the MODIS data. These were examined to find those images least affected by cloud cover, which greatly limited the number of images available, given that deep clouds and sustained rain prevail during the wet season across northern Australia. The Fmask quality band for Sentinel-2 does not always detect clouds, so images affected by significant remnant clouds were removed. The remaining images were then converted to the geographic latitude/longitude (EPSG:4326) coordinate system and GeoTIFF format for use with the hydrodynamic models.

2.5 Inundation mapping using Sentinel-1

2.5.1 ALGORITHM USED

Sentinel-1 backscatter data for the flood events were processed to normalised radar backscatter, an analysis-ready format, and filtered to reduce speckle effects. The radar backscatter was converted from intensity to decibels for better contrast between water and land. A low backscatter threshold was used to identify surface water. After testing various methods, this threshold was calculated based on the likelihood of flooding generated from the HAND algorithm. Areas with a low HAND value (i.e. along the valley floor) were more likely to be flooded, so the backscatter threshold was increased there compared with those pixels further from the valley bottom. To reduce commission errors, small 'clumps' of pixels (up to 10 pixels in size) that were misclassified as water bodies were removed using a sieve filter. The HAND algorithm was applied to mask pixels in steep terrain.

2.5.2 EVENT MAPS

Sentinel-1 images for 14 dates were processed to water maps. Due to the large catchment size, no single date had images available for the entire Southern Gulf catchments. The images were provided in the geographic latitude/longitude (EPSG:4326) coordinate system and GeoTIFF format for use with the hydrodynamic model.

2.6 Combined summary maps

There were a limited number of images identifying flooding among the Landsat, Sentinel-2 and Sentinel-1 images. However, because they were of a similar spatial resolution and quality, these images were able to be combined to produce a summary map. Those water maps produced for the flood events used in the hydrodynamic modelling were combined to delineate the maximum flooding extent, and to calculate the percentage of clear observations in which a pixel was inundated (Figure 2-2).

2.7 Summary

Flood inundation maps were produced using MODIS, Landsat, Sentinel-2 and Sentinel-1 imagery for the Southern Gulf catchments. MODIS surface reflectance data are available since 2000 for the whole of Australia. Daily images of surface reflectance from the TERRA sensor (MOD09GA), and 8-day composite images of surface reflectance from the TERRA MODIS sensor (MOD09A1) were used in the analysis. Landsat data are available from DEA from 1987 until the present in a consistent analysis-ready format. Sentinel-2 data are available from DEA from 2015 until the present.

The OWL algorithm was used for mapping open surface water with MODIS imagery at a 500 m pixel resolution. The OWL was developed using empirical statistical modelling and calculates the fraction of water within a MODIS pixel. The daily MODIS OWL water maps (from TERRA – MOD) were extracted and subset for the Southern Gulf catchments hydrodynamic model domain, and a

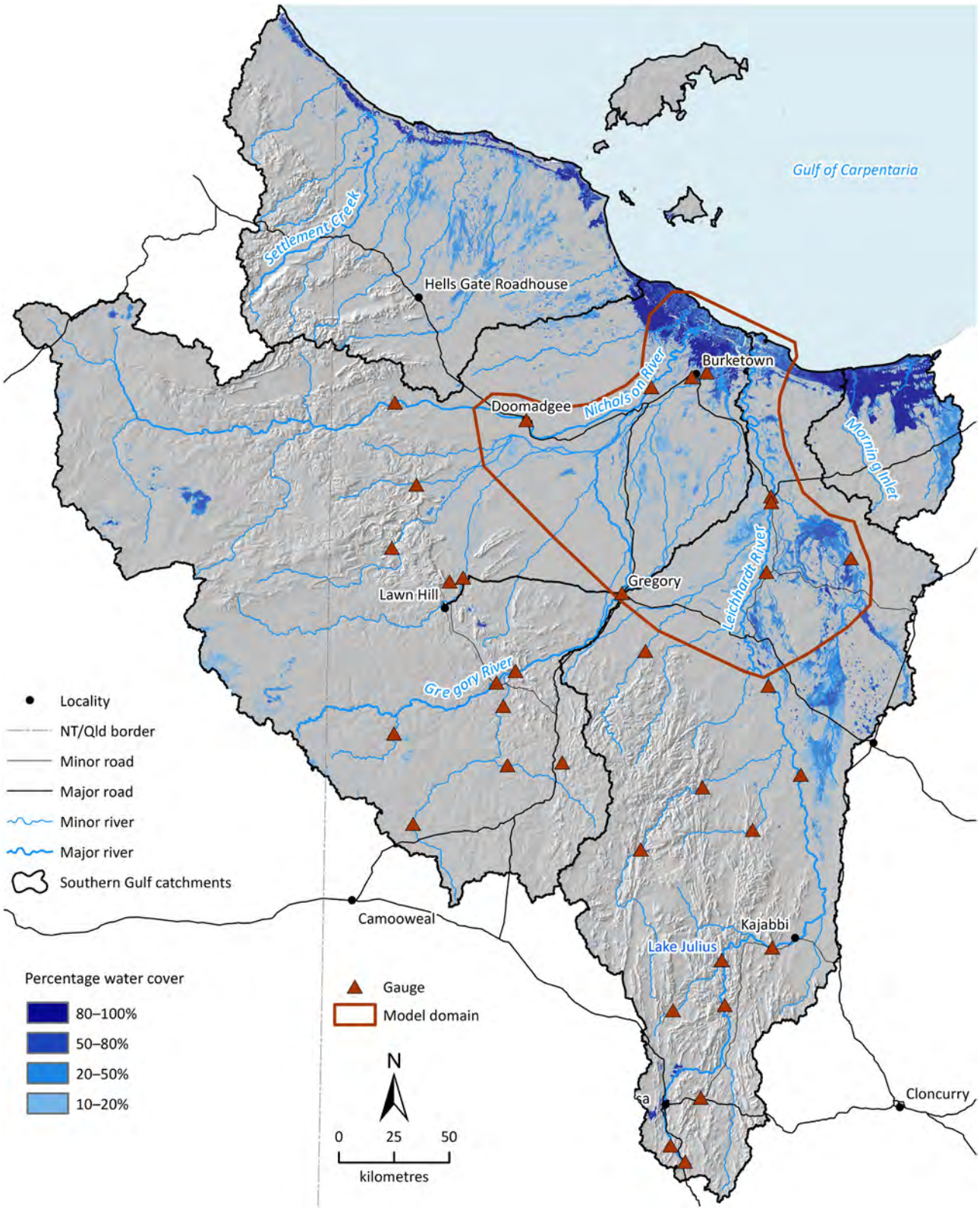

Figure 2-2 Combined Landsat, Sentinel-2 and Sentinel-1 satellite–based flood inundation map of the Southern Gulf catchments

Data captured using Landsat, Sentinel-2 and Sentinel-1 satellite imagery. This figure illustrates the percentage of clear observations in which a pixel was inundated during the flood events used in the hydrodynamic modelling.

series of flood maps were produced for selected flood days for the hydrodynamic model calibration.

Sentinel-1 data, which are not affected by cloud cover, were also used to identify flooding, based on a low radar backscatter. These images were able to capture some flooding in parts of the Southern Gulf catchments.

The NDWI algorithm was used for mapping flood inundation based on Landsat and Sentinel-2 imagery. Water was separated from other features using a threshold of NDWI ≥ −0.3, which balances errors of omission and commission, in the Southern Gulf catchments. Similarly, for MODIS, a set of event-based and summary maps were produced using the combined Landsat, Sentinel-2 and Sentinel-1 data.

Water maps generated from satellite imagery are particularly useful for encompassing large areas at a reasonable temporal frequency. While MODIS can provide daily water maps, it is of a poorer spatial resolution (~500 m) compared with Landsat (30 m pixels), Sentinel-2 (10–20 m pixels) and Sentinel-1 (10 m pixels), and surface water of less than 1 pixel in width (~500 m) cannot be mapped, particularly if there is vegetation along the riverbanks. In general, it was found that in northern Australia's wet–dry tropical/monsoonal climate, MODIS produces better flood maps for large floodplains and/or big flood events. Care must be taken when interpreting the MODIS water maps, due to artefacts in the imagery and confusion with dark soils, dark rocks, residual cloud and topographic shadow. Unusual water features appearing in only one image need to be treated with caution, and a flood-likelihood mask would be of great benefit in interpretation of the data.

The Landsat and Sentinel-2 water maps are very useful for detecting fine water features. However, the temporal frequency of the imagery made it difficult to analyse flood events, as the flood peak was often missed due to the timing of satellite overpass or cloud cover. As for MODIS, the Landsat and Sentinel-2 water maps will be affected by the difficulty of detecting water under flooded vegetation, and by confusion with dark features (e.g. residual cloud and topographic shadow).

The maximum percentage water cover based on MODIS imagery is higher than that determined from combined Landsat/Sentinel-2/Sentinel-1 imagery. The reason for this is that MODIS OWL water maps can identify wet soil as water (Sims et al., 2016). Another reason for the difference could be that MODIS has a much higher temporal frequency (daily) than Landsat (every 16 days), Sentinel-2 (every 5 days) and Sentinel-1 (every 12 days), which means that these sensors will fail to coincide with as many flood events as MODIS, especially as there can be high cloud cover in the Southern Gulf catchments.

3 Floodplain inundation modelling

3.1 Hydrodynamic models

Two-dimensional hydrodynamic models (e.g. MIKE 21 FM, TUFLOW, LISFLOOD-FP) are commonly used to simulate flood levels and inundation extent in a river–floodplain system (Kumar et al., 2023; Kvocka et al., 2015; Neal et al., 2012). The main strengths of the hydrodynamic models are that they produce floodplain hydraulics that can be used to estimate inundation extent and duration, and depth and frequency of wetting and drying at desired spatial (e.g. 5 to 10 m–grid) and temporal (e.g. hourly) scales (Horritt and Bates, 2002). Based on the modelling objectives and the availability of input data, either a two-dimensional regular-grid model (DHI, 2012) or a two-dimensional flexible-grid model (DHI, 2016) can be selected. Technical considerations include the size of the hydrodynamic model domain, irregularity in land topography, the availability of topography data, and the complexity of the hydraulic regime. These two-dimensional models can be coupled with one-dimensional river models, which allows finer-scale representation of the highly dynamic river processes, including river cross-sections.

For the Assessment, a two-dimensional flexible-mesh model (MIKE 21 FM) was selected for the Southern Gulf catchments, primarily based on the availability of fine-scale laser altimetry (LiDAR) data. A brief description of the MIKE 21 FM model is presented in the following sections.

3.1.1 TWO-DIMENSIONAL HYDRODYNAMIC MODEL – MIKE 21 FM

The hydrodynamic module of the MIKE 21 FM is based on the two-dimensional incompressible Reynolds-averaged Navier–Stokes equations (DHI, 2016). The model simulates the water level and velocity flux in response to a variety of forcing functions in floodplains, lakes, estuaries, bays and coastal areas. The boundary conditions in MIKE 21 FM can vary in both time and space. Point sources and sinks can also be incorporated into the model. The model has been widely used across the world, including in Australia, for flood inundation modelling (Teng et al., 2017). The main strength of the MIKE 21 FM model is its ability to simulate wetting and drying of a floodplain during a flood event, and the large number of computational cells that it can handle (in the range of millions). Model input includes river bathymetry, floodplain topography, land surface roughness (constant or spatially variable), inflow and outflow conditions, eddy viscosity and radiation stresses. Rainfall, evaporation and surface infiltration can also be incorporated in MIKE 21 FM. The model output includes time series of water depth, velocity and discharge for the entire computational domain and user-specified time intervals. In the Assessment, a triangular mesh of varying size was used, and the modelling domain was divided into three subzones based on mesh size. The flexible-mesh model is preferable over the classic MIKE 21 FM regular-grid model, because it allows selection of a very small grid at the area of interest and also the alignment of model grids to the riverbanks.

3.1.2 SOLVING GOVERNING EQUATIONS AND HARDWARE REQUIREMENTS

The primitive variables of the governing equations are discretised using an element-centred finite-volume method. The spatial domain is discretised into non-overlapping elements, which can be either triangular or quadrilateral (DHI, 2016). The finite-volume method sets up an equivalent Riemann problem (ERP) across each element interface and solves it to determine the variable fluxes between the elements. The technique used in MIKE 21 FM determines an exact solution to an approximate Riemann problem. The approach treats the problem as one-dimensional in the direction perpendicular to each element interface. MIKE 21 FM has two options for time integration accuracy: a first-order explicit Euler method (referred to as the lower temporal order scheme) and a second-order Runge–Kutta method (referred to as the higher temporal order scheme). There are also two options for spatial integration, with the second-order (higher-order) accuracy being achieved through a variable gradient reconstruction technique prior to the ERP formulation (DHI, 2016). The model can be simulated on either a central processing unit (CPU) machine or a graphics processing unit (GPU) machines. In the present Assessment, the models were run using GPU machines containing 16 CPU cores and 3 GPU cards (each with 4 P100 Nvidia GPUs). Each run took about 3 days of computer time to simulate a 30-day flood event.

3.2 Data requirement for model configuration

Hydrodynamic models are data intensive. A large amount of temporal and spatial data is required for setting up a hydrodynamic model for flood inundation modelling. While some input data (e.g. stream network, water level, discharge) can be extracted from the secondary sources, most input data are case-specific and need to be prepared before running the model. To configure the MIKE 21 FM model, data needed across each of the hydrodynamic model domains included:

- topography
- surface roughness
- stream network
- Inflow/outflow
- water level
- local runoff.

4 Southern Gulf catchments hydrodynamic model calibration

4.1 Physical and hydro-meteorological properties

4.1.1 PHYSIOGRAPHIC CHARACTERISTICS

The Southern Gulf catchments comprise four northerly draining catchments defined by the Australian Water Resources Council (AWRC) river basin boundaries – Settlement Creek (17,600 km^2), Nicholson River (52,200 km^2), Leichhardt River (33,400 km^2) and Morning Inlet (3700 km^2) – and the islands within the AWRC Mornington Island Basin (total 1200 km^2) (Figure 4-1). The catchments are characterised by several uplands and plains. The upland area in the south and west reaches 620 m above sea level. The uplands have been eroded into a complex pattern of easterly flowing streams and valleys separated by ranges and outcrops of sedimentary formations. The Nicholson and South Nicholson rivers are the primary systems draining this area. Musselbrook, Lagoon, Settlement, Gold and Running creeks also drain this area The Cloncurry Plain consists of gently sloping colluvial and fluvial sedimentary plains. Streams are few and incised into the pediments, with narrow alluvial plains. The Cloncurry Plain extends from the middle reach of the Leichhardt River to Lawn Hill Creek. In the north, the Doomadgee Plain lies below and adjacent to the Cloncurry Plain. Widely spaced creeks drain the plains towards the coast. In the south, the Armraynald Plain lies below and adjacent to the Cloncurry Plain. Stream channels are few, widely spaced, and deeply incised due to sea-level changes. The plains extend up the Lawn Hill Creek, and Gregory and Leichhardt valleys. Lawn Hill Creek and Gregory River are spring-fed permanent running streams. The Gregory River splits into a giant braid (20 km at its widest) of permanent streams (consisting of the Gregory River, Beames Brook, Barkly River and Running Creek) downstream of the Gregory Crossing. Downslope of both the Doomadgee Plain and the Armraynald Plain lies the coastal Karumba Plain. This coastal unit extends 10 to 35 km inland from the Gulf of Carpentaria coast, and the plain is most extensive near the Albert River mouth. Some of the inland plains only flood when the rivers are in spate or when the north-westerly winds cause exceptionally high tides during the monsoon. Because the plain is wide and the tidal range is moderate (~3.5 m), and because the plain is generally flat, tidal waters can rapidly inundate the land. Mangroves and tidal flats dominate the coastline (Gibbs et al., 2024a). For the hydrodynamic modelling study, the focus was the floodplains of the Nicholson, Gregory and Leichhardt rivers.

The main land use in the Southern Gulf catchments is grazing of beef cattle (84%), including on productive black soil plains, with nature conservation through national parks (including Boodjamulla (formerly Lawn Hill) National Park and Indigenous Protected Areas) comprising 13% of the catchments' area. Century Zinc Mine – formerly one of the world's largest zinc mines – is located near Lawn Hill, and there are large mining operations in and near Mount Isa. The catchments incorporate the edge of the Barkly Tableland and are characterised by extensive alluvial grassy plains, distinctive marine plains, dissected hilly regions, and erosional plains.

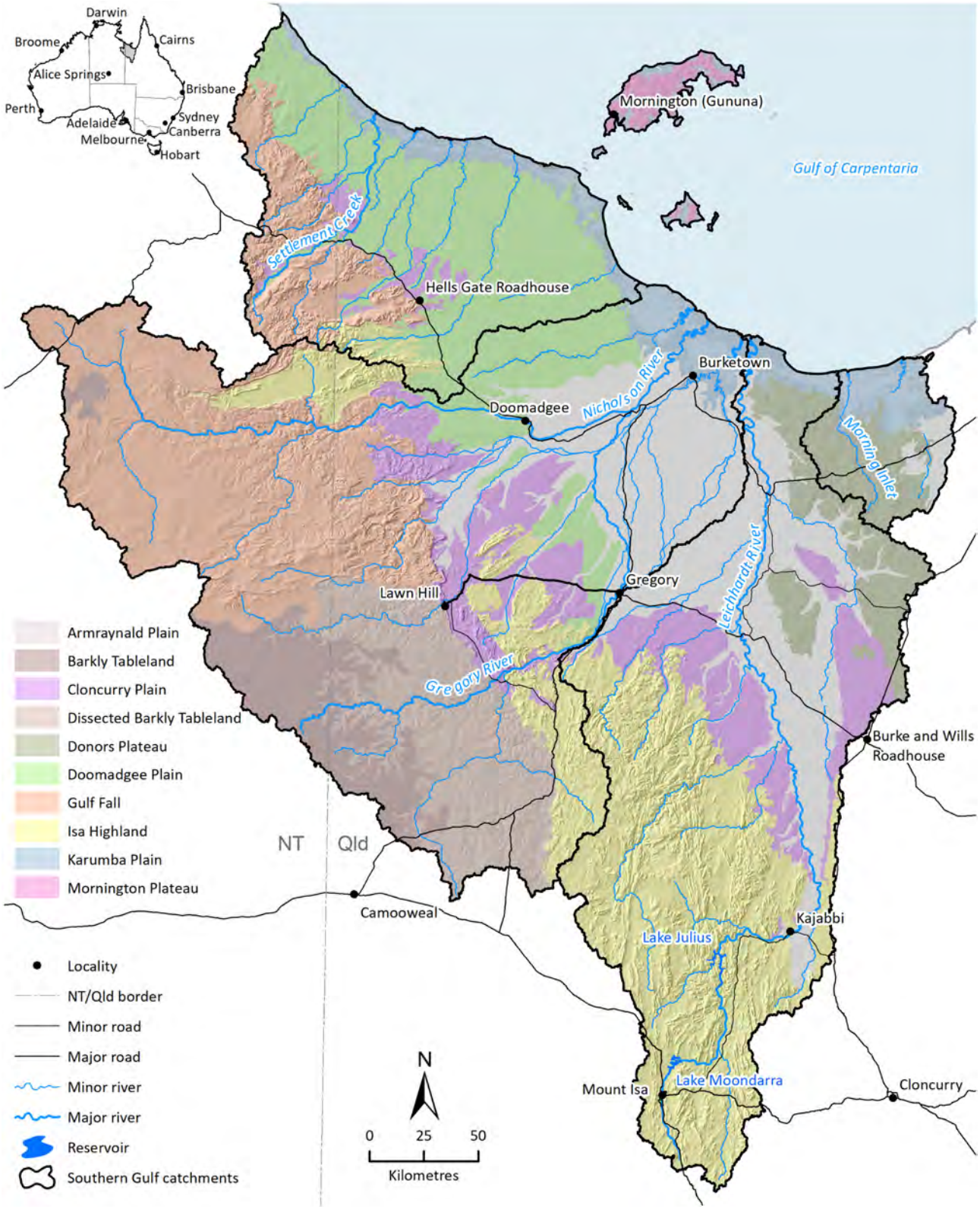

Figure 4-1 Southern Gulf catchments map showing physiography and river network. From Thomas et al. (2024)

4.1.2 CLIMATE

The Southern Gulf catchments are characterised by a distinctive wet and dry season due to their location in the northern Australia tropics. The mean annual rainfall, averaged over the Southern Gulf catchments for the 133-year historical period (1 September 1890 to 31 August 2022) is 602 mm. Rainfall totals are highest near the coast and decline in a southerly direction. In the Southern Gulf catchments, approximately 94% of rain falls during the wet-season months (1 November to 30 April). The mean and median annual rainfall is highest near the coast, primarily due to the monsoonal activity, which generates significant rainfall during the wet season (McJannet et al., 2023). The highest rainfall totals typically occur during January and February (Figure 4-2).

Mean areal potential evapotranspiration in the Southern Gulf catchments is approximately 1900 mm. Evaporation is high all year round, but exhibits a strong seasonal pattern, ranging from about 200 mm per month during November and December to about 100 mm per month during the middle of the dry season (June). The high mean annual PE and moderate mean annual rainfall result in a mean annual rainfall deficit across all of the Southern Gulf catchments (Figure 4-2). Consequently, most of the study area is semi-arid.

Tropical cyclones and lows contribute large quantities of rainfall over the Southern Gulf catchments in some years and result in high daily rainfall values. Increased rainfall, storm surge, and wind speeds are associated with tropical cyclones. The cyclone season in the Southern Gulf catchments falls between November and April. From 1969 to 2022, the Southern Gulf catchments experienced 53 tropical cyclones. Sixty percent of seasons experienced no tropical cyclones, 36% one, and 4% two (McJannet et al., 2023).

Approximately a third of GCMs project an increase in mean annual rainfall by more than 5%, a fifth of GCMs project a decrease in mean annual rainfall by more than 5%, and about half project ‘little change’ (McJannet et al., 2023).

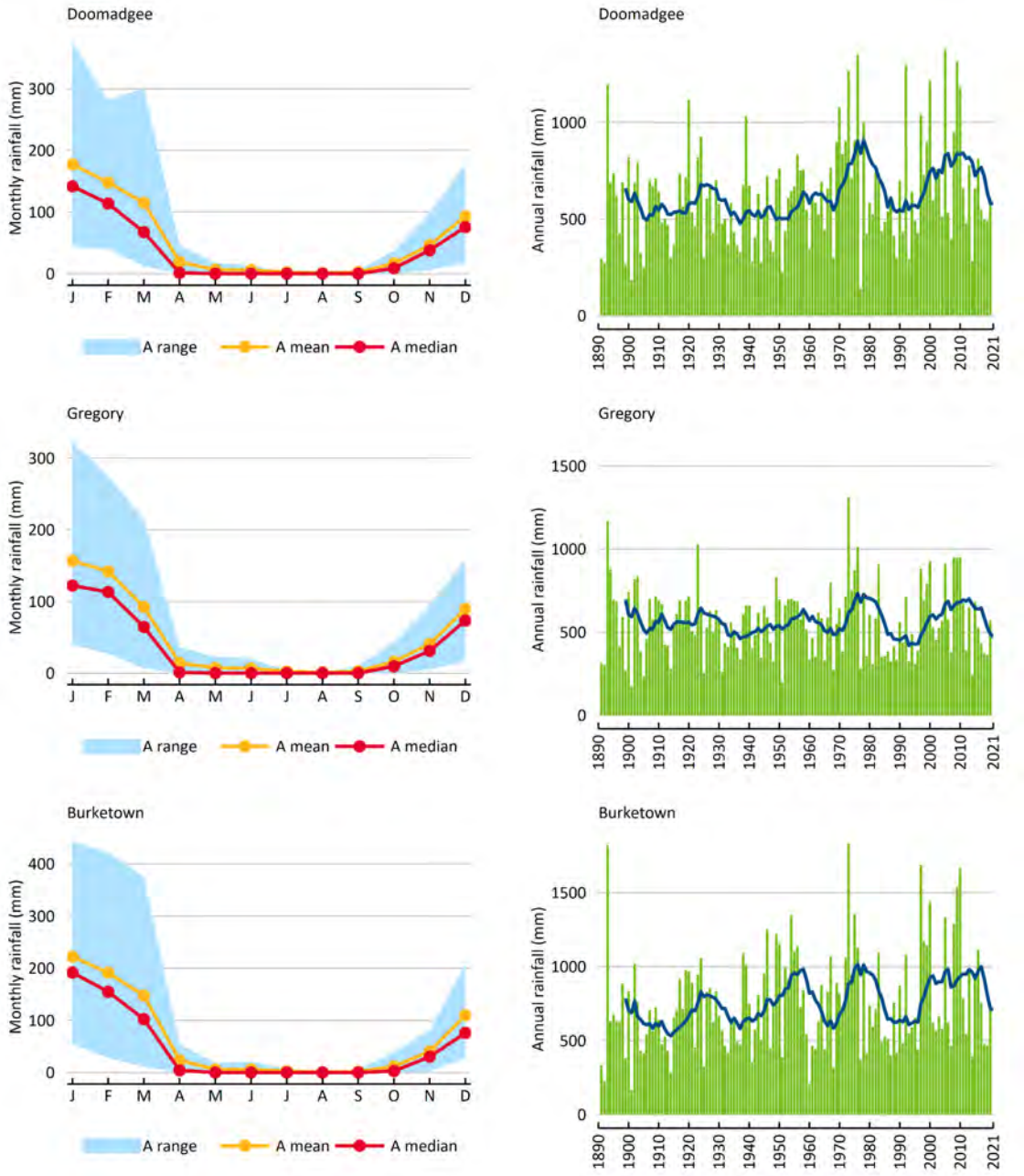

Figure 4-2 Historical monthly rainfall (showing the range in values between the 20% and 80% monthly exceedance rainfall) and annual rainfall in the Southern Gulf catchments at Doomadgee, Gregory and Burketown (from McJannet et al., 2023)

The left-hand column shows the monthly rainfall, and the right-hand column shows time series of the annual rainfall. (The range in the left-hand column is the 10th to 90th percentile for the monthly rainfall, and the blue line in the right-hand column represents the 10 years moving mean).

4.1.3 STREAMFLOW

Streamflow across the Southern Gulf catchments varies significantly based on river network and location. There were 23 gauging stations, but only 7 stations are currently operating across the Leichhardt, Gregory and Nicholson catchments. The only site with streamflow gauging over the past 35 years and maximum gauging covering at least 75% of the total volume is the gauge on Gunpowder Creek at Gunpowder (913006A). The streamflow gauging station on the Gregory River at Riversleigh (912105A) also has relatively extensive gauging data. The Nicholson River at Connolly's Hole (912007A) has gauging data that cover most of the flow regime (86% of the total estimated volume); however, this station was closed in 1988. Most gauges are located towards the southern portion of the Assessment area, in the upper reaches of the catchments (Figure 4-3). The only gauge available in the lower reaches of the Assessment area is on the Leichhardt River at Floraville Homestead (913007B). There are a number of anabranches on the Gregory River near the gauge at Gregory (912101A). The proportion of flow occurring in each of the flow paths will have an influence on the flow remaining in the Gregory River, and ultimately flowing towards the Nicholson River, and the proportion that splits off into Beames Brook and ultimately the Albert River at Burketown.

Driven by the highly seasonal climate, streamflow in the Southern Gulf catchments displays very strong seasonal patterns (Figure 4-4). The Southern Gulf catchments comprise four northerly draining catchments: the catchments of Settlement Creek, the Nicholson River, the Leichhardt River and Morning Inlet. The rivers and creeks in the area are seasonal (January to March) due to the vast majority of rainfall occurring during the wet season, with cease-to-flow periods for 30%–60% of the time. The watercourses in the Gregory River catchment are a notable exception, with perennial flow that is associated with limestone and dolostone aquifers.

For the period of 1890 to 2022, the mean (median) annual end-of-system volume for the Leichhardt River catchment is 1721 GL (804 GL). For the Gregory–Nicholson catchment, the mean (median) annual end-of-system volume was 2448 GL (1159 GL). Across all catchments in the Assessment area, the mean (median) annual end-of-system volume was estimated to be 7360 GL (3816 GL) (Gibbs et al., 2024a).

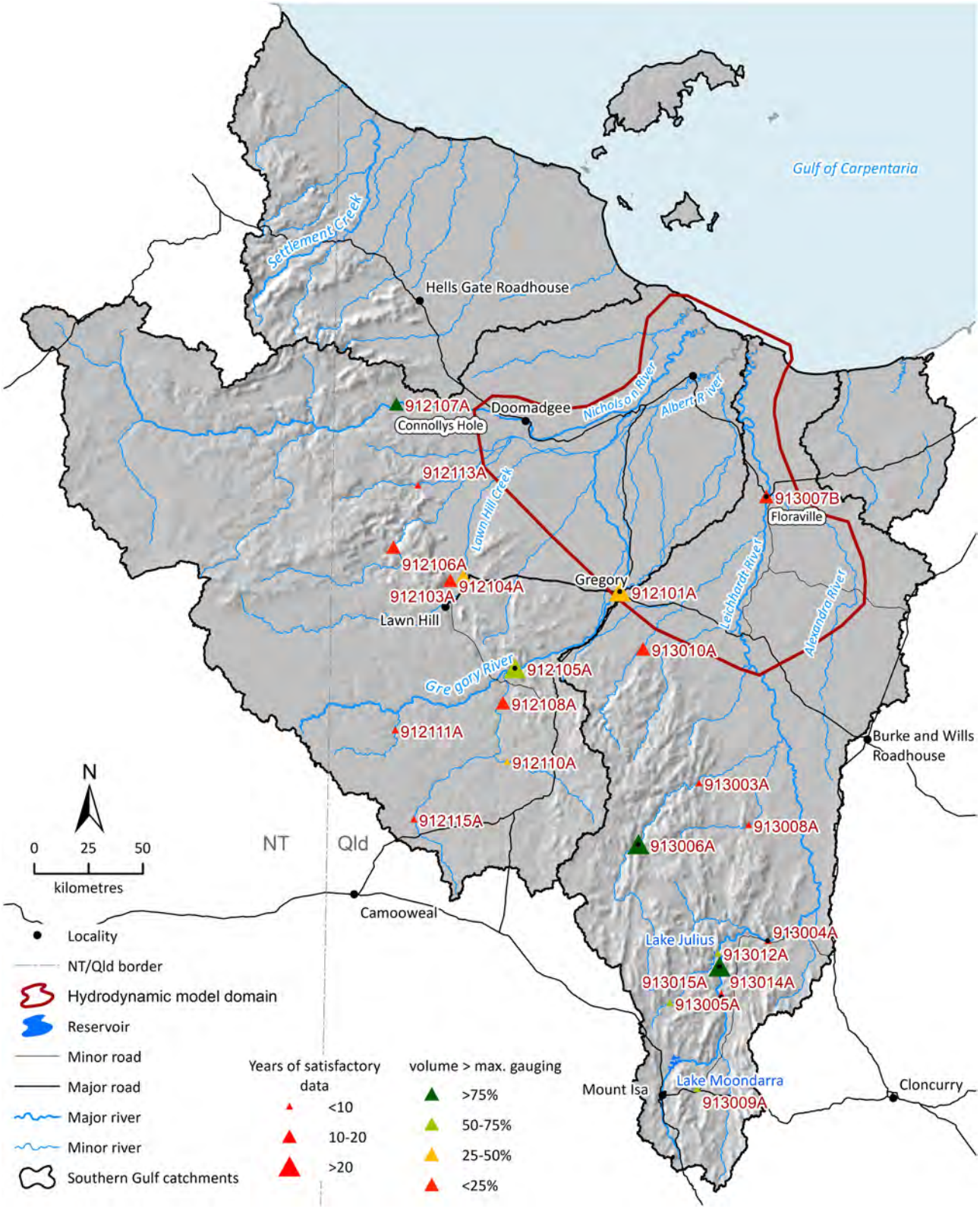

Figure 4-3 Location of streamflow gauges in the Southern Gulf catchments

Colours indicate the proportion of the total estimated volume that occurred below the maximum gauging at the site, with the size of the symbol indicating the number of years with satisfactory data (defined as having a good- or fair-quality code). Sites that are currently open are indicated by a black dot inside the triangle

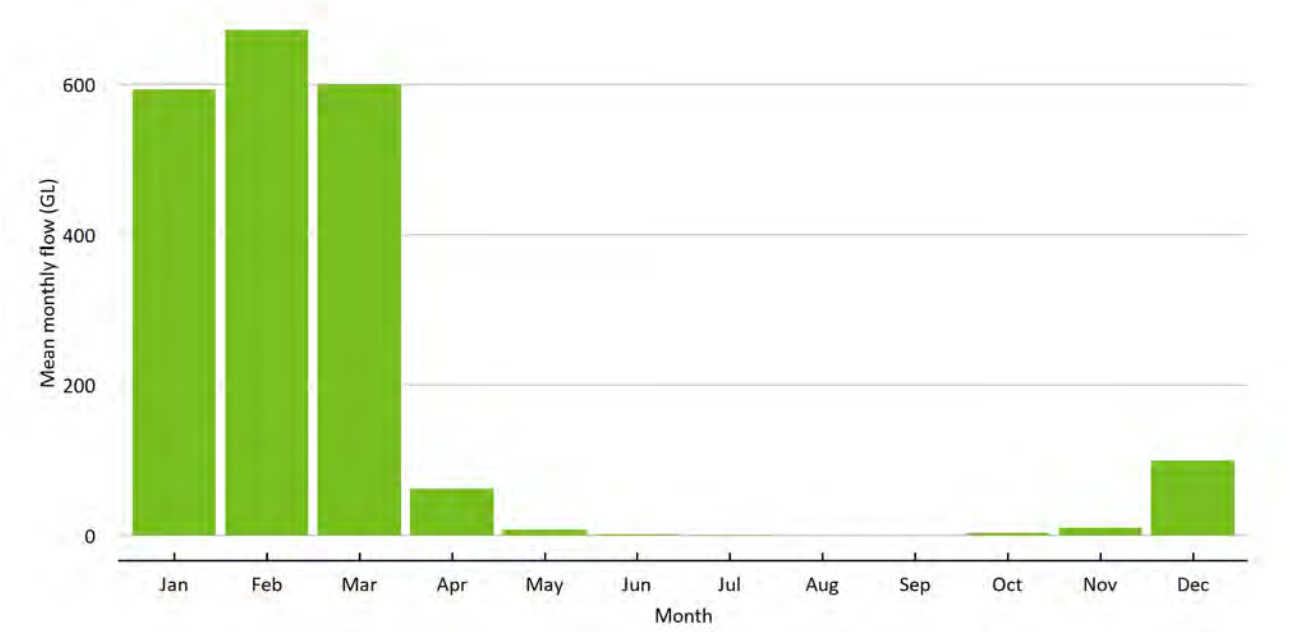

Figure 4-4 Monthly flow distribution at Floraville on the Leichhardt River, based on the observed flow data for 1984 to 2023

4.1.4 FLOODING

Intense seasonal rains from monsoonal bursts and tropical cyclones in the period of November to March create flooding in parts of the Southern Gulf catchments and inundate large areas of floodplains, mostly in the downstream reaches between the Nicholson, Gregory and Leichhardt rivers. The floodplains along the Alexandra and Albert rivers are also heavily flooded (Figure 2-1). Flooding is common in the Burketown area, which is located on a remnant of the main channel of the Albert River and represents the most eastward extent of a very flat ridgeline that provides the highest ground (~5 m above sea level) on the western bank of the river. Burketown is susceptible to flooding from the Albert River floodplain, as well as from overland flow paths within the town area. Flooding of the Albert River could also occur from floodwater breakout from the Nicholson or Gregory rivers. Rivers in the Southern Gulf catchments are unregulated, and their overbank flow is generally governed by the topography of the floodplain. Characterising these flood events is important for a number of reasons. Flooding can be catastrophic to agricultural production in terms of loss of stock, fodder and topsoil, and damage to crops and infrastructure. In addition, it can isolate properties and disrupt vehicle traffic providing goods and services to people in the catchment. However, flood events also provide the opportunity for offstream wetlands to be connected to the main river channel. The high biodiversity found in many unregulated floodplain systems in northern Australia is thought to largely depend on seasonal flood pulses, which allow for biophysical exchanges to occur between rivers and offstream wetlands.

Flooding is widespread in parts of Lawn Hill Creek and the Gregory, Leichhardt and Albert rivers near Burketown. In the last 40 years (1984 to 2023), there have been 41 floods ranging from small to large in the catchments. This was based on an overbank threshold of 709 m^3/second, which was estimated by obtaining daily streamflow at Floraville on the Leichhardt River (913007) and comparing it against floodplain inundation on the available satellite imagery. For flood events with an AEP of 1 in 2, 1 in 5 and 1 in 10, the peak discharge at the Floraville gauging station on the

Leichhardt River was 1220, 3350 and 7140 m^3/second, respectively. Figure 4-5 shows the annual maximum daily discharge at Floraville for 1953 to 2023. While floods can occur in any month from October to May, approximately 90% of historical floods have occurred between December and March, with the maximum in January (33.3%) (Figure 4-6). Of the ten largest flood peak discharge rates at Floraville, four events occurred during January, four in March, one in February and one in December. Flood peaks typically take about 2 days to travel from Gregory to Burketown, with a mean speed of 3.2 km/hour.

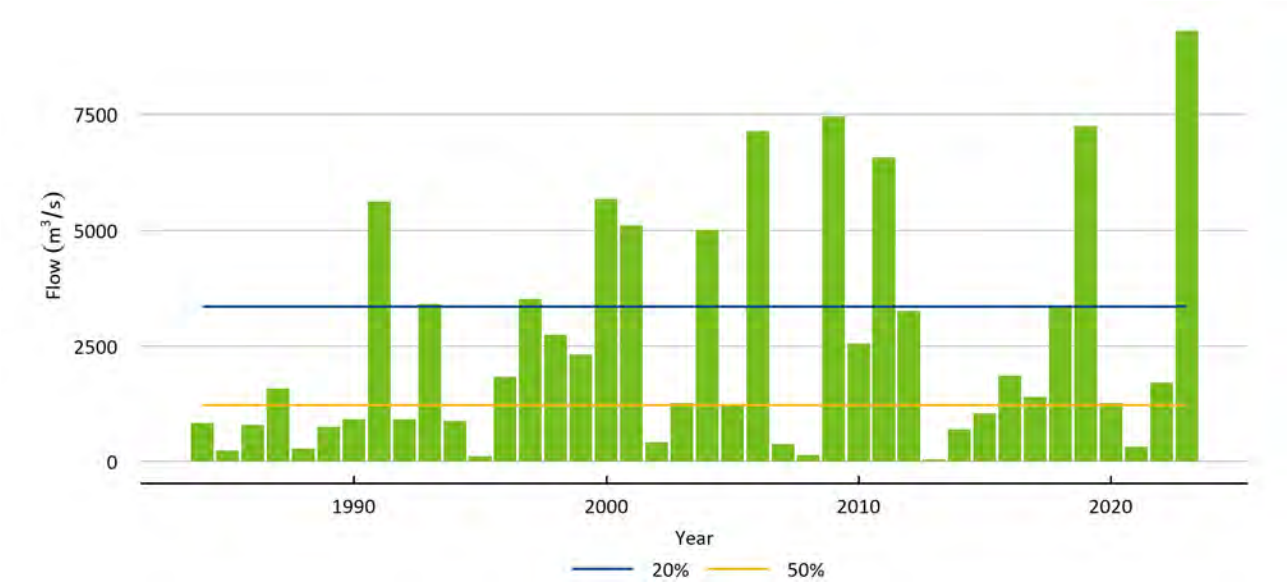

Figure 4-5 Annual maximum daily discharge at Floraville on the Leichhardt River, based on the observed flow data for 1984 to 2023

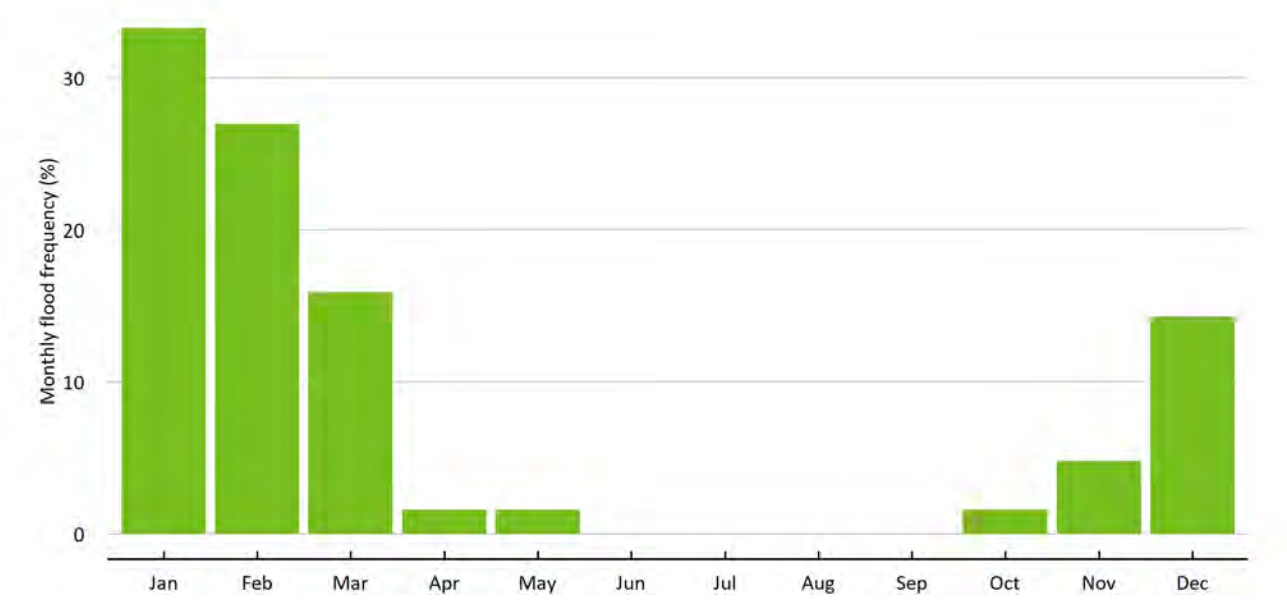

Figure 4-6 Monthly flood frequency in the Southern Gulf catchments (floods defined as an AEP of ≥1 in 1, based on flow data for 1984 to 2023) at Floraville on the Leichhardt River

4.2 Model configuration

The hydrodynamic model was configured for the proportion of the Southern Gulf catchments encompassing the floodplains of the major rivers and the tidal flats at the mouth of the Nicholson, Albert and Leichhardt rivers and Gin Arm Creek (Figure 4-7). The modelling domain included areas downstream of Doomadgee on the Nicholson River, Gregory on the Gregory River and Lorraine on the Leichhardt River, encompassing an area of 17,130 km^2. The model domain included six inflow boundaries across the river network and one water-level boundary off the coast (Figure 4-7). The model domain included 45 subcatchment outlets, incorporating local runoff, as described in Section 4.3.4.

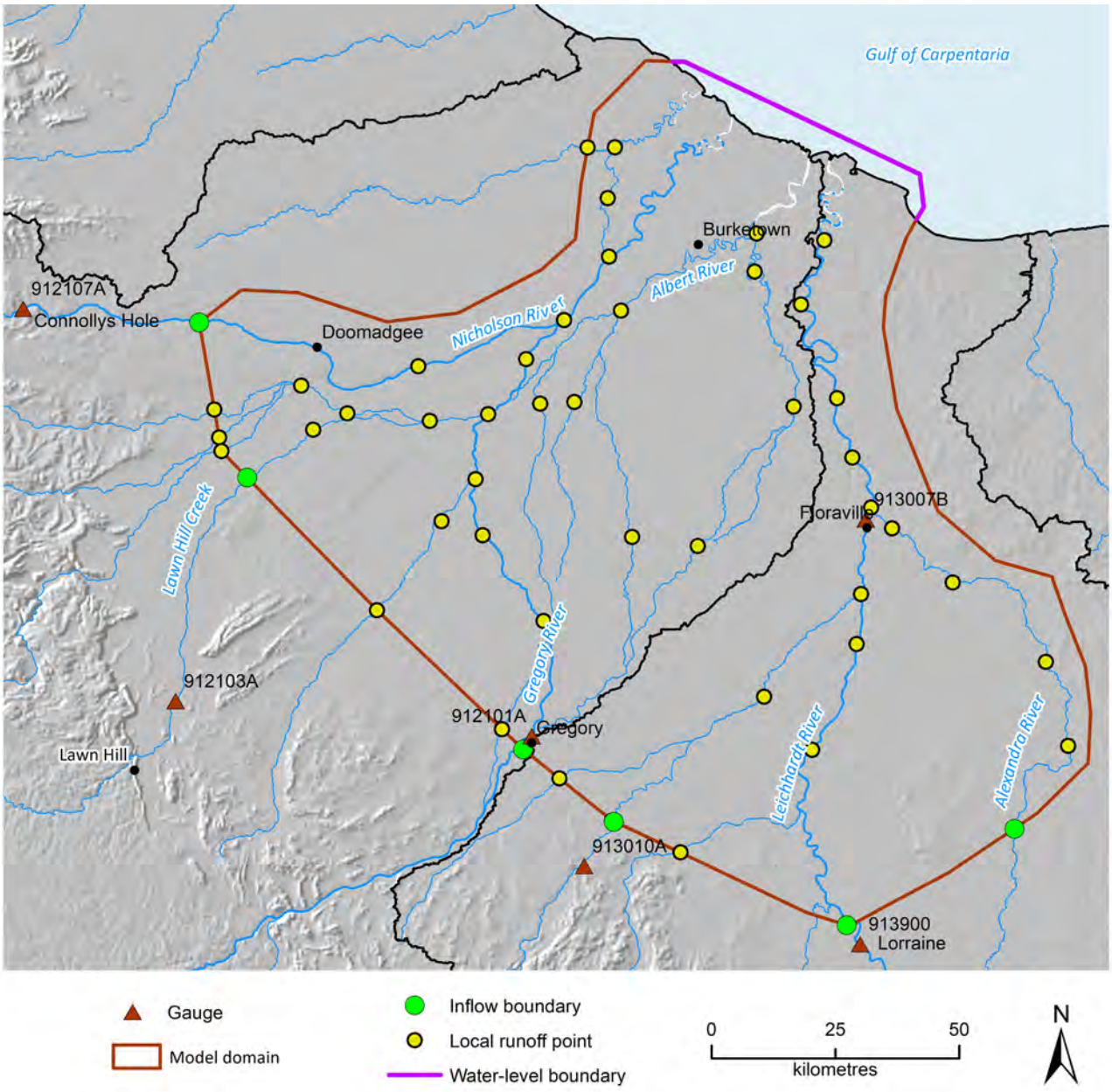

Figure 4-7 Hydrodynamic model configuration of the Southern Gulf catchments, showing the river network, model boundaries, and local runoff points in the model domain

4.3 Model input

4.3.1 TOPOGRAPHY

Land surface topography data are essential for flood inundation modelling, in addition to hydro-meteorological inputs (Sanders, 2007). The vertical accuracy of these data is critical, since the inundation depths and extents simulated by hydrodynamic models are highly sensitive to vertical errors of topographic data, especially on low-gradient floodplains (Horritt and Bates, 2002).

A digital elevation model (DEM) was produced for the Southern Gulf catchments MIKE 21 FM model domain based on a LiDAR 5-m DEM (±0.3 m horizontal and ±0.1 m vertical accuracy) patched with a 30 m Forest And Buildings removed Copernicus) digital elevation model (FABDEM). The highest resolution publicly available topographic information that encompasses the whole of the Southern Gulf catchments is based on a 1-second (i.e. ~30 m) Shuttle Radar Topography Mission (SRTM) DEM (Gallant et al., 2011) and a 1-second FABDEM (Hawker et al., 2022). These two global DEMs were compared, and FAB DEM was chosen due to its superior vertical accuracy in the Assessment area (Meadows et al., 2024). The FABDEM was used for the hydrodynamic modelling domain to cover areas for which LiDAR data were not available. The final combined DEM was created by resampling the FABDEM to 5 m (to match the original LiDAR resolution) and merging it with the LiDAR data using methods described by Gallant (2019). The Gallant method attenuates the difference between the resampled coarse DEM and the LiDAR data at the interface to zero over a distance beyond the LiDAR extent. The LiDAR elevations remain intact, while the coarse DEM elevations are modified by the attenuated difference, resulting in a ‘seamless’ combination while retaining hydrological connectivity. The final product of the Southern Gulf DEM is a 5 m–grid raster file of size 7 GB.

The LiDAR data covers the major proportion of the Gregory and Albert rivers and only a small proportion of the Nicholson River (Figure 4-8). The hydrodynamic modelling domain encompasses an area of 17,130 km^2, and the area covered by LiDAR is 7490 km^2 (i.e. ~43.7% of the model domain).

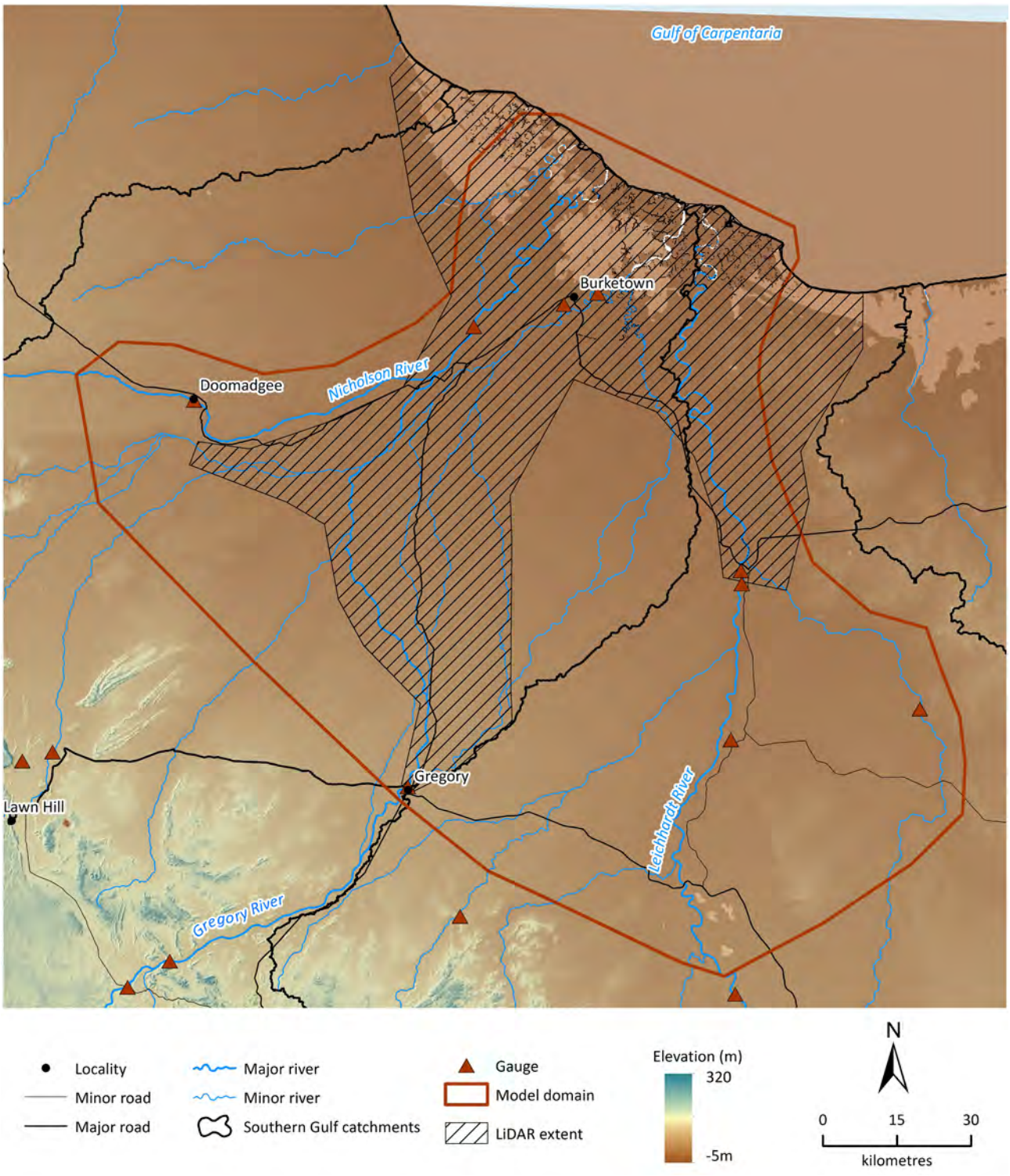

Figure 4-8 LiDAR data coverage in the hydrodynamic model domain of the Southern Gulf catchments

4.3.2 SURFACE ROUGHNESS

The hydraulic roughness coefficients of the land surface were derived from DEA Land Cover, which is a collection of annual land-cover maps for Australia for the period 1988 to 2020 (Owers et al., 2021) in which Australia's landscapes are classified into six basic land-cover categories (Table 4-1). The categories were represented in the model by Manning's roughness coefficient (*n*), as estimated in the published literature (Arcement and Schneider, 1989; Chow, 1959; LWA, 2009) (Table 4-1), and a roughness map was produced.

Table 4-1 Manning's roughness coefficient (*n*) for various types of land cover occurring in the Southern Gulf catchments

LAND-COVER TYPE	MANNING'S *n* ($s/m^{1/3}$) RECOMMENDED RANGE	MANNING'S *n* ($s/m^{1/3}$) CALIBRATED
Artificial surface	0.035–0.050	0.04
Cultivated terrestrial vegetation	0.035–0.060	0.04
Natural bare surface	0.03–0.035	0.03
Natural aquatic vegetation	0.04–0.060	0.05
Natural terrestrial vegetation	0.04–0.080	0.06
Open water	0.03–0.033	0.03

4.3.3 INFLOW AND OUTFLOW BOUNDARY CONDITIONS

The hydrodynamic model consisted of four inflow boundaries, but gauge data were available for only one boundary (i.e. Gregory River at Gregory). The upstream river boundary conditions of the hydrodynamic models were obtained from the Australian Water Resource Assessment – River model (AWRA-R) simulations (see the companion technical report on river model calibration for the Southern Gulf catchments, Gibbs et al., 2024a). The river model discharge gauge nodes used in the hydrodynamic models are shown in Table 4-2. In addition to these, the tidal sea-level data was used for the downstream water-level boundary. The Karumba station was used, which is the closest to the Southern Gulf catchments. The remaining inflows to the boundary of the hydrodynamic model domain that were not captured by the river model were simulated using the Sacramento rainfall-runoff model based on the residual reach parameters from the AWRA-R calibrations (Gibbs et al., 2024b).

Table 4-2 List of stream gauges that were used for the Southern Gulf hydrodynamic model configuration and calibration

STATION ID	STATION NAME	CATCHMENT AREA (km^2)	GAUGE RECORD	YEARS OF GOOD-QUALITY DATA	GAUGE STATUS	DATA USED FOR
912101A	Gregory River at Gregory	12,567	1969–2023	54	Open	Inflow boundary
912103A	Lawn Hill Creek at Lawn Hill No. 2	4,003	1919–1988	69	Closed	Inflow boundary
912107A	Nicholson River at Connolly's Hole	13,875	1968–1988	20	Closed	Inflow boundary
913007B	Leichhardt River at Floraville Homestead	23,679	1984–2023	39	Open	Calibration
913010A	Fiery Creek at 16 Mile Waterhole	721	1972–2019	47	Closed	Inflow boundary

4.3.4 LOCALLY GENERATED STREAMFLOW

The hydrodynamic model domain was subdivided into 53 subcatchments based on the topography and stream network (Figure 4-7). The Sacramento-based gridded runoff was averaged for each subcatchment by assigning Scientific Information for Land Owners (SILO) cells to the subcatchments in accordance with the intersecting cells. Streamflow at the outlet (also called the 'pour point') of each subcatchment was calculated by multiplying the runoff by the subcatchment area. This locally generated runoff was added into the hydrodynamic model as a point source of water in the system. Subcatchment boundaries and pour points were generated using ArcGIS tools. The locations of some pour points were manually changed to ensure all subcatchments delivered the local flow directly into a river or creek (Figure 4-7).

4.4 Flood frequency and selected events for model calibration

The magnitudes of flood events in the Southern Gulf catchments were calculated based on the observed flow data at Floraville on the Leichhardt River (913007) using a flood frequency analysis. A flood event was defined as the occurrence of overbank flows that could be identified through satellite imagery. Based on these observations, a threshold flow rate of 709 m^3/second was used to identify the overbank flow as the starting point for flood events. If the flow rate dropped below the overbank flow threshold for five consecutive days, the event was considered to have ended. To determine the number of times each event was exceeded events with higher peak discharge and larger total event volume were counted.

Flood frequency analysis (FFA) was performed in the Southern Gulf catchments to establish streamflow thresholds above which a flood event would occur. Flood frequency was estimated for the three major rivers, the Nicholson River at Connolly's Hole (912107), the Gregory River at Riversleigh (912105) and the Leichhardt River at Floraville (913007). Traditionally, flood frequencies are estimated based on maximum discharge for an individual event. However, in this Assessment, to help determine the true magnitude of the events, the FFA took into account both the total flow volume and the peak discharge for each event. This was motivated by the knowledge that not only the maximum discharge but also the duration of an event can have a great impact on the inundated area. Figure 4-9 displays the relationship between peak flow and AEP for the three gauges, one on the Nicholson River, one on the Gregory River and the other on the Leichhardt River. However, the Leichhardt River gauge at Floraville is the only gauge within the hydrodynamic model domain that has 30 years or more of observed data.

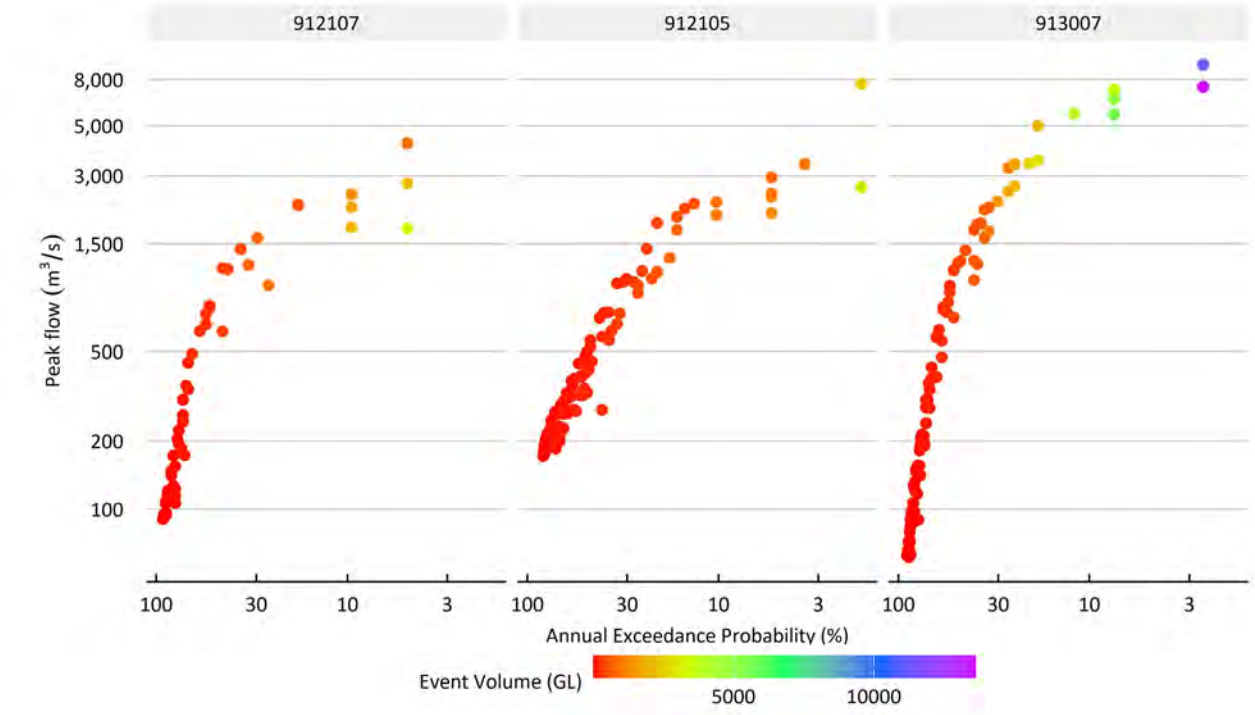

Figure 4-9 Peak flood discharge and annual exceedance probability at gauge: (a) 912107 (Nicholson River at Connolly's Hole, (b) 912105 (Gregory River at Riversleigh) and (c) 913007 (Leichhardt River on Floraville)

Flood events were selected for the model calibration based on the availability of cloud-free Landsat satellite imagery, while ensuring the magnitude of the flood events spanned the AEPs of interest to ecologists and the land suitability analysis. Five events were chosen, with flood magnitudes ranging from an AEP of 1 in 2 to 1 in 38, based on the flow data at Floraville on the Leichhardt River (Table 4-3). The requirement for a large number of simulations involving all combinations of scenarios and calibration events necessitated the use of only two flood events (in 2016 and 2023) for scenario modelling.

Table 4-3 Flood events used for calibration

EVENT PERIOD	DURATION (DAYS)	PEAK DATE	PEAK FLOW (m^3/s)	EXCEEDANCE PROBABILITY (YEARS)	PURPOSE
8/01/2005 – 18/01/2005	10	9/01/2005	1231	1 in 2	Calibration
29/12/2015 – 10/01/2016	12	2/01/2016	1853	1 in 3	Calibration, scenario modelling
4/3/2018 – 21/03/2018	17	12/03/2018	3382	1 in 5	Calibration
2/02/2019 – 20/02/2019	18	8/02/2019	7255	1 in 10	Calibration
15/02/2023 – 1/04/2023	45	12/03/2023	9320	1 in 38	Calibration, scenario modelling

4.5 Hydrodynamic model simulation and outputs

The simulations for hydrodynamic models in the calibration and scenario modelling were undertaken with a 1-second time step to satisfy the numerical stability criteria for the biggest flood event in the analysis. Each event was simulated for 30 days (longer than the flood durations) irrespective of the time of flood recession, to ensure the entire rising and falling limbs were included in the simulation. The models were run using GPU machines consisting of 16 CPU cores and 3 GPU cards (each with 4 P100 Nvidia GPUs). For each run, it took about 2 days of computer time to simulate a 30-day flood event. At the hydrodynamic model boundaries, daily discharges were specified in all inflow boundaries, and hourly tide levels were specified at the seaside boundary. The model used an inbuilt interpolation technique to derive flow variables at each computational time step. The model outputs included the water surface elevation, depth and velocity for each mesh element. While the model has the option of producing output at any time interval, all outputs in this analysis were recorded at 6-hour time intervals. A separate model was configured and simulated for each flood event.

Total water depths and water velocities were obtained from each model run and converted to three-column XYZ format American Standard Code for Information Interchange (ASCII) data. In the post-processing, two-dimensional triangular flexible-mesh data were converted to 5 m $\times$ 5 m gridded data via an inverse distance weighted interpolation algorithm.

4.6 Hydrodynamic model calibration

The calibration process was constrained by the excessive time required by the hydrodynamic model simulation, which limited the number of iterations possible for tuning. However, the simulations were checked to ensure correct activation of the anabranches and connectivity to the various floodplain water bodies. The duration of the floodplain inundation was tuned by adjusting the surface roughness coefficient and the infiltration rates to ensure inundation patterns were consistent with the satellite imagery. In addition to evaluations against the satellite imagery, simulated stage height outputs were compared with observed stage heights at the Floraville gauging station on the Leichhardt River (913007), which is the only gauge with recent data records in the hydrodynamic model domain.

The evaluation of hydrodynamic modelled inundation extent was performed using available and suitable Landsat and MODIS inundation maps for the selected flood events (including at least one image for each flood event). To evaluate the performance of the hydrodynamic model using the remotely sensed flood extent observations, two evaluation methods were employed:

- A visual comparison of the spatial inundation areas indicated by the satellite image and the model simulation was undertaken to assess how the main inundation patterns were represented by the hydrodynamic model.
- A quantitative assessment of the spatial inundation metrics (whether the model correctly simulated inundated pixels or not) was undertaken to assess how well the hydrodynamic model captured the overall inundation extent.

Both evaluation methods were performed by resampling of the remotely sensed inundation maps (Landsat 30 m and MODIS 500 m) at 5 m–grid pixel horizontal resolution, to be consistent with the

hydrodynamic model gridded output. The satellite inundation maps were masked so as to only include the modelled area within the hydrodynamic model domain.

In many cases, satellite-derived inundation maps (even for a sensor like MODIS, with a twice-daily satellite overpass frequency) will only capture portions of the hydrodynamic model domain due to the persistent cloud cover that can occur during flood events. Thus, only pixels in the satellite images showing 'inundated' or 'non-inundated' were considered; this meant that all 'cloudy' or 'no data' pixels were removed from the analysis.

4.6.1 CATEGORICAL STATISTICS

Detection metrics were computed for each adjusted hydrodynamic model domain and for each grid cell. Every satellite inundation map and modelled inundation extent was classified as a hit (H, observed inundation by the satellite correctly detected by the model), miss (M, observed inundation not detected by the model), or false alarm (F, inundation detected by the model but none observed by the satellite) using a contingency table, following Ebert et al. (2007) (Figure 4-10).

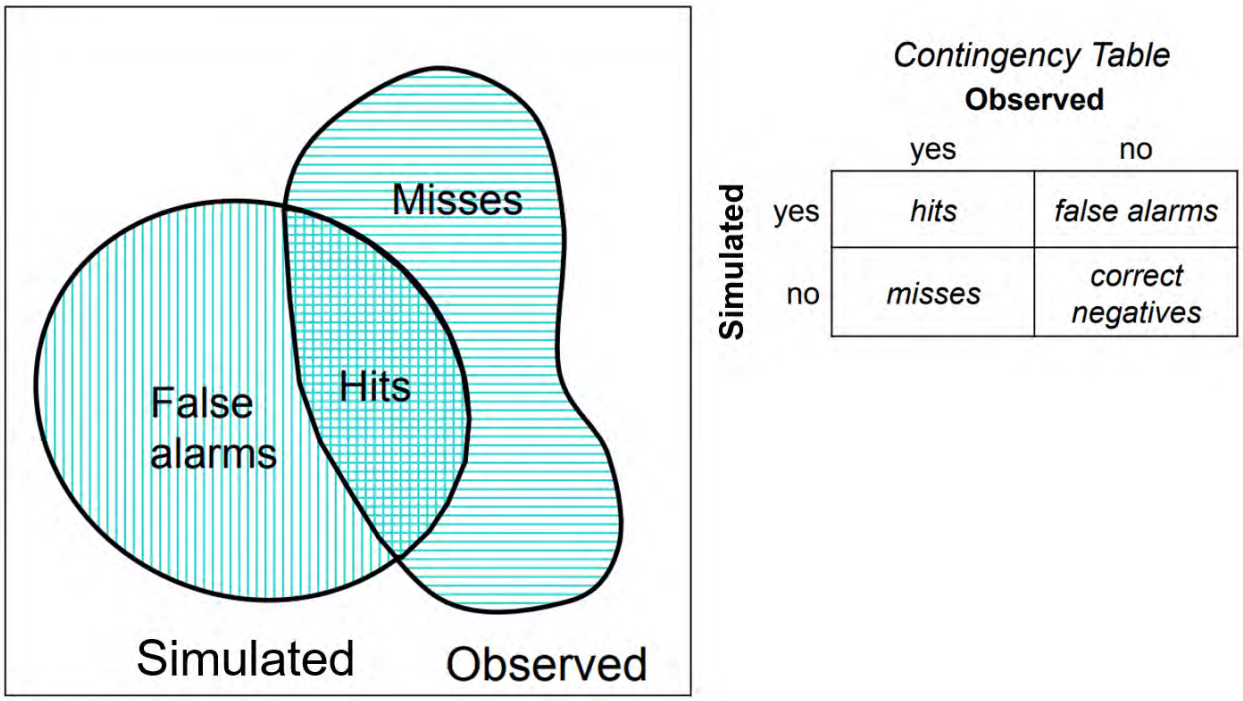

Figure 4-10 Classification at the grid cell level using a contingency table

The following statistics were computed from the contingency table (see Collaboration for Australian Weather and Climate Research (CAWCR)):

- The Probability Of Detection, POD = H/(H + M), gives the fraction of inundated pixels correctly detected (range 0 to 1, 1 indicating a perfect score). It is sensitive to hits, but ignores false alarms, and it should be used in conjunction with the False Alarm Ratio (FAR; see next bullet point).
- FAR = F/(H + F), gives the fraction of wrongly detected inundated pixels (range 0 to 1, 0 indicating a perfect score). It is sensitive to false alarms, but ignores misses.

- The Frequency Bias, FB = (H + F)/(H + M), gives the ratio of the simulated to observed inundated pixels frequency (range 0 to ∞, 1 indicating a perfect score). It measures the ratio of the frequency of modelled inundated pixels to the frequency of the satellite imagery inundated pixels, and it indicates whether the hydrodynamic model has tended to underestimate (FB < 1) or overestimate (FB > 1) events. It does not measure how well the modelled inundation extent corresponds to the satellite inundation extents, as it only measures relative frequencies.
- The equitable threat score (ETS), used as an overall performance metric, gives the fraction of the inundated pixels that were correctly detected, adjusted for correct detections (He) that would be expected due to random chance: ETS = (H – He)/(H + M + F – He), where He = (H + M)(H + F)/N and N = the total number of estimates (range –1/3 to 1, 1 indicating a perfect score and 0 indicating no skill). It is sensitive to hits. Because it penalises both misses and false alarms in the same way, it does not distinguish the sources of error.

Although the detection statistics described above are well constrained, there are issues to consider in the interpretation of the results, such as:

- Satellite inundation images may show inundated areas that remain in the landscape as ponded areas in between flood events, because of the gentle topography and the low infiltration rates.
- The results of the cell to cell comparison between the hydrodynamic model output and the satellite imagery will be inherently poor where the satellite images (from MODIS in particular) are of a lower spatial resolution than the river channel widths, the river morphology and the resulting inundation dynamics.

The two approaches mentioned above (visual comparison and detection statistics) complement each other – visual comparisons, although labour-intensive and subjective, highlight the sources or nature of the errors and provide diagnostic information regarding necessary changes to the inputs or hydrodynamic model set-up. On the other hand, statistical metrics provide an objective and comparable metric for assessing overall model performance. The calibration is considered successful if the two approaches assess the performance of the model output as reasonable (in terms of overall inundation patterns captured and detection statistics).

4.7 Results and discussion

4.7.1 STAGE HEIGHT

Figure 4-11 shows a typical comparison between simulated and observed stage heights for the various flood events at Floraville on the Leichhardt River (913007B). In general, the simulated flood peaks match well with the observed data, except for the 2005 flood event, for which the model overpredicted stage height. While a good match was obtained for the flood peak, there were differences in stage heights for the rising and falling limbs of the flood hydrograph. Also, there were differences in the timing of the flood peak. For most of the events, the simulated stage heights for the receding floods were smaller than the observed heights. In addition, the hydrodynamic model failed to simulate stage heights between the two peaks correctly for flood events with two or more peaks (e.g. 2018 flood).

The possible reasons for the discrepancies between simulated and observed stage heights include: (i) coarse topography data for the major proportion of the Leichhardt River, (ii) lack of good-

quality bathymetry data, (iii) lack of observed river flow data, and (iv) poor representation of some river channels. In addition, there are uncertainties in the river model–simulated inflows to the hydrodynamic model domain.

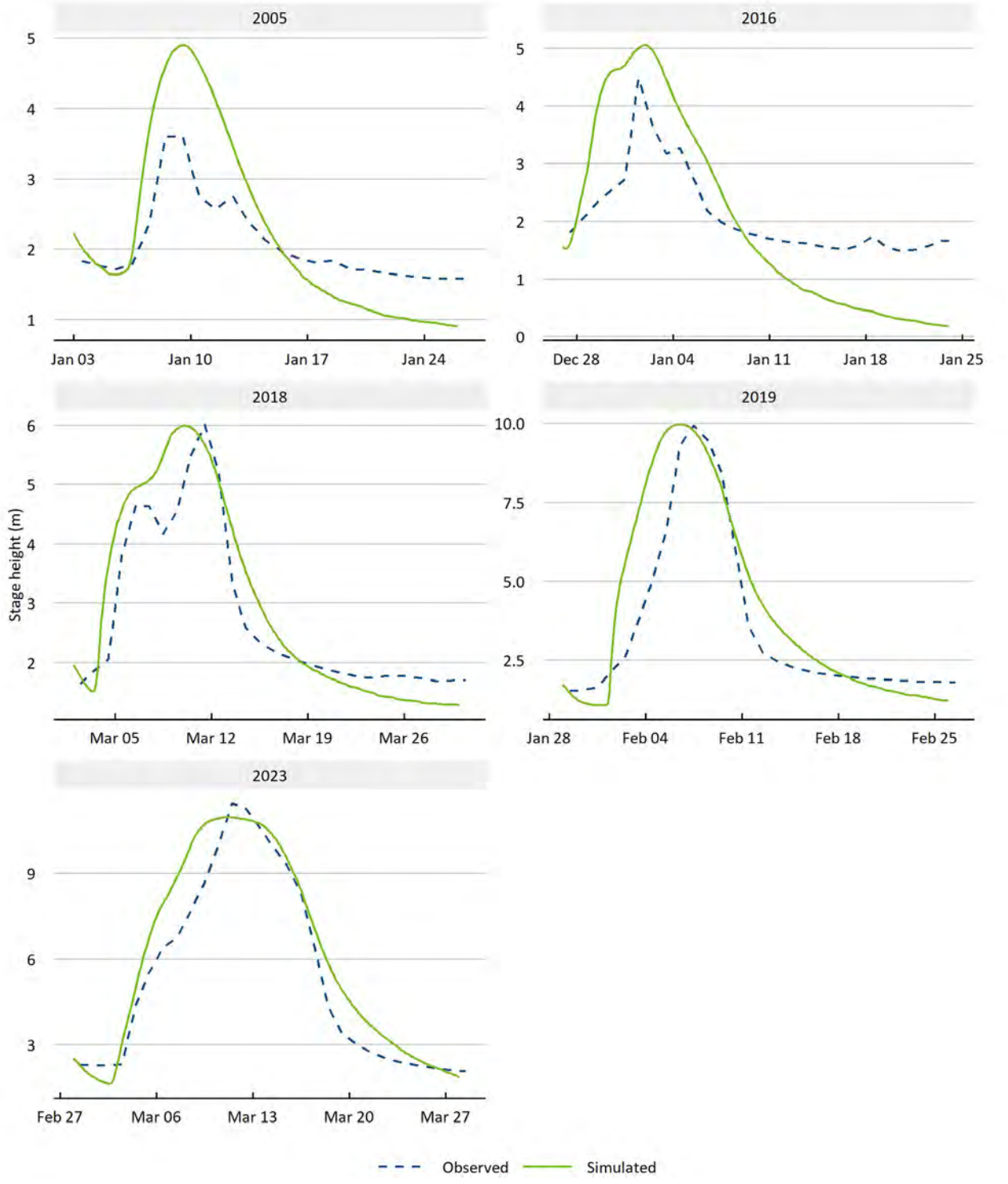

Figure 4-11 Comparison of the model-simulated stage height and the observed stage height at Floraville (913007B) on the Leichhardt River in the Southern Gulf catchments

4.7.2 SATELLITE-BASED FLOOD MAPS

The available Landsat, MODIS and Sentinel images were processed for the Southern Gulf hydrodynamic model domain for the calibration periods (Table 4-4). The availability of images and the proportion of cloud/null effects were reported. Due to the large number of MODIS images, only those images containing 80% or less clouds/nulls were processed to obtain inundation maps. Also, to exclude images with little or no flooding, only images with 5% or more observed inundated area were used for comparison with the hydrodynamic model results.

Table 4-4 Flood event dates and number of satellite images (Landsat, MODIS and Sentinel) processed for the Southern Gulf catchments hydrodynamic model calibration

START DATE	END DATE	FLOOD MAGNITUDE	NUMBER OF LANDSAT IMAGES	NUMBER OF SENTINEL -1 IMAGES	NUMBER OF SENTINEL-2 IMAGES	NUMBER OF MODIS IMAGES
8/01/2005	18/01/2005	1 in 2 AEP	3	0	0	4
29/12/2015	10/01/2016	1 in 3 AEP	3	0	1	9
4/03/2018	21/03/2018	1 in 5 AEP	2	1	7	11
2/02/2019	20/02/2019	1 in 10 AEP	4	1	8	15
15/02/2023	1/04/2023	1 in 38 AEP	9	12	8	22

AEP = annual exceedance probability

4.7.3 INUNDATION EXTENT

The results of the hydrodynamic model simulation of inundation across the Southern Gulf catchments were compared with satellite inundation maps through a direct visual comparison and detection metrics. In the first instance, images that passed the first cloud cover filtering were further scrutinised to identify flood patterns that could be used to inform the calibration of the hydrodynamic modelling. The images within the modelling simulation period (see Table 4-4) that showed limited inundation, or images with large cloud cover over the inundated areas, were omitted from further analysis. Generally, at least one image was retained for each flood event to assist in the calibration. Figure 4-12 shows an example of Landsat, MODIS and Sentinel inundation maps with corresponding hydrodynamic model inundation maps for the same date.

Table 4-5 presents the detection statistics for selected images considered in the analysis, including images from all five flood events (see Table 4-4 for the flood events). The POD, which gives the fraction of inundated pixels correctly detected, varies within a range of 0.08 to 0.56 (range 0 to 1, 1 indicating a perfect score), with a mean of 0.28. The FAR, which gives the fraction of wrongly detected inundated pixels, varied within a range of 0.33 to 0.96 (range 0 to 1, 0 indicating a perfect score), with a mean of 0.67. This indicates over estimation of the inundation area by the model compared with the satellite imagery. The ETS varied within the range of 0.03 to 0.39 (1 indicating a perfect score and 0 indicating no skill), with a mean of 0.14. This indicates poor overall matching between the simulated and the observed inundation. In general, the simulated inundation was greater than that identified in the satellite images for all flood events (FB > 1). The FB varied within a range of 0.14 to 4.24 (range 0 to ∞, 1 indicating a perfect score), with a mean of 1.42, that there was generally overprediction of inundation by the model, although there was some underestimation as well.

Locations of poor fit generally coincided with complex anabranching networks. Closer inspection of the satellite imagery for these locations revealed that they often did not display flooding of these anabranches. The inability of MODIS to capture inundation in narrow floodplains has been reported for the Fitzroy catchment in WA (Karim et al., 2011) and for other catchments in northern Australia (Ticehurst et al., 2013). Furthermore, MODIS regularly falsely identifies cloud shadow as inundation, which is particularly an issue when using imagery with high (up to 80%) cloud cover.

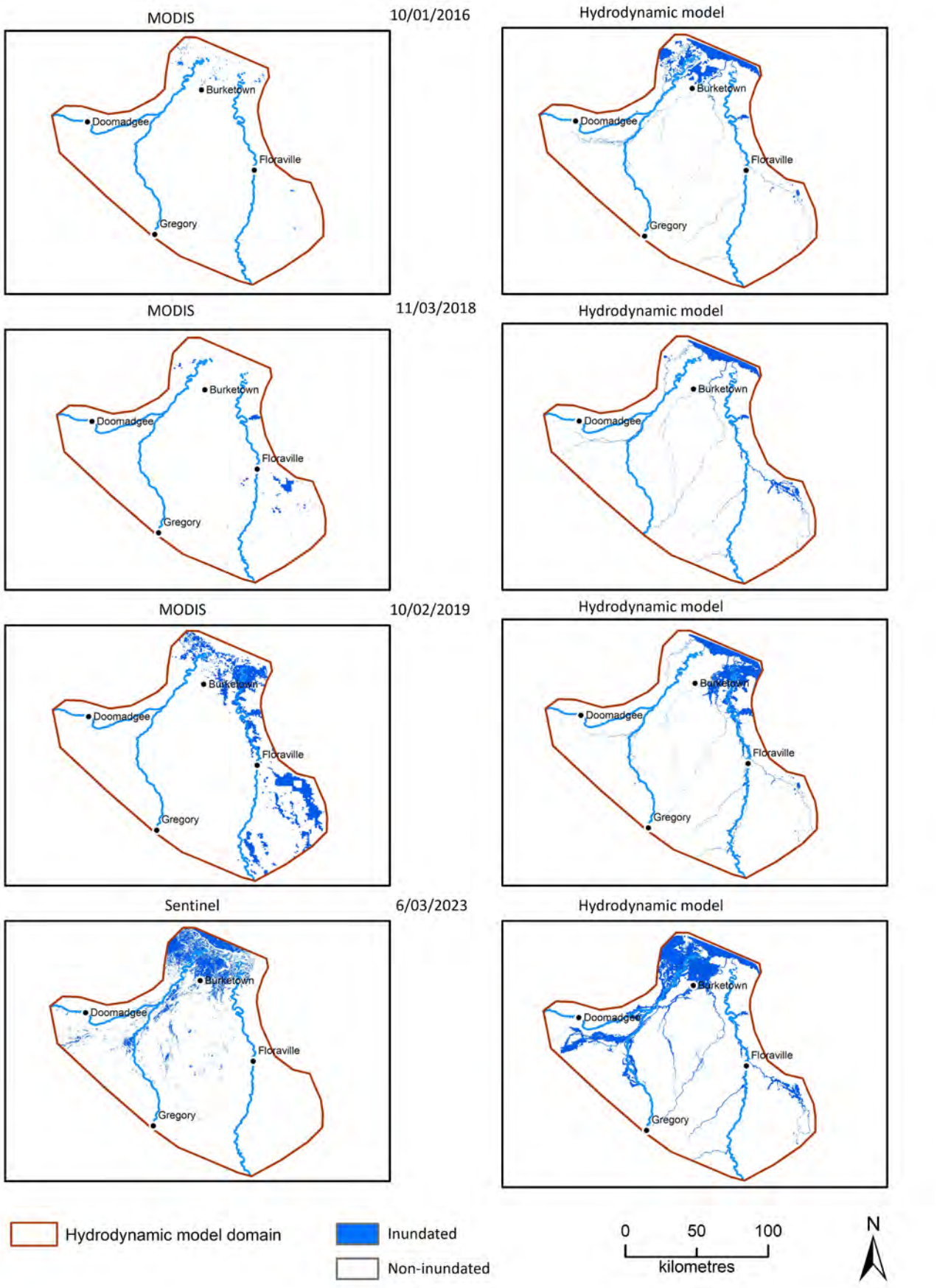

Figure 4-12 Comparison of (MODIS and Sentinel) satellite–based inundation maps with hydrodynamic model results for the Southern Gulf catchments

Table 4-5 Detection statistics for the Landsat, MODIS and Sentinel images considered in the analysis for the Southern Gulf hydrodynamic model calibration

Percentage available refers to pixels other than cloud/null (including inundated and non-inundated pixels) within the hydrodynamic model domain. ETS stands for Equivalent Threat Score (a measure of overall performance), POD for the Probability Of Detection, FAR for the False Alarm Ratio and FB for Frequency Bias.

SATELLITE	DATE	% AVAILABLE	ETS	POD	FAR	FB
MODIS	9/01/2016	84	0.07	0.32	0.91	3.61
MODIS	10/01/2016	26	0.06	0.32	0.92	4.24
MODIS	11/03/2018	9	0.25	0.34	0.47	0.65
MODIS	12/03/2018	64	0.05	0.08	0.74	0.32
MODIS	13/03/2018	91	0.06	0.11	0.84	0.73
MODIS	16/03/2018	90	0.06	0.12	0.86	0.84
MODIS	18/03/2018	88	0.03	0.11	0.96	2.57
MODIS	9/02/2019	60	0.14	0.18	0.49	0.36
MODIS	10/02/2019	87	0.21	0.31	0.49	0.60
MODIS	11/02/2019	92	0.16	0.22	0.50	0.44
Landsat	14/02/2019	56	0.07	0.12	0.34	0.17
MODIS	15/02/2019	92	0.08	0.17	0.85	1.16
MODIS	16/02/2019	80	0.05	0.15	0.91	1.71
MODIS	19/02/2019	50	0.04	0.13	0.91	1.38
Sentinel-1	1/03/2023	54	0.06	0.08	0.38	0.14
Sentinel-1	6/03/2023	62	0.25	0.54	0.60	1.34
MODIS	14/03/2023	52	0.39	0.56	0.33	0.84
MODIS	15/03/2023	59	0.29	0.49	0.52	1.03
MODIS	16/03/2023	91	0.27	0.40	0.44	0.72
MODIS	19/03/2023	19	0.21	0.40	0.64	1.11
MODIS	25/03/2023	90	0.08	0.43	0.90	4.24
MODIS	26/03/2023	93	0.10	0.44	0.87	3.39
Landsat	28/03/2023	45	0.21	0.38	0.62	1.00

4.8 Summary

Intense seasonal rains from monsoonal bursts and tropical cyclones in the period of November to March create flooding in parts of the Southern Gulf catchments and inundate large areas of floodplains, mostly in the downstream reaches between the Nicholson, Gregory and Leichhardt rivers. The floodplains along the Alexandra River are also heavily flooded. During large events (e.g. 2023), flooding is widespread on both sides of the Albert River, including at Burketown. The Lawn Hill Creek and Gregory Rivers burst their banks, and the inundation area is large, especially at the junction. There are large tidal floods in between the Nicolson and the Albert rivers, as well as between the Albert and the Leichhardt rivers, where there is regular inundation by tides and a combination of tidal and river flow (Figure 2-1 and Figure 4-12).

Flood inundation maps were produced using Landsat, MODIS and Sentinel imagery. MODIS imagery of 500 m resolution at1-day intervals was acquired from November 2001 to March 2023 and processed using the OWL algorithm. Landsat imagery of 30 m resolution at 16-day intervals was acquired from 2001 to 2023 and processed using the NDWI algorithm. A total of 21 Landsat images, 61 MODIS images, 14 Sentinel-1 images and 24 Sentinel-2 images were selected for processing for the hydrodynamic model calibration. Event-based inundation maps were produced for individual floods, and composite flood maps were produced by combining all images. Cloud cover was a challenge when producing event-based inundation maps. Both Landsat and MODIS show inconsistencies in the spatial flood extent due to the limited number of cloud-free observations. In addition, the inability of MODIS to capture inundation in narrow floodplains has been reported for the Fitzroy catchment (Karim et al., 2011) and for other catchments in Australia (Ticehurst et al., 2013).

Inundations on the floodplains of the Gregory, Nicholson, Leichhardt and Albert rivers and their tributaries, covering an area of 17,130 km^2, were modelled for five flood events ranging from an AEP of 1 in 2 to an AEP of 1 in 38. Inundation is primarily driven by high flows down the Nicholson, Gregory and Leichhardt rivers and to a lesser extent down the Alexandra River and Lawn Hill Creek. Flooding is widespread in the downstream reaches of the major rivers near Burketown and at the junction of Gregory River and Lawn Hill Creek. Most rivers in the Southern Gulf catchments consist of a network of braided channels that produce large inundation during floods.

A two-dimensional hydrodynamic model (MIKE 21 FM) was used to simulate flood inundation. The model was calibrated for the 2005, 2016, 2018, 2019 and 2023 flood events using inundation maps derived from satellite imagery and gauged stage height data. The models were calibrated primarily by adjusting the roughness coefficient and the infiltration rate.

Compared with the Landsat and MODIS inundation maps, the hydrodynamic model captured the overall inundation patterns better along the main river channels and their tributaries. However, the detection statistics showed that the cell-to-cell matching of the model-generated data against the observed satellite data was overall poor, largely due to the inability of MODIS to detect inundation of narrow floodplains. The detection metrics suggest that there is overestimation of inundation area by the hydrodynamic model, especially during receding floods, as well as a general misalignment of inundation patterns. The locations of poor fit generally coincided with complex anabranching rivers. Closer inspection of the satellite imagery in these locations revealed that it often does not display flooding of these anabranches. The inability of MODIS to capture inundation in narrow floodplains has been reported for the Fitzroy catchment in WA (Karim et al., 2011) and for other catchments in northern Australia (Ticehurst et al., 2013). Furthermore, MODIS regularly falsely identifies cloud shadow as inundation, which is particularly an issue when using imagery with high (up to 80%) cloud cover. The hydrodynamic model has some limitations. However, lack of good-quality satellite images and gauged data, which restricts rigorous calibration of the model results. Moreover, there are uncertainties in the river model simulations for inflows to the hydrodynamic model domain.

5 Flood modelling under future climate and development scenarios

5.1 Introduction

Rising global air temperatures are likely to be accompanied by changes in the intensity and patterns of rainfall in Australia. The Australian Academy of Science released a report (Australian Academy of Science, 2021) stating that current emissions trajectories will likely result in Australia experiencing a 3 °C temperature increase by 2100. McJannet et al. (2023) found that GCMs indicated changes in rainfall across the Victoria, Roper and Southern Gulf catchments. These changes in rainfall are usually amplified in runoff. Consequently, increases in global temperatures may be accompanied by changes in the extent and patterns of flood inundation.

In addition, the development of the surface water resources for irrigated agriculture in the highly seasonal streamflow regime prevailing in the Southern Gulf catchments is likely to require some degree of storage and river regulation. Surface water storage options have been evaluated at several hypothetical dam locations in the Southern Gulf catchments (Yang et al., 2024). Flood waters stored during the wet season and their gradual release during the dry season will modify the timing and magnitude of floods and the subsequent inundation of floodplains. The impacts of water harvesting during high-flow events were also evaluated during the flood study.

To explore how flood characteristics may change under projected future climate and hypothetical development scenarios, a series of simulation experiments or scenarios were devised. Due to the long run times of the hydrodynamic model, it was only possible to explore a limited number of scenarios. Hence, scenarios were selected to enable general conclusions about likely impacts on floodplain inundation. A summary of the future climate and development scenarios undertaken in the Assessment area is presented in Table 5-1.

Table 5-1 Summary of selected future climate and development scenarios

ASSESSMENT AREA	SCENARIO NAME	FLOOD START DATE (DURATION OF SIMULATION IN DAYS)	EXCEEDANCE PROBABILITY (YEARS)
Southern Gulf catchments, Queensland	Scenario B Historical climate and hypothetical dam (Scenario B-Dam) and water harvesting (Scenario B- Water Harvesting)	25/12/2015 (30) 26/02/2023 (30)	1 in 3 1 in 38
	Scenario C Projected future dry climate (Cdry) and future wet climate (Cwet) with current levels of development	25/12/2015 (30) 26/02/2023 (30)	1 in 3 1 in 38
	Scenario D Projected future dry climate and hypothetical dam (Cdry-Dam) and future dry climate and water harvesting (Cdry- Water Harvesting)	25/12/2015 (30) 26/02/2023 (30)	1 in 3 1 in 38

5.2 Future climate scenarios

GCMs are an important tool for simulating global and regional climate. To assess the level of uncertainty in the range of future runoff projections, future climate projections from a large range of archived GCM simulations were downloaded from the Coupled Model Intercomparison Project 6 (CMIP6) website (https://pcmdi.llnl.gov/CMIP6/). Of the 92 available GCMs, 32 included the rainfall, temperature, solar radiation, and humidity data required for the Australian Water Resource Assessment Landscape model (AWRA-L) and AWRA-R hydrological modelling. The IPCC in its Sixth Assessment Report (AR6) presented five different climate scenarios based on a SSP for the future (IPCC, 2022). For the Assessment, SSP2-4.5 was used to investigate the sensitivity to changes in rainfall and PE of streamflow at approximately the year 2060 (McJannet et al., 2023). Under SSP2-4.5, emissions rise slightly before declining after 2050, but they do not reach net zero by 2100. At approximately 2060, SSP2-4.5 is representative of a 1.6 °C temperature rise relative to a time slice centred around 1990.

GCMs provide information at a resolution that is too coarse to be used directly in catchment-scale hydrological modelling. Hence, an intermediate step is generally performed: the broad-scale GCM outputs are transformed to catchment-scale variables. For this reason, and due to the scale of the catchments being assessed (which makes it resource-intensive to undertake dynamic or statistical downscaling), a simple scaling technique – the pattern scaling (PS) method (Chiew et al., 2009) – was adopted. The seasonal PS method employed used output from the 32 GCMs to scale the 133-year historical daily rainfall, temperature, radiation and humidity sequences (i.e. SILO climate data) to construct the 32 by 133-year sequences of future daily rainfall, temperature, radiation and humidity. The method is described in the companion technical report on future climate across the Victoria, Roper and Southern Gulf catchments (McJannet et al., 2023).

The resulting percentage changes in rainfall and PE spatially averaged across the Southern Gulf catchments under SSP2-4.5 at approximately 2060 for each GCM are shown in Figure 5-1. As outlined by McJannet et al. (2023), scenarios Cwet and Cdry were selected to represent the range of projections from the 32 GCMs shown in Figure 5-1. They were selected based on the 10th and 90th percentile exceedance changes in rainfall. That is, the global climate model – pattern scaling (GCM-PS) time series derived from the GISS-E2-1-G (3rd-ranked GCM) and CMCC-ESM2 GCMs (29th-ranked GCM) were used for the Cdry and Cwet scenarios, respectively. The calibrated river model was used to simulate the river flow at the boundary of the Southern Gulf hydrodynamic model domain under Cdry and Cwet scenarios (Gibbs et al., 2024b).

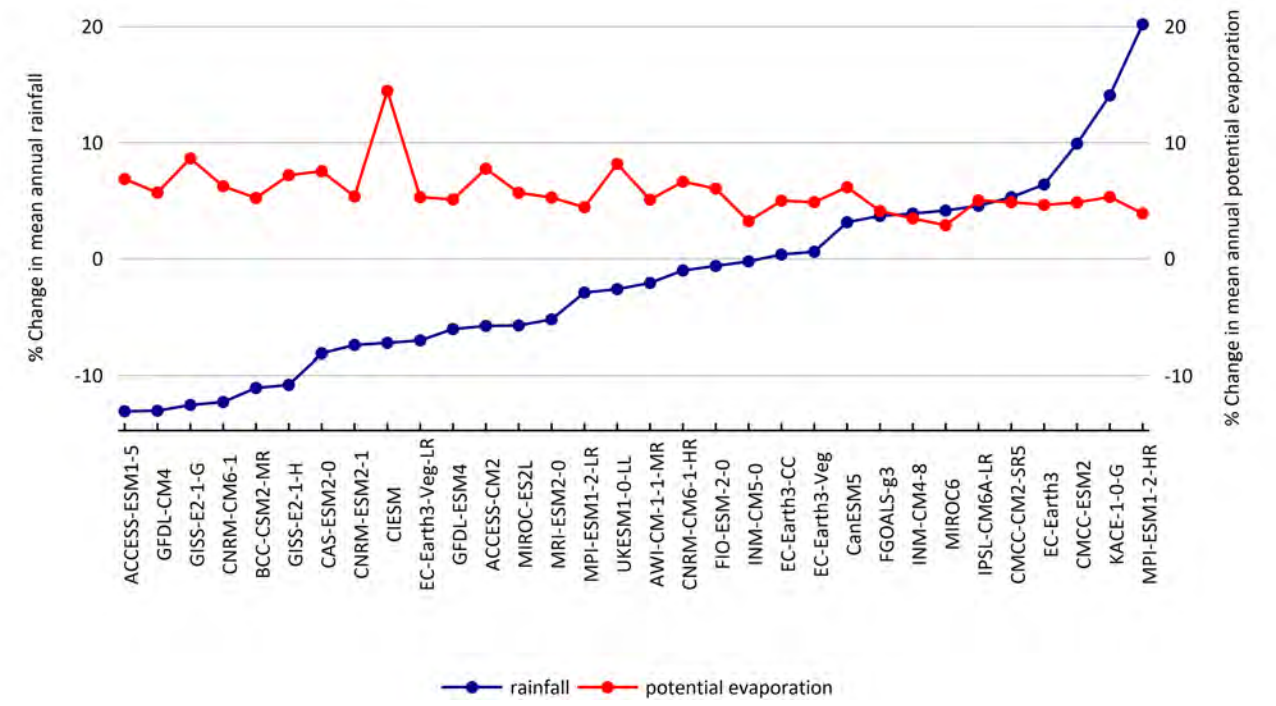

Figure 5-1 Percentage change in mean annual rainfall and potential evaporation under Scenario C relative to Scenario A

Simple scaling of rainfall and potential evaporation have been applied to global climate model output. GCMs are ranked by increasing rainfall.

Figure 5-2 shows simulated monthly streamflow (catchment mean runoff, used as an input to the hydrodynamic model) under scenarios A, Cdry and Cwet from 2000 to 2023 (the hydrodynamic model was calibrated for flood events within this period). Under scenario Cwet, the mean annual catchment streamflow increased by 25%, 21% and 19% for the Nicholson, Gregory and Leichhardt rivers, respectively, and for the wet season (December to March) these increases were 24%, 21% and 17%, respectively. Under Scenario Cdry, the mean annual streamflow decreased by 33%, 26% and 31% for the Nicholson, Gregory and Leichhardt rivers, respectively, and for the wet season (December to March) these reductions were 32%, 25% and 29%, respectively.

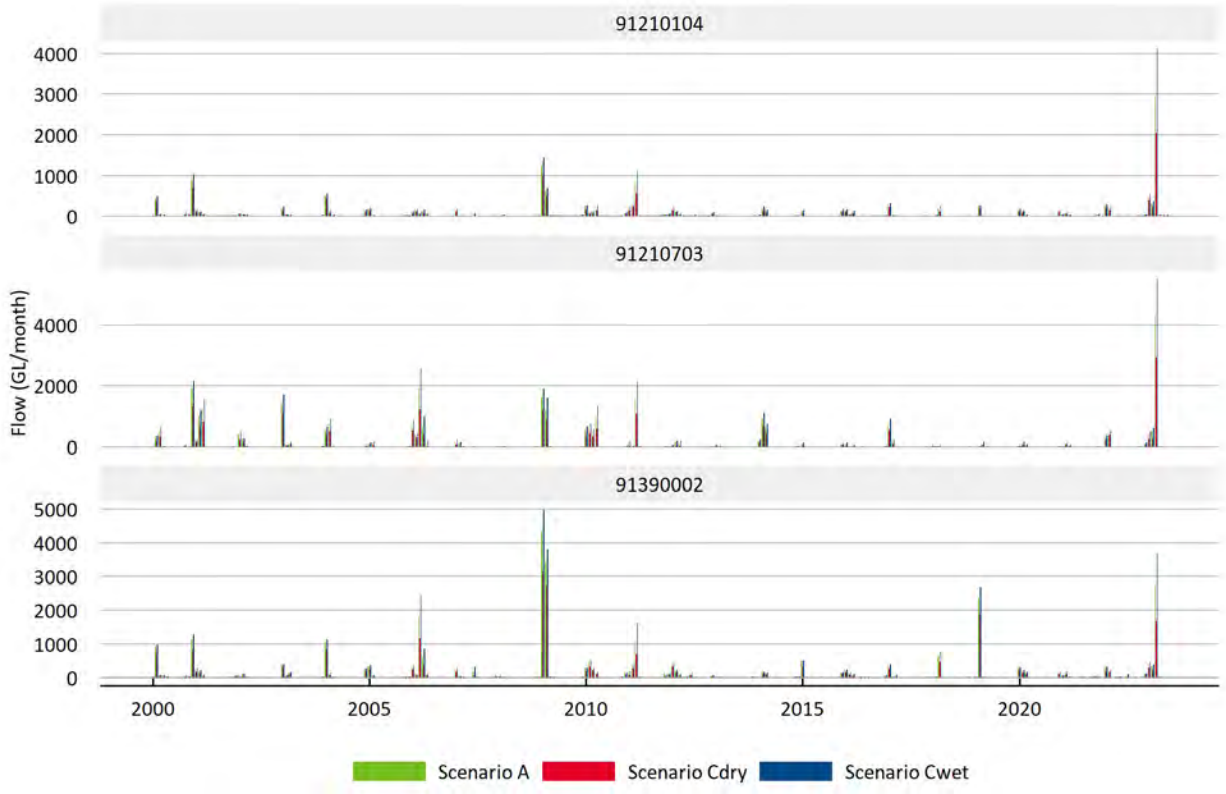

Figure 5-2 River flow under Cdry and Cwet scenarios relative to Scenario A (Baseline) (for 2000 to 2023) at the boundary of Southern Gulf catchments hydrodynamic model, gauge 91210104 on the Gregory River at Gregory, 91210703 on the Nicholson River at Connolly's Hole and 91390002 on the Leichhardt River at Lorraine

Figure 5-3 compares the river flow under the current and future climate for the major rivers in the Southern Gulf catchments, used as inflows to the hydrodynamic model for flood simulation (Section 4.4). It shows relatively large changes in peak and total discharge under scenarios Cwet and Cdry relative to Scenario A for each event. Under Scenario Cdry, the peak streamflow decreased by 21%, 43% and 17% for the Gregory, Nicholson and Leichhardt rivers, respectively, for the 2016 flood, and the respective reductions were 34%, 31% and 38% for the 2023 flood. Under Cwet, the peak streamflow increased by 13%, 40% and 11% for the Gregory, Nicholson and Leichhardt rivers, respectively, for the 2016 flood, and the respective increases were 46%, 28% and 33% for the 2023 flood. For all three river systems, the increases and decreases in total event flow were similar to the maximum flow, but slightly less in magnitude.

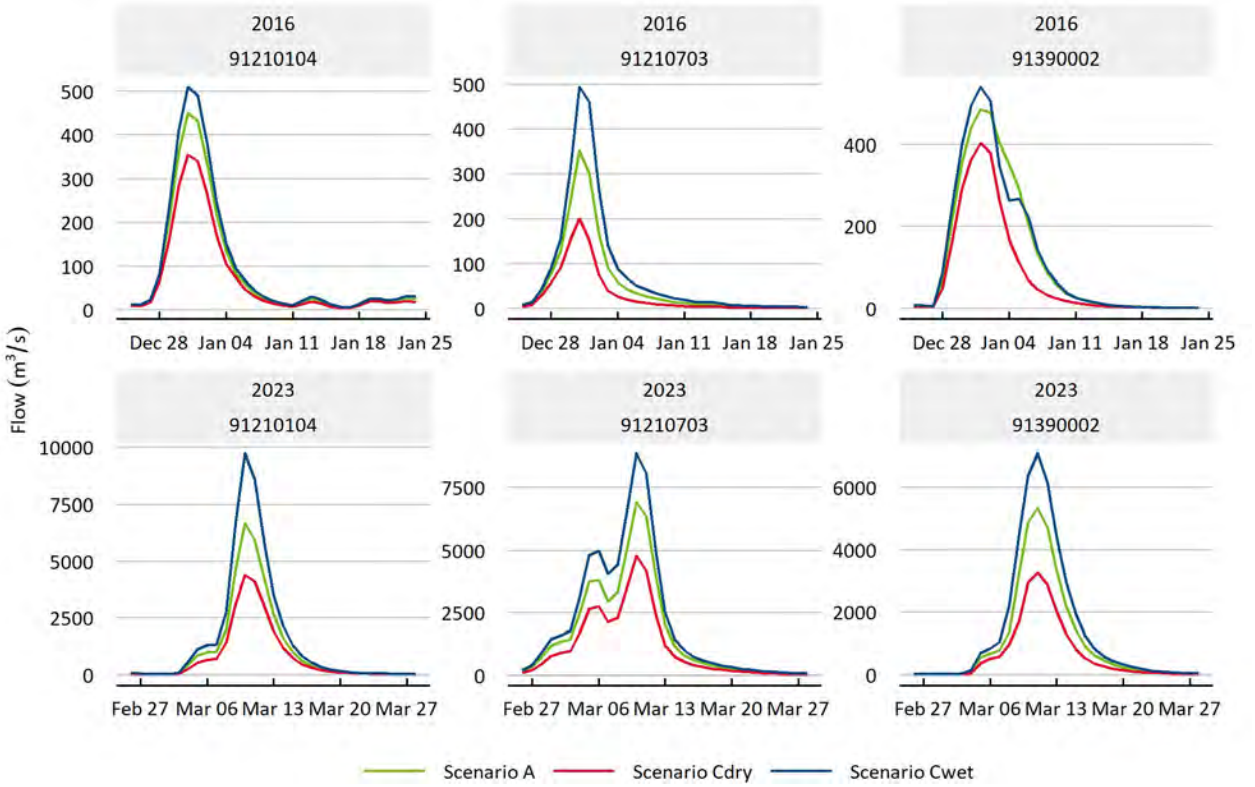

Figure 5-3 Simulated aggregated streamflow used as inflows in the hydrodynamic model (91210104 on the Gregory River, 91210703 on the Nicholson River and 91390002 on the Leichhardt River) for two different flood events – 2016 (AEP of 1 in 3) and 2023 (AEP of 1 in 38) – under scenarios A (Baseline), Cdry (future dry climate) and Cwet (future wet climate)

5.3 Potential development scenarios

5.3.1 INSTREAM DAMS

Potential dams identified in the companion technical report on surface water storage (Yang et al., 2024) were located outside the hydrodynamic model domain. Hence, to explore the impact of instream dams and water harvesting on flood inundation downstream, river system models were configured for various scenarios (refer to the companion technical report on river model calibration and scenario analysis, Gibbs et al., 2024b), and the resulting river system model output provided for the upstream boundary of the hydrodynamic model domains. Only streamflows at the upstream boundaries of the hydrodynamic model domains were updated; the remaining input datasets and boundary conditions in the calibrated hydrodynamic models remained unchanged.

Several potential dam sites were investigated in the Southern Gulf catchments for irrigation and hydro-electric power generation (Table 5-2). However, only three of the potential dams (Dam 1, Dam 3 and Dam 28) were considered for inundation impact assessment. The capacities of these dams at full supply level are 441, 1403 and 716 GL, respectively. At the beginning of each flood event, the dams were set to 50% full.

Figure 5-4 Locations of existing water users under scenarios A and C, and additional hypothetical options considered under scenarios B and D

AMTD = Adopted Middle Thread Distance. FSL = full supply level. Qld = Queensland.

Table 5-2 Surface area and reservoir capacity at full supply level (FSL) of the short-listed hypothetical dams in the Southern Gulf catchments

NAME	LOCATION	FSL (mEGM96)	MODEL NODE	RESERVOIR SURFACE AREA (ha)	RESERVOIR CAPACITY (GL)
Dam 1	Gregory River at AMTD 174 km	145	9121050	7,090	441
Dam 3	Nicholson River AMTD 198 km	108	9121070	12,417	1403
Dam 28	Gunpowder Creek AMTD 66 km	186	9130030	4,021	716
Dam 165	Mistake Creek AMTD 60 km	149	9130080	2,320	158
Dam 206	Gold Creek AMTD 58 km	84	9121097	756	119
Dam 275	Ewen Creek AMTD 6 km	217	9130040	2,515	245

† AMTD = Adopted Middle Thread Distance.

The Southern Gulf catchments feature a highly seasonal climate, with the majority of streamflow occurring in the months December to March (Gibbs et al., 2024a). The effects of instream dams were simulated in the catchment at various locations for 133 years (1890 to 2022). One characteristic of the dams used for simulated irrigation supply was the annual cycle of filling across the wet season and of emptying across the dry season, due to irrigation diversion and evaporation from the dams. This pattern can be seen in the plot of mean monthly dam storage at three sites in the Southern Gulf catchments (Figure 5-5), noting that there can be substantial variability in the storage level from year to year.

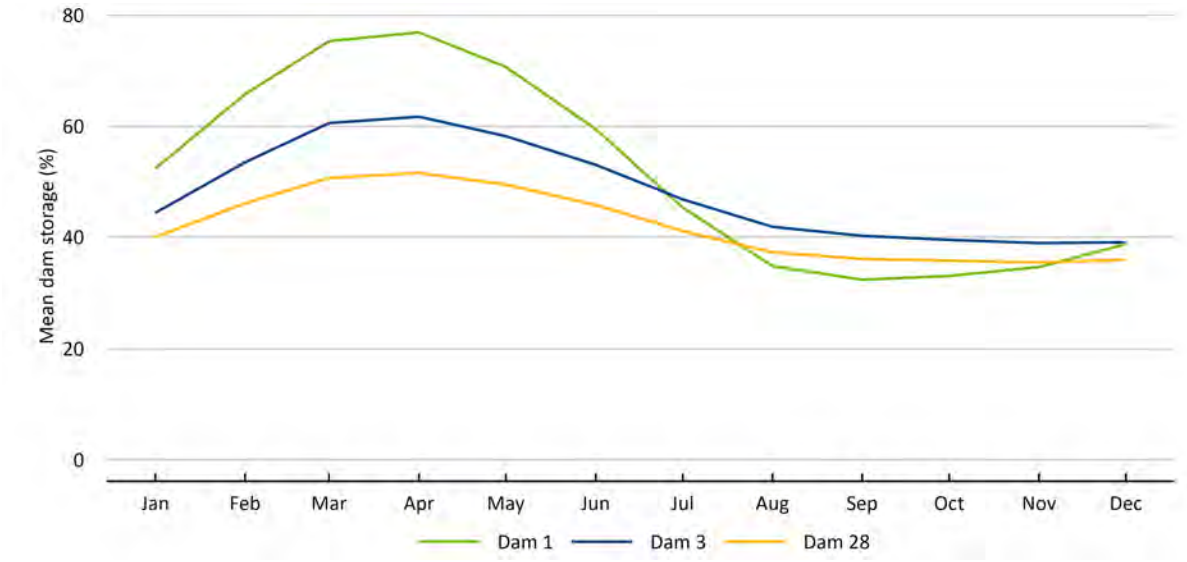

Figure 5-5 Mean monthly dam storage in different months at three dam sites in the Southern Gulf catchments

As a percentage of total dam capacity, dam storage reaches its peak towards the end of the wet season in April and empties across the dry season with irrigation diversion. With regard to floods, this means that, generally, there would be reduced capacity for mitigation of flood events later in the wet season, particularly in March and April; maximum flood mitigation would be expected to be possible for events in the late dry/early wet season (November and December).

These patterns of storage have consequences for hydrodynamic simulation of instream dam scenarios. In particular, simulated flood events later in the wet season are less likely to generate substantial change in the estimated flooded area due to the antecedent storage. Ideally,

hydrodynamic models would be run for the entire 133-year period, as for the Southern Gulf catchment model. This would give a better understanding of the effects of dams on flood mitigation. However, due to the very high computational demand of hydrodynamic models, only selected flood events can be simulated, which are affected by the particular antecedent conditions prior to those events. To counter this, two approaches were taken. First, for each simulated event, the reservoir storage was reduced to 50% immediately prior to the event. Second, a regression between river flow at multiple locations and the estimated flooded area was derived. This was then used to estimate the total flooded area for various scenarios across the entire time series of the river model. This was denoted the flood 'emulator' and allowed for a more balanced assessment of the relative effects of each scenario on flooded area, since it enabled a daily estimate of the flooded area that took into account any antecedent effects. More detailed information on the emulator can be found in Section 5.5.

5.3.2 WATER HARVESTING

Water harvesting was implemented at five locations for an annual limit of 150 GL withdrawal, with a pump rate of 600 ML/day (Gibbs et al., 2024b). For the Water Harvesting scenario, extractions were delayed so as to commence at the start of the hydrodynamic simulation at all five nodes. The pumps were operated assuming a pump start threshold of 600 ML/day, selected to prevent impacts to downstream users. A system target across all five nodes was set at 150 GL, and the pumping rate was adjusted to enable this target volume to be extracted in 20 days. The volume and pump capacity were selected, because they could be physically supported with an annual reliability of 75%, taking into account soil and water limitations, mitigating impacts on existing users, and providing an annual DCFR that protects early-season flows (Gibbs et al., 2024b).

5.4 Floodplain inundation scenario analysis

Evaluation of hydrodynamic modelled scenarios was undertaken by comparing future development (Scenario B), future climate (Scenario C) and future climate and development (Scenario D) scenarios with the baseline simulation (Scenario A). Two types of evaluations were performed across the hydrodynamic model domains for each scenario (Table 5-1):

- a spatial comparison using maps of percentage inundation frequency (the ratio of the number of times a pixel was inundated to the entire duration of the simulation), maximum inundation extent, and inundated depth at maximum inundation extent
- a time-series comparison of the inundated area.

5.4.1 SCENARIO B CURRENT CLIMATE AND INSTREAM DAMS

Figure 5-6 shows the maximum inundation extent as well as the spatial variation in inundation frequencies for 2016 (AEP of 1 in 3) and 2023 (AEP of 1 in 38) flood events. The dams decreased the inundation extent and frequency, but the effects were relatively small in the model domain. Similarly to inundation frequency, the effects on spatial inundation depth were also small (Figure 5-7). However, changes in inundation area due to the dams were noticeable for both the 2016 and 2023 flood events (Figure 5-8). The maximum inundated area for the 2016 event (AEP of 1 in 3)

was 999.3 km^2 under Scenario A (Baseline) and 662.0 km^2 under Scenario B (3-dams). This represents a decrease in inundated area of approximately 33.8%. The maximum inundated area for the 2023 event (AEP of 1 in 38) was 5983.3 km^2 under Scenario A (Baseline) and 5677.6 km^2 under Scenario B (3-dams), representing a decrease of approximately 5.1%. The smaller volume of floodwater in the 1 in 3 AEP event during 2016 caused a larger relative impact. The larger relative impact may also have been due to the difference in the antecedent conditions at the beginning of the two events.

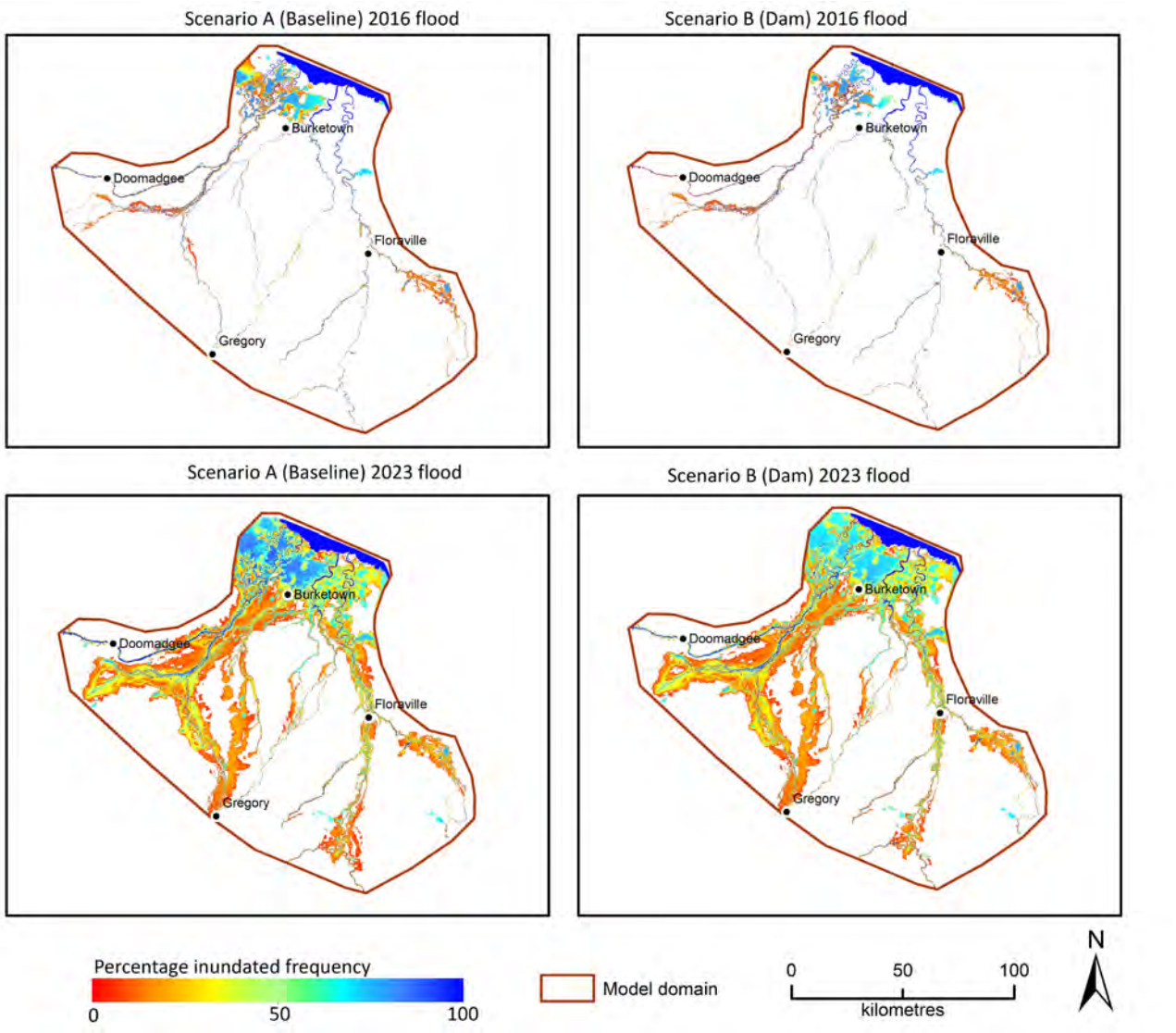

Figure 5-6 Percentage inundation frequency in the Southern Gulf hydrodynamic model domain under scenarios A (Baseline) and B (3-dams)

The 2016 flood event had an AEP of 1 in 3, and the 2023 flood event had an AEP of 1 in 38.

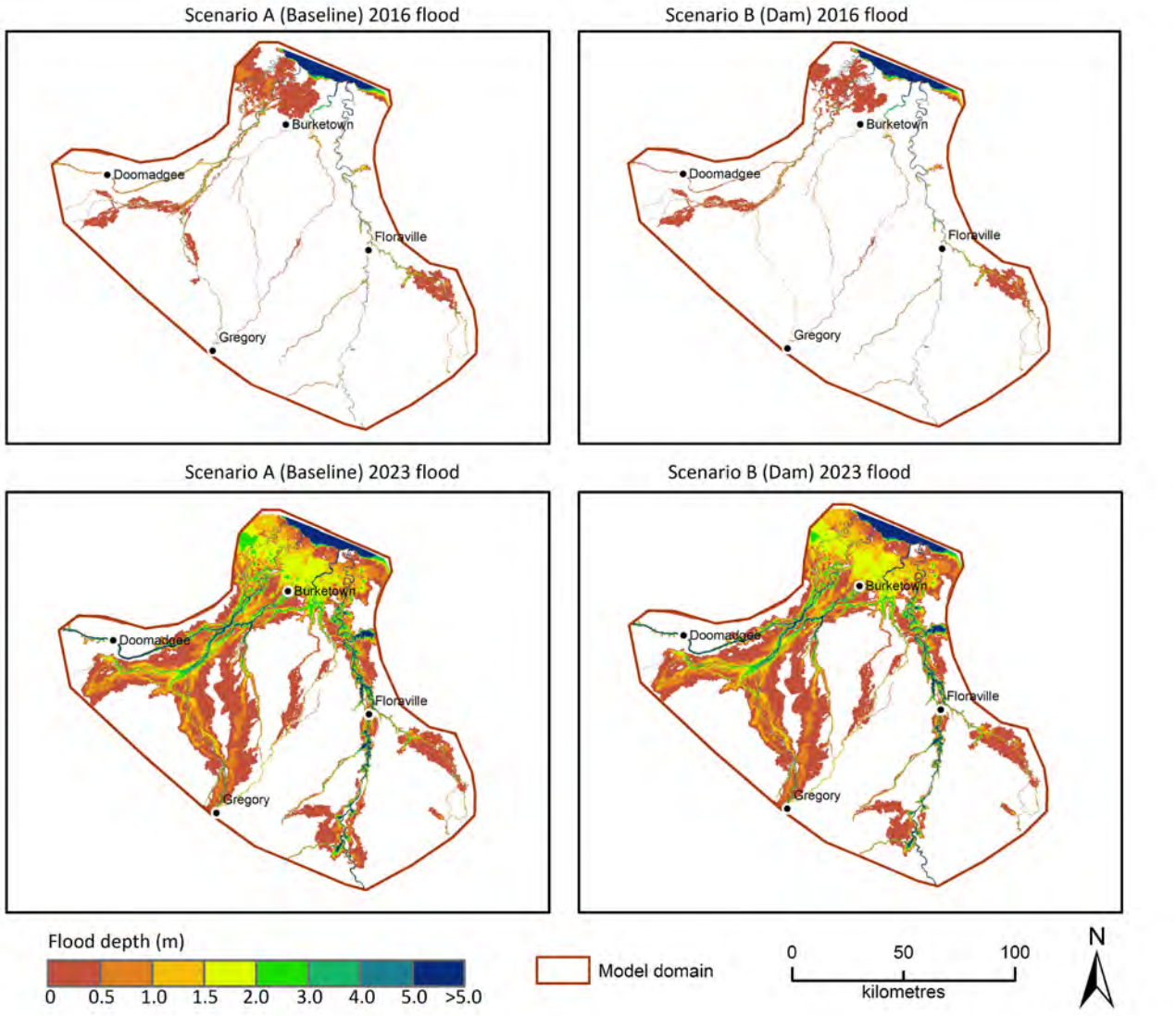

Figure 5-7 Depth at maximum inundation extent in the Southern Gulf hydrodynamic model domain under scenarios A (Baseline) and B (Dam)

The 2016 flood event had an AEP of 1 in 3, and the 2023 flood event had an AEP of 1 in 38.

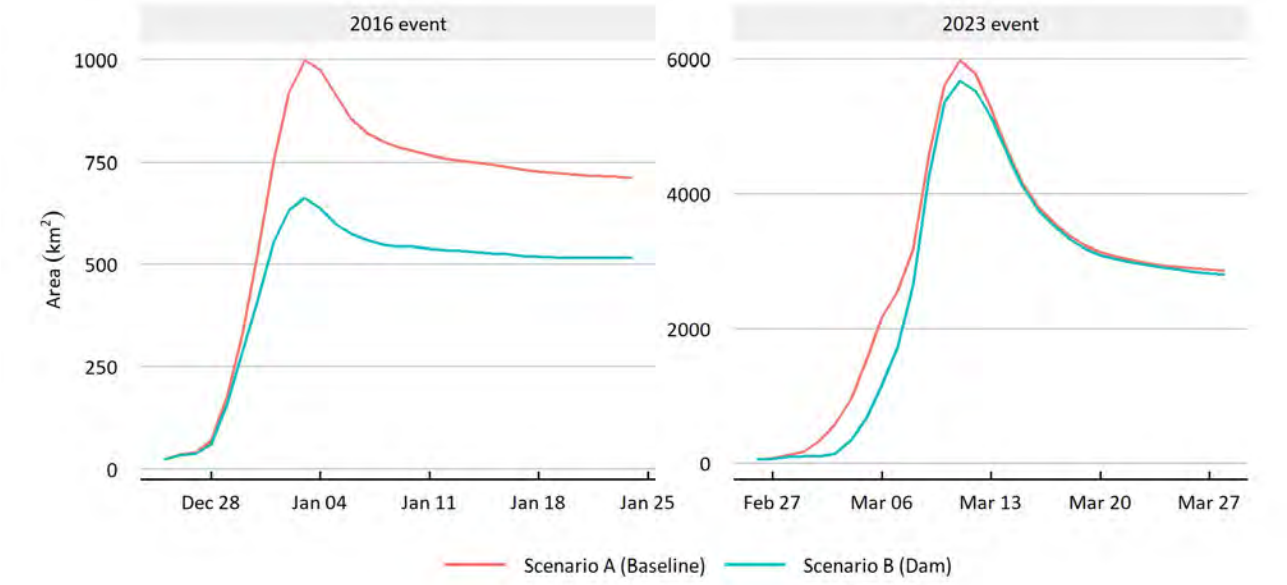

Figure 5-8 Comparison of inundated area (in square kilometres) under scenarios A (Baseline) and B (Dam) in the Southern Gulf hydrodynamic model

The 2016 flood event had an AEP of 1 in 3, and the 2023 flood event had an AEP of 1 in 38.

5.4.2 SCENARIO B CURRENT CLIMATE AND WATER HARVESTING

Figure 5-9 shows the maximum inundation extent as well as the spatial variation in inundation frequencies for the 2016 (AEP of 1 in 3) and 2023 (AEP of 1 in 38) flood events. Water extraction reduced the flow in the river and produced less inundation. In general, the effect of the water harvesting was small for the maximum inundation extent and the inundation frequency. As for inundation frequency, the effect on inundation depth was very small for both the 2016 and 2023 events (Figure 5-10). The changes in inundation areas due to water harvesting were noticeable for the 2016 flood event, but for the 2023 event the effects were minimal (Figure 5-11). The impacts of water harvesting on flood characteristics over the hydrodynamic model domain were larger for the smaller event than those for the larger event. The maximum inundated area for the 2016 event (AEP of 1 in 3) under Scenario A was 999.3 km^2 and 945.3 km^2 under Scenario B (Water Harvesting of 150 GL). This represents a decrease in inundated area of approximately 5.4%. The maximum inundated area under Scenario A for the 2023 event (AEP of 1 in 18) was 5983.3 km^2 and 5934.1 km^2 under Scenario B (Water Harvesting of 150 GL), representing a decrease of only approximately 0.8%. As expected, the impacts were relatively large for the smaller flood event, given the same amount of water was extracted for both flood events.

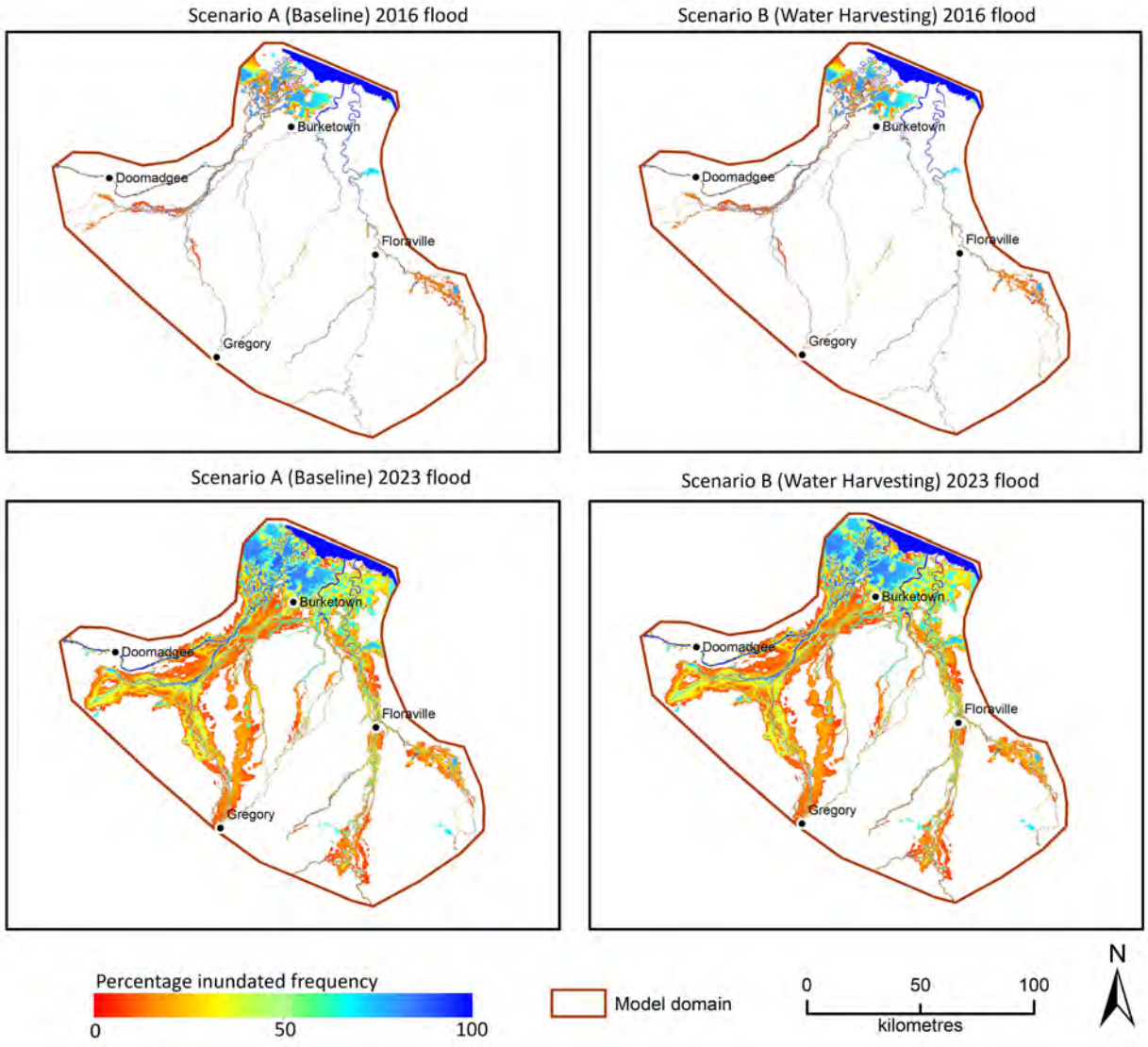

Figure 5-9 Percentage inundation frequency in the Southern Gulf catchments under scenarios A (Baseline) and B (Water Harvesting of 150 GL)

The 2016 flood event had an AEP of 1 in 3, and the 2023 flood event had an AEP of 1 in 38.

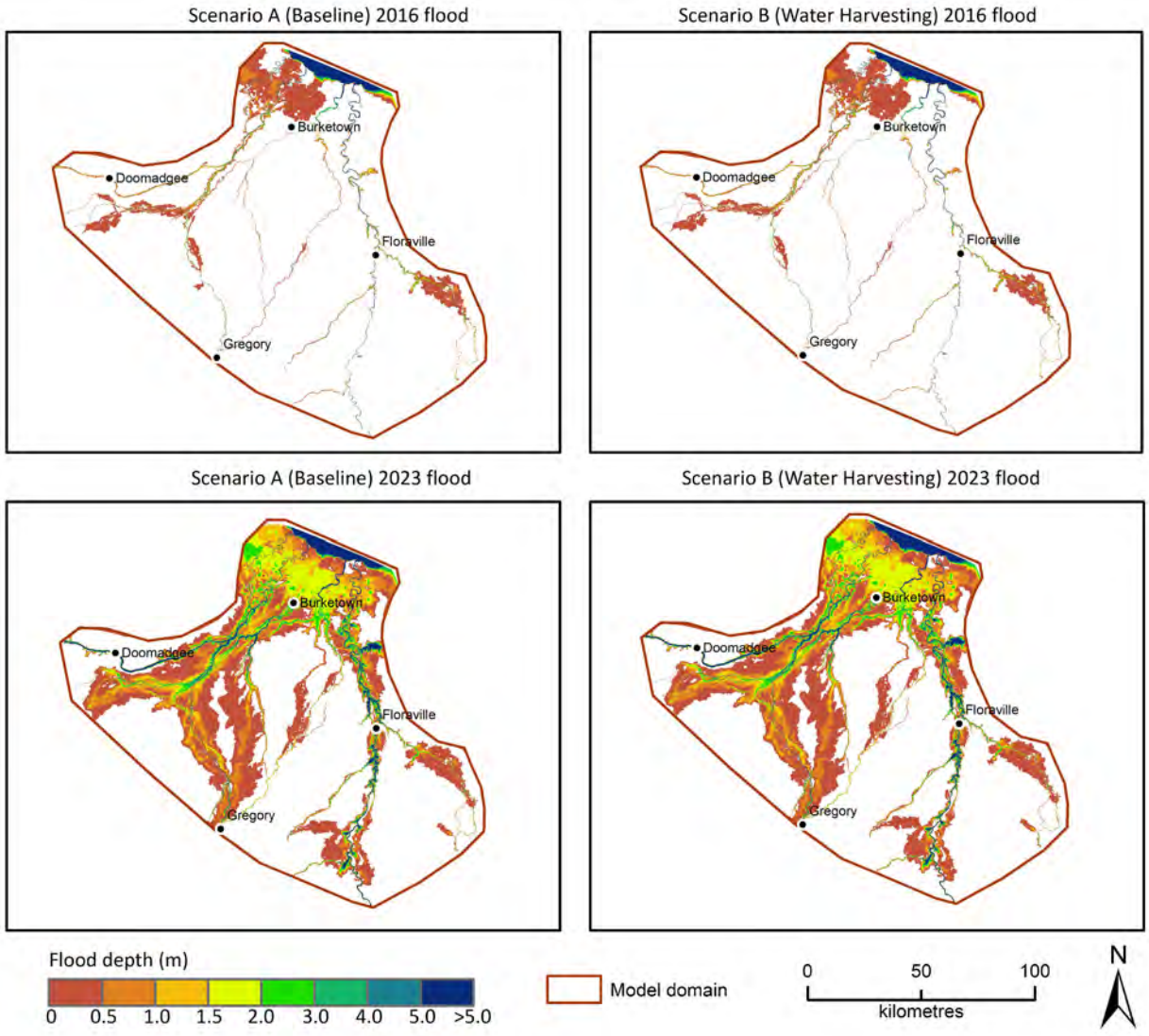

Figure 5-10 Depth at maximum inundation extent in the Southern Gulf hydrodynamic model domain under scenarios A (Baseline) and B (Water Harvesting of 150 GL)

The 2016 flood event had an AEP of 1 in 3, and the 2023 flood event had an AEP of 1 in 38.

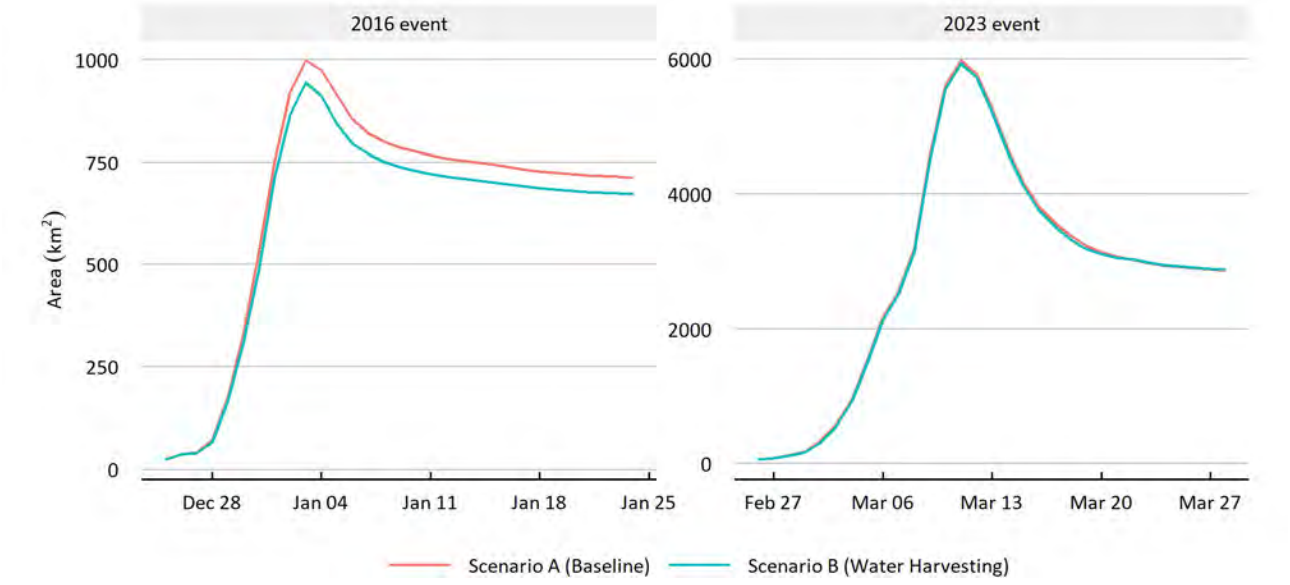

Figure 5-11 Comparison of inundated area (in square kilometres) in the Southern Gulf hydrodynamic model domain under scenarios A (Baseline) and B (Water Harvesting of 150 GL)

The 2016 flood event had an AEP of 1 in 3, and the 2023 flood event had an AEP of 1 in 38.

5.4.3 SCENARIO C FUTURE CLIMATE SCENARIOS

Figure 5-12 shows the difference between scenarios A, Cdry and Cwet in terms of percentage inundated frequency and maximum inundation extent. The results show decreases in inundation frequency and inundation extent under Scenario Cdry relative to Scenario A. Similarly, a significant increase can be seen under Scenario Cwet relative to Scenario A. Similar changes are noticed for spatial inundation depth (Figure 5-13). The maximum inundated area under Scenario Cdry and Cwet for the 2016 event (AEP of 1 in 3) were 689.1 km^2 and 1186.7 km^2, respectively, a reduction of approximately 31.0% under Cdry and an increase of approximately 18.8% under Cwet. For the 2023 event (AEP of 1 in 38), the maximum inundated area under scenarios Cdry and Cwet were 4790.0 km^2 and 6927.4 km^2, respectively, indicating a reduction of approximately 19.9% under Scenario Cdry and an increase of approximately 15.8% under Scenario Cwet. Although the relative increase in inundation area for the 2016 event (~18.8%) was higher than for the 2023 event (~15.8%), the absolute increase in inundation area was higher for the 2023 flood (944.1 km^2) compared with the 2016 flood (187.4 km^2).

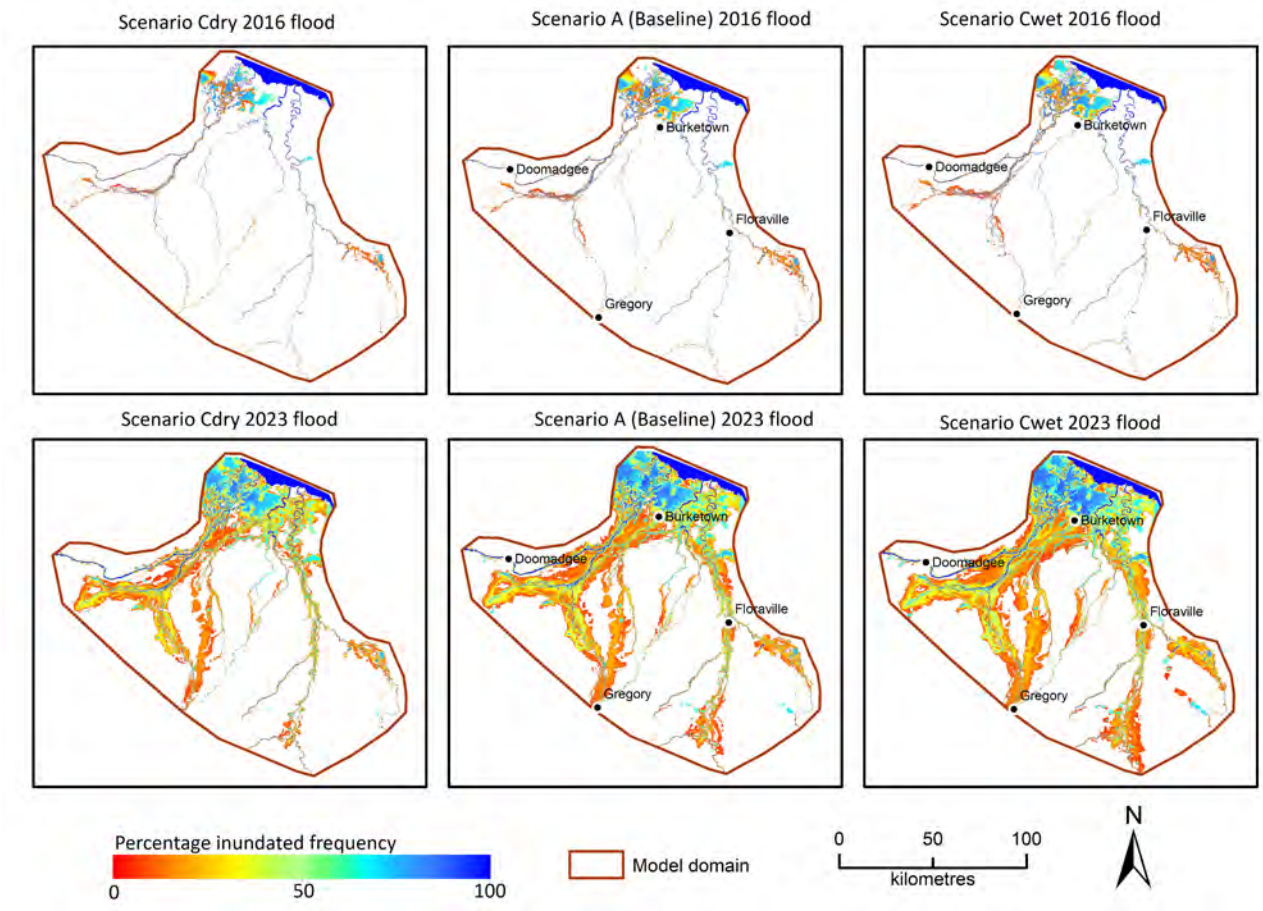

Figure 5-12 Percentage inundated frequency in the Southern Gulf hydrodynamic model domain under scenarios A (Baseline) and C (Future Climate)

The 2016 flood event had an AEP of 1 in 3, and the 2023 flood event had an AEP of 1 in 38.

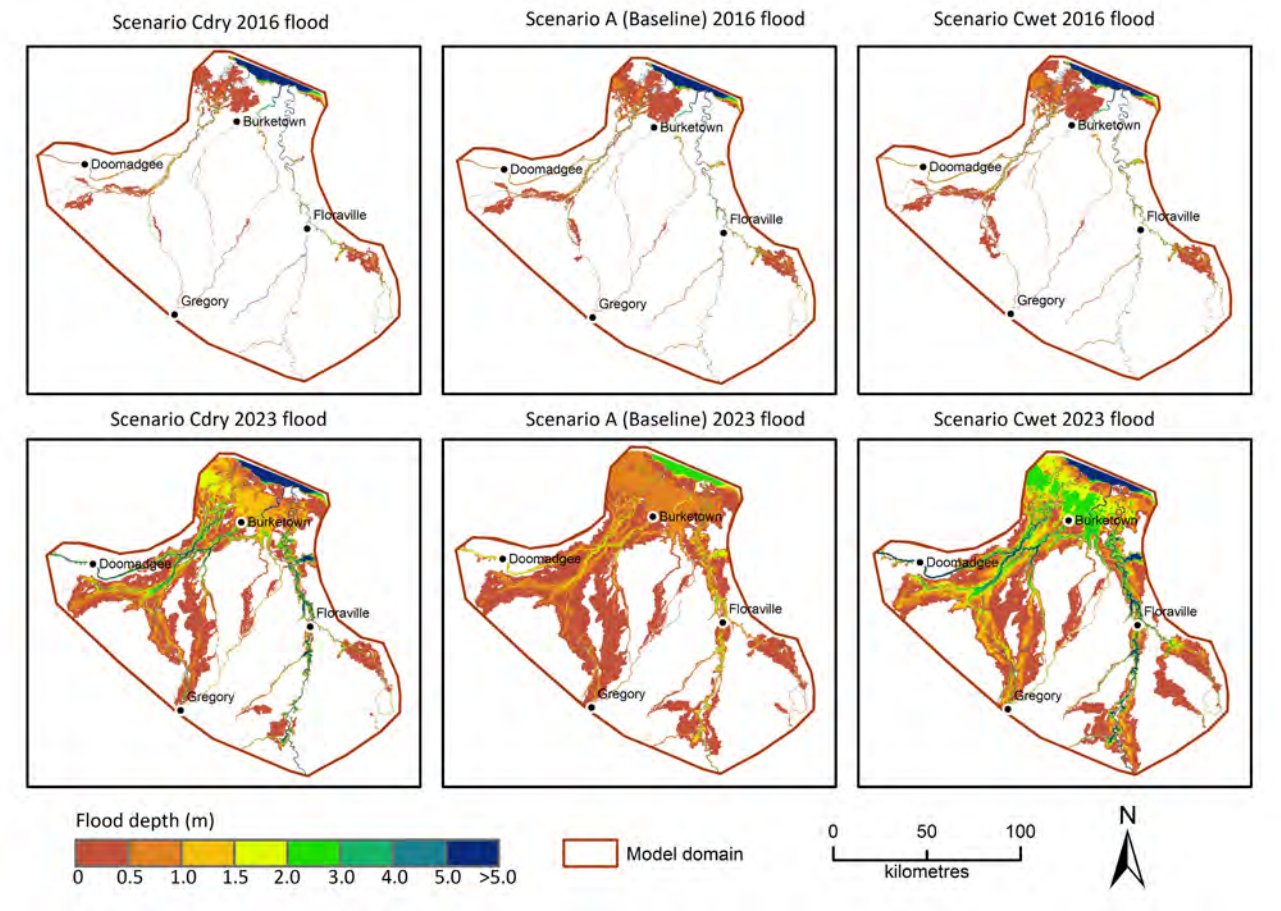

Figure 5-13 Depth at maximum inundation extent in the Southern Gulf hydrodynamic model domain under scenarios A (Baseline) and C (Future climate)

The 2016 flood event had an AEP of 1 in 3, and the 2023 flood event had an AEP of 1 in 38.

The time series in Figure 5-14 shows the large differences between the climate scenarios in the inundated area that occurred under scenarios Cdry and Cwet relative to Scenario A for both events. The differences were largest at the times of peak inundation under both the Cdry and Cwet scenarios. Under Cdry, the peak in inundated area decreased by approximately 29.6% and approximately 19.8% for the 2016 and 2023 flood events, respectively. Under Scenario Cwet, the peak in inundated area increased by approximately 17.9% and approximately 15.6% for the 2016 and 2023 flood events, respectively. Table 5-3 summarises the inundated area under Scenario C and the changes in maximum and mean inundation areas relative to Scenario A.

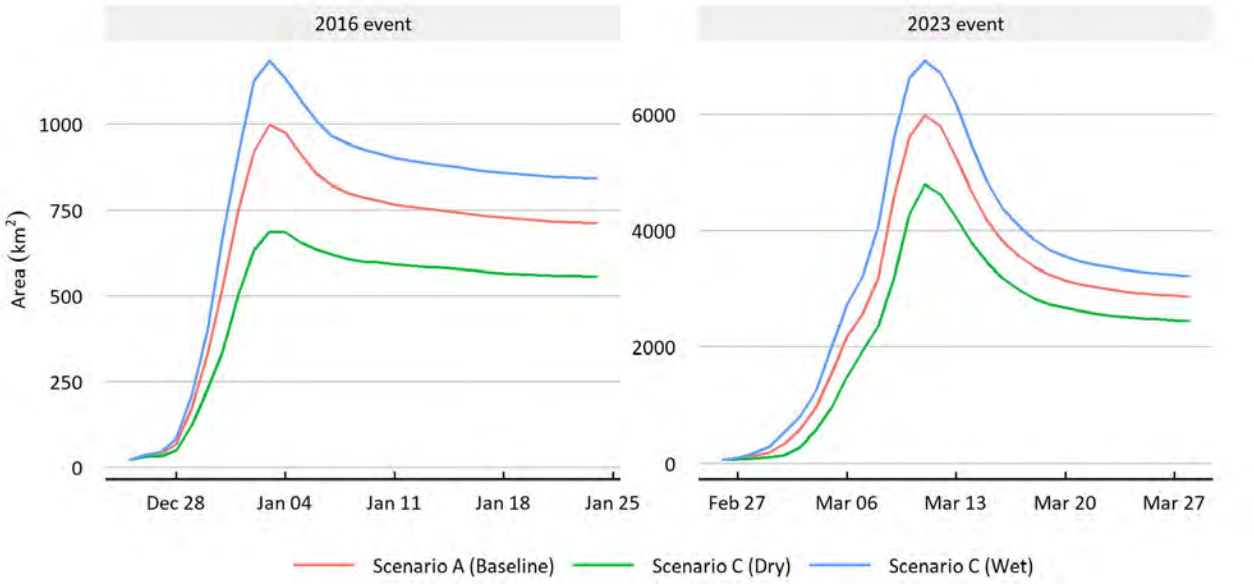

Figure 5-14 Comparison of inundated area (in square kilometres) (left) in the Southern Gulf hydrodynamic model domain under scenarios A (Baseline) and C (Future Climate)

The 2016 flood event had an AEP of 1 in 3, and the 2023 flood event had an AEP of 1 in 38.

Table 5-3 Comparison of the inundated area and associated changes under Scenario C (Future Climate) relative to Scenario A (Baseline)

The 2016 flood event had an AEP of 1 in 3, and the 2023 flood event had an AEP of 1 in 38.

* decrease.

	2016 FLOOD SCENARIO A	2023 FLOOD SCENARIO A	2016 FLOOD Cdry	2023 FLOOD Cdry	2016 FLOOD Cwet	2023 FLOOD Cwet
Maximum inundated area (km²)	999	5983	689	4790	1187	6927
% change in maximum inundated area	–	–	31.0*	19.9*	18.8	15.8
Mean inundated area (km²)	648	2858	486	2288	767	3342
% change in mean inundated area	–	–	25.0*	19.9*	18.4	16.9

5.4.4 SCENARIO D DRY CLIMATE AND INSTREAM DAMS

The maps of percentage inundated frequency (Figure 5-15) and depth at maximum inundation (Figure 5-16) show that the dams combined with future dry climate decreased inundation (frequency, extent and depth) for both the 2016 (AEP of 1 in 3) and 2023 (AEP of 1 in 38) flood events. As expected, the combined impacts of the future dry climate and 3-dams on the inundation extent and frequency were significant, although the climate appears to have been the main driver of the differences. The maximum inundated area under scenarios A (Baseline) and D (Dry Climate and Dam) for the 2016 event was 999.3 km^2 and 375.7 km^2, respectively (Figure 5-17). This represents a decrease in inundated area of approximately 62.4%. The maximum inundated area under scenarios A (Baseline) and D (Dry Climate and Dam) for the 2023 event was 5983.3 km^2 and 3999.6 km^2, respectively, representing a decrease of approximately 33.2%.

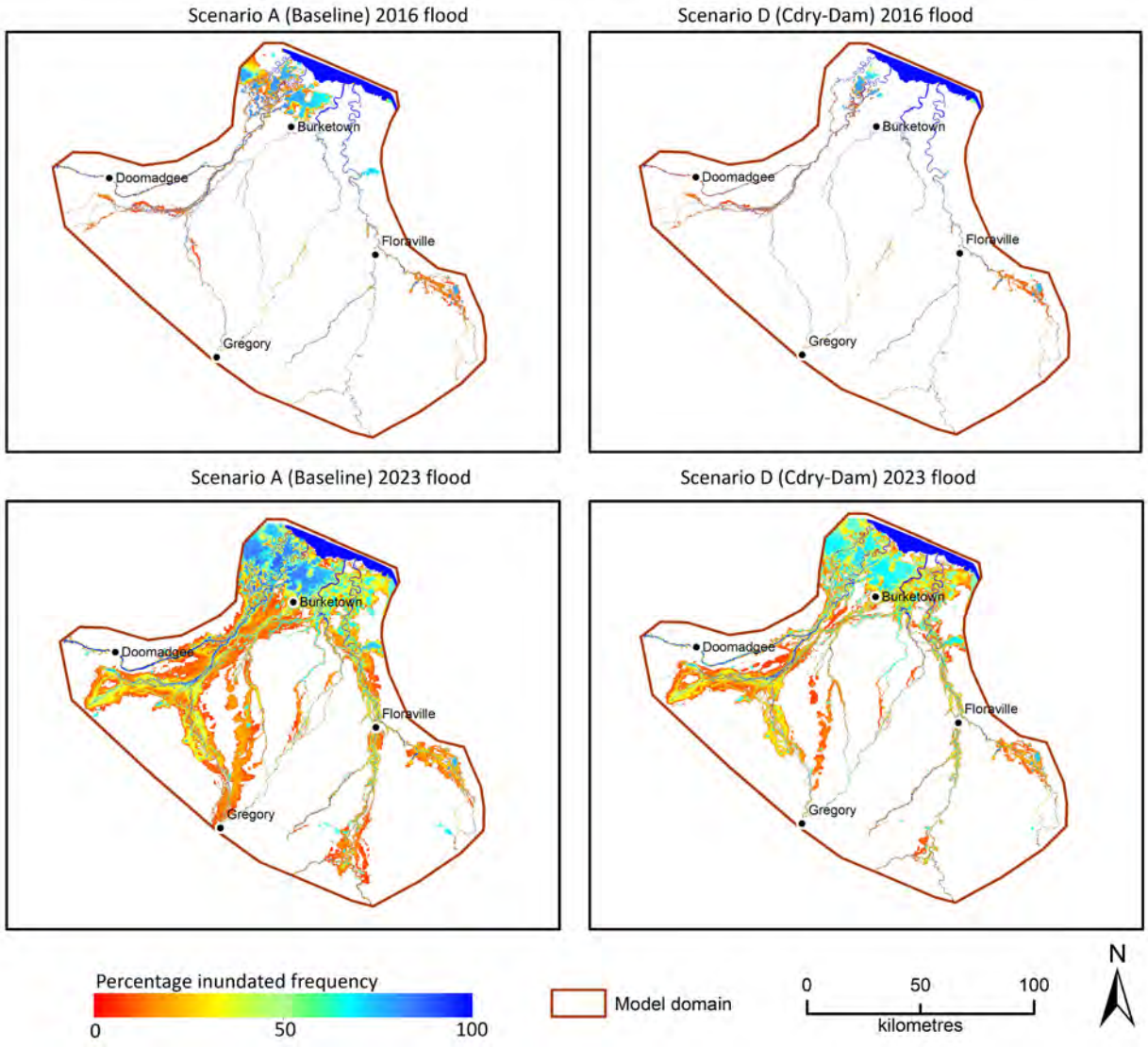

Figure 5-15 Percentage inundation frequency in the Southern Gulf hydrodynamic model domain under scenarios A (Baseline) and D (Dry Climate and Dam)

The 2016 flood event had an AEP of 1 in 3, and the 2023 flood event had an AEP of 1 in 38.

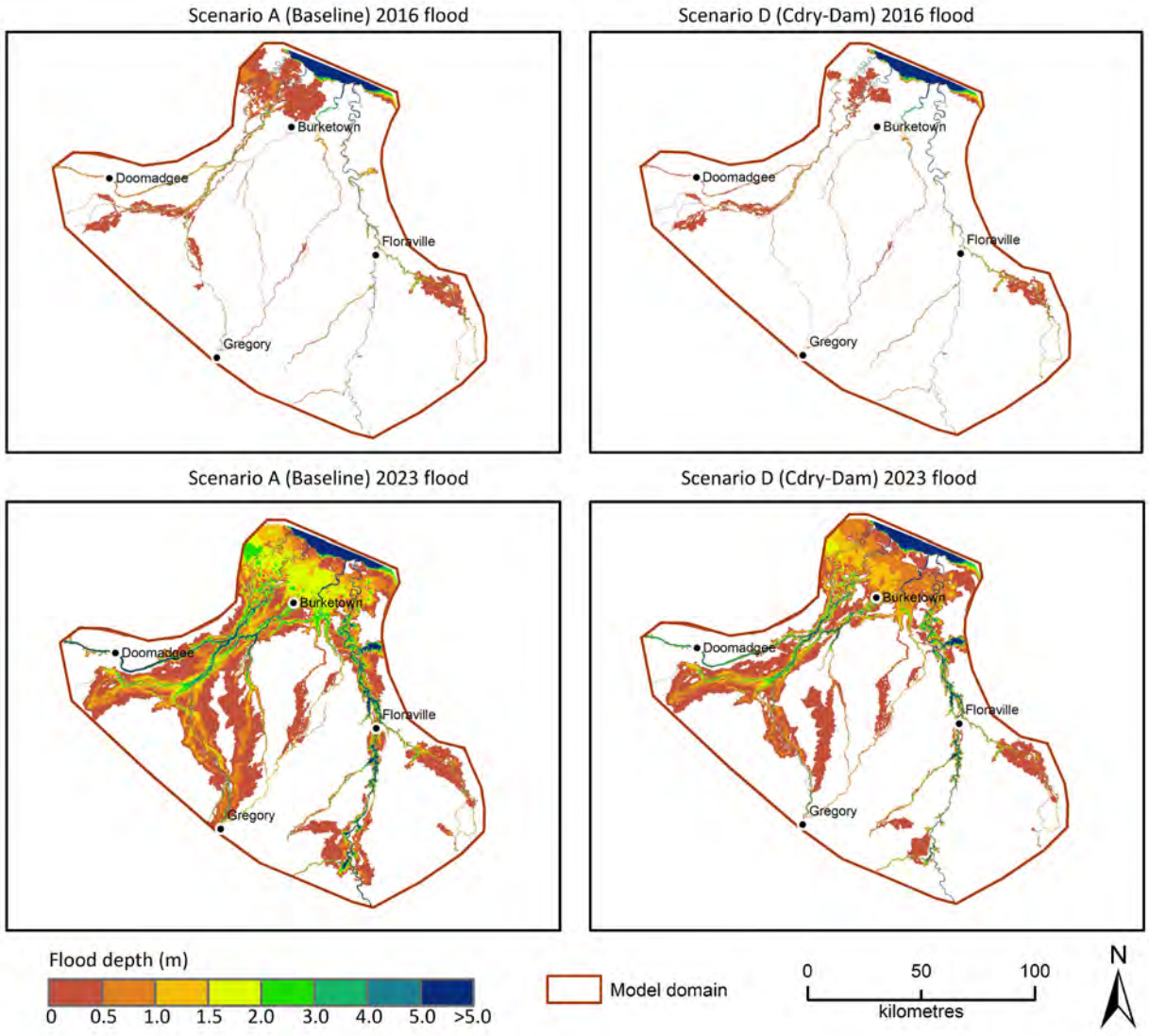

Figure 5-16 Depth at maximum inundation extent in the Southern Gulf hydrodynamic model domain under scenarios A (Baseline) and D (Dry Climate and Dam)

The 2016 flood event had an AEP of 1 in 3, and the 2023 flood event had an AEP of 1 in 38.

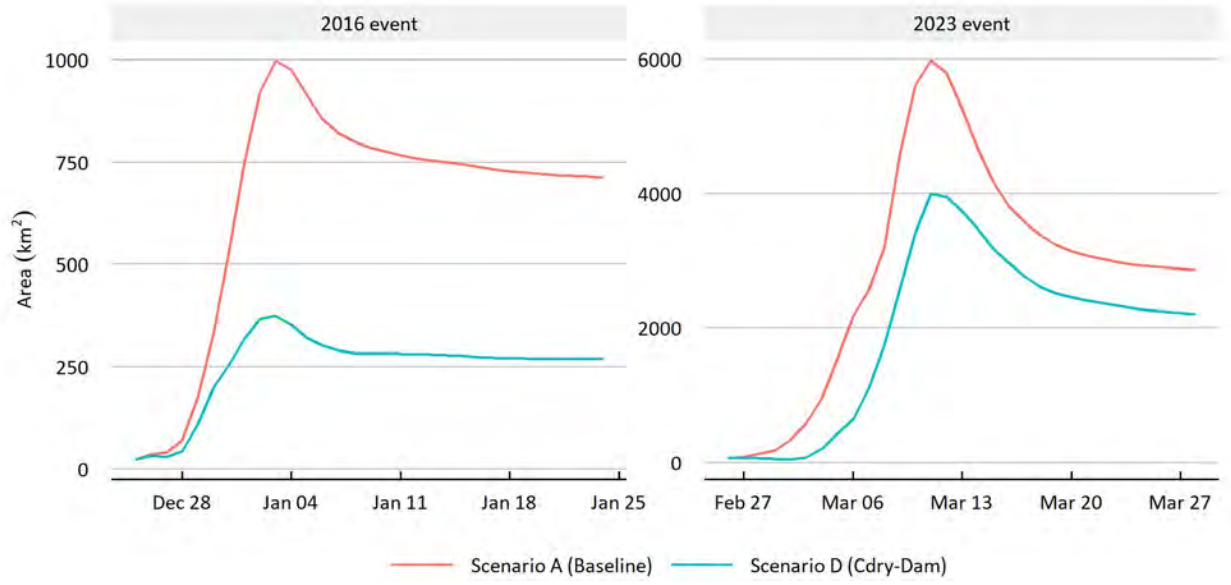

Figure 5-17 Comparison of inundated area (in square kilometres) in the Southern Gulf catchments under scenarios A (Baseline) and D (Dry Climate and Dam)

The 2016 flood event had an AEP of 1 in 3, and the 2023 flood event had an AEP of 1 in 38.

5.4.5 SCENARIO D DRY CLIMATE AND WATER HARVESTING

Maps of percentage inundated frequency (Figure 5-18) and depth at maximum inundation (Figure 5-19) show that water harvesting under a future dry climate scenario substantially decreased inundation for the 2016 (AEP of 1 in 3) and 2023 (AEP of 1 in 38) events. The maximum inundated area under scenarios A (Baseline) and D (Dry Climate and Water Harvesting of 150 GL) for the 2016 event was 999.3 km^2 and 678.3.0 km^2, respectively. This represents a decrease in inundated area of approximately 32.1%. The maximum inundated area for the 2023 event was 5983.3 km^2 and 4747.7 km^2 under scenarios A (Baseline) and D (Dry Climate and Water Harvesting of 150 GL), respectively, representing a decrease of approximately 20.7%. The mean inundations under Scenario D were 481.2 km^2 and 2269.1 km^2 for the 2016 and 2023 floods, respectively, and respectively 648.1 km^2 and 2858.6 km^2 under Scenario A, representing an approximately 25.8% reduction for the 2016 flood and an approximately 20.6% reduction for the 2023 flood. As seen earlier, the relative impacts were higher for smaller events (Figure 5-20).

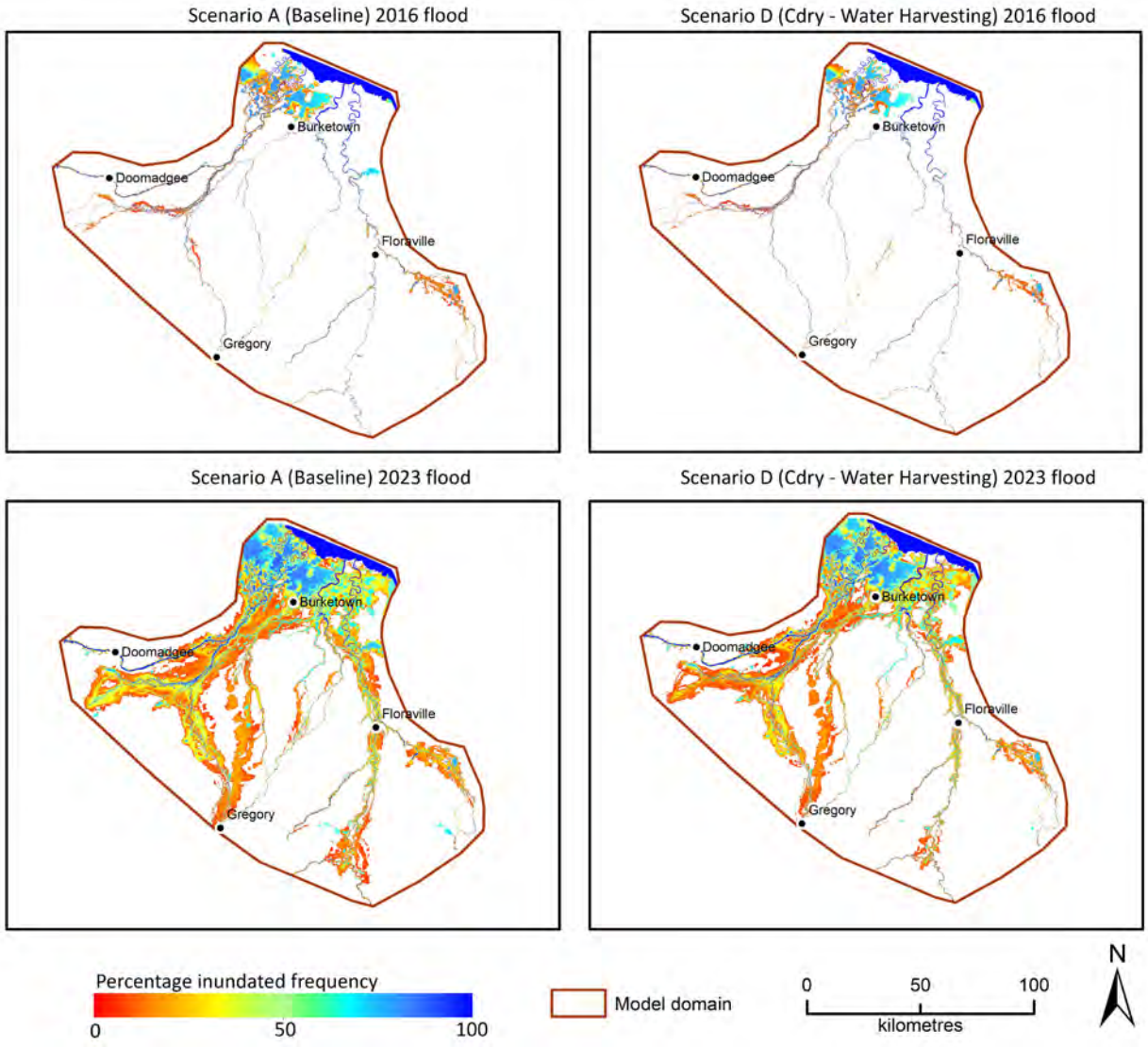

Figure 5-18 Percentage inundation frequency in the Southern Gulf hydrodynamic model domain under scenarios A (Baseline) and D (Dry Climate and Water Harvesting)

The 2016 flood event had an AEP of 1 in 3, and the 2023 flood event had an AEP of 1 in 38.

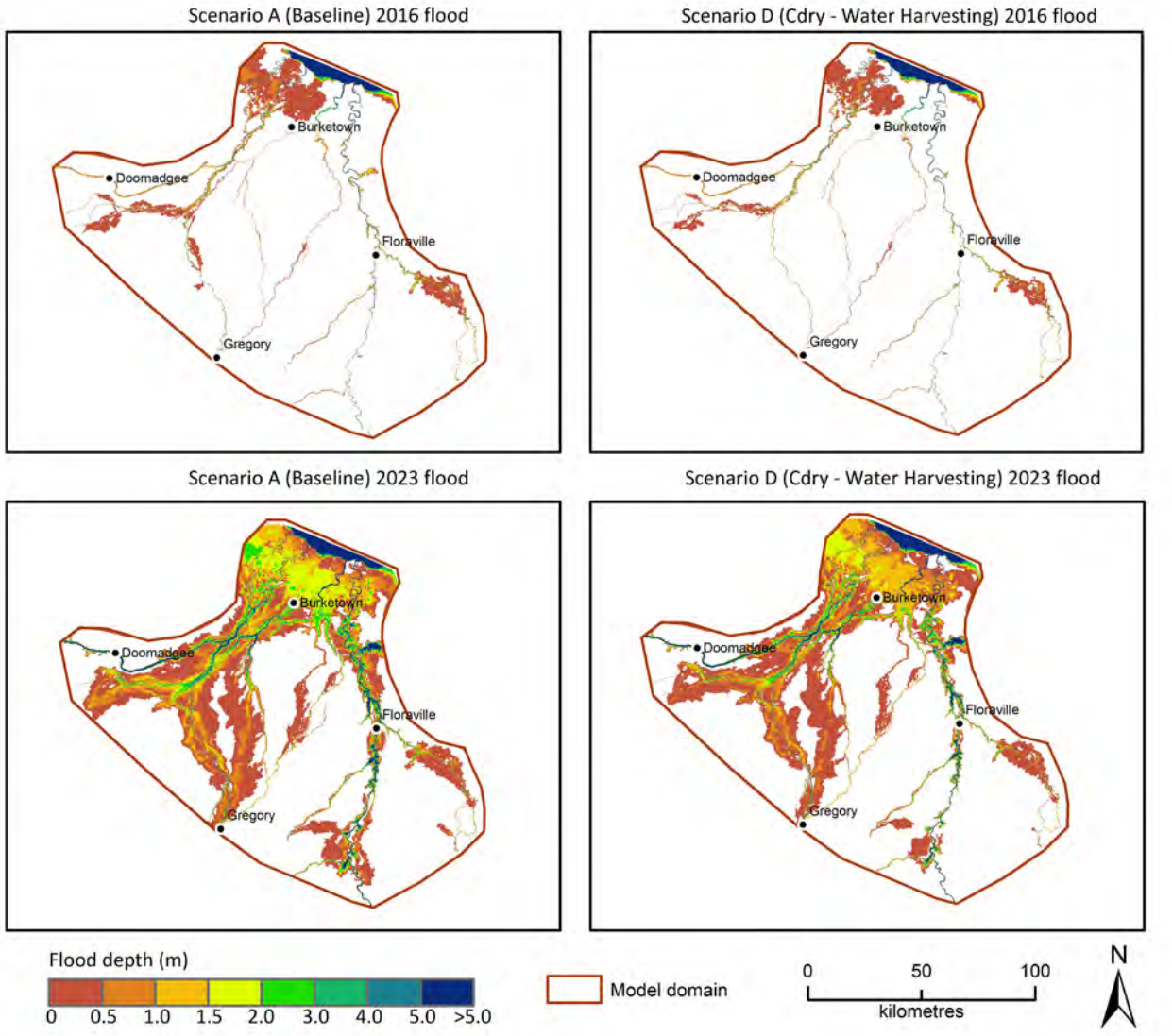

Figure 5-19 Depth at maximum inundation extent in the Southern Gulf hydrodynamic model domain under scenarios A (Baseline) and D (Dry Climate and Water Harvesting)

The 2016 flood event had an AEP of 1 in 3, and the 2023 flood event had an AEP of 1 in 38.

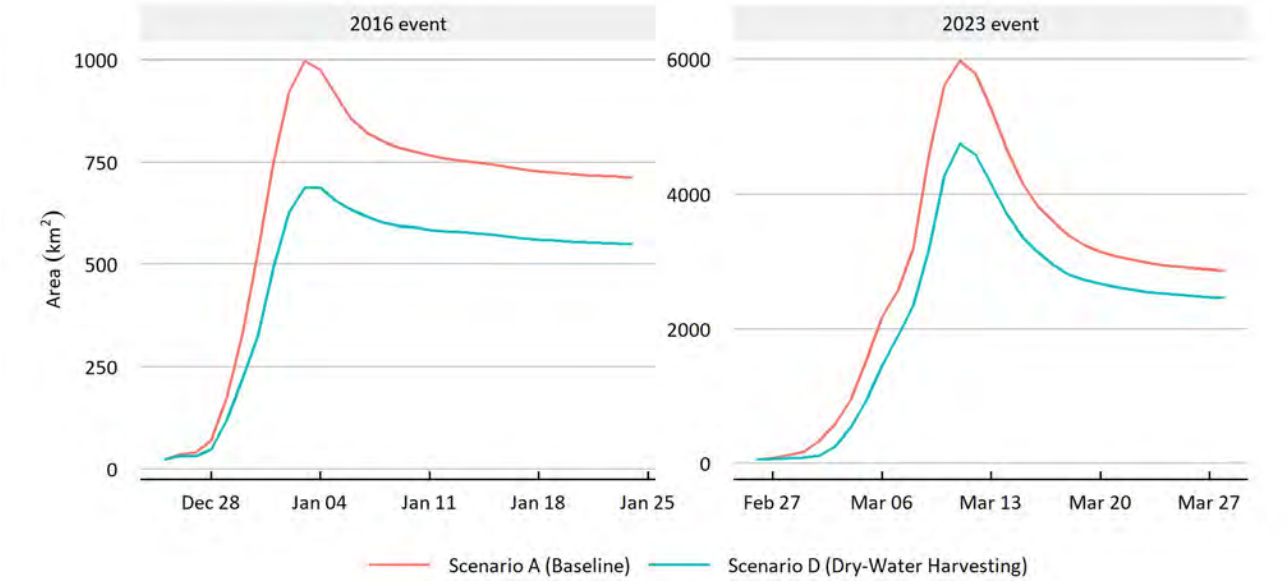

Figure 5-20 Comparison of inundated area (in square kilometres) in the Southern Gulf catchments under scenarios A (Baseline) and D (Dry Climate and Water Harvesting)

The 2016 flood event had an AEP of 1 in 3, and the 2023 flood event had an AEP of 1 in 38.

5.5 Floodplain inundation emulator

5.5.1 DEVELOPMENT OF EMULATOR

An emulator was developed for the Assessment area by relating hydrodynamic model–simulated inundation area to flood discharge through a regression model. Inflows to the hydrodynamic model domain through the three major rivers (Gauge 912116 on the Nicholson River, 912101 on the Gregory River and 913900 on the Leichhardt River) were aggregated in order to produce a time series of flood discharge. Two measures of flow data were compared with the flooding extent data. The first was total volume over the event period, and the second was peak flow during the event period. These were graphed against maximum inundation area. In both cases, there was a clear relationship between flow and inundation area. Of the two measures, peak flow during the event period was determined to give the best relationship and chosen as the measure for use in the regression model. To ensure the calibration data covered a large range, all five calibration events, plus Scenario B (Water Harvesting), Scenario B (3-dams), Scenario Cdry (Future Dry Climate) and Scenario Cwet (Future Wet Climate) estimates of the flooded area for the two events were utilised.

A power curve in the form of $A = bQ^c$ was tested and found to suitable for the Southern Gulf catchments. The parameters were optimised using the following objective function:

$$OF = \frac{\sum_i^n |\hat{A}_i - A_i|}{n} \quad (1)$$

where $\hat{A}_i$ is the estimated flooded area, A_i is the hydrodynamic model–simulated flooded area and n is the number of events.

The calibrated emulator had the following relationship between flow and inundation area:

$$\widehat{\boldsymbol{A}} = 8.6776 * (\boldsymbol{Q}_1 + \boldsymbol{Q}_2 + \boldsymbol{Q}_3)^{0.6633} \quad (2)$$

where $\widehat{\boldsymbol{A}}$ is the estimated time series of the flooded area (km^2), and $\boldsymbol{Q}_1$, $\boldsymbol{Q}_2$ and $\boldsymbol{Q}_3$ are the time series of flow (m^3/second) at nodes 9121160, 9121010 and 9139000.

Overall, the emulator produced a good estimate of the hydrodynamic model–simulated inundation area, with an R^2 value of 0.97 (Figure 5-21). It can be seen that the calibration data covers a large range of data, although there are no data points for the area range of 2000 to 4000 km^2, and estimates in this range will be more uncertain.

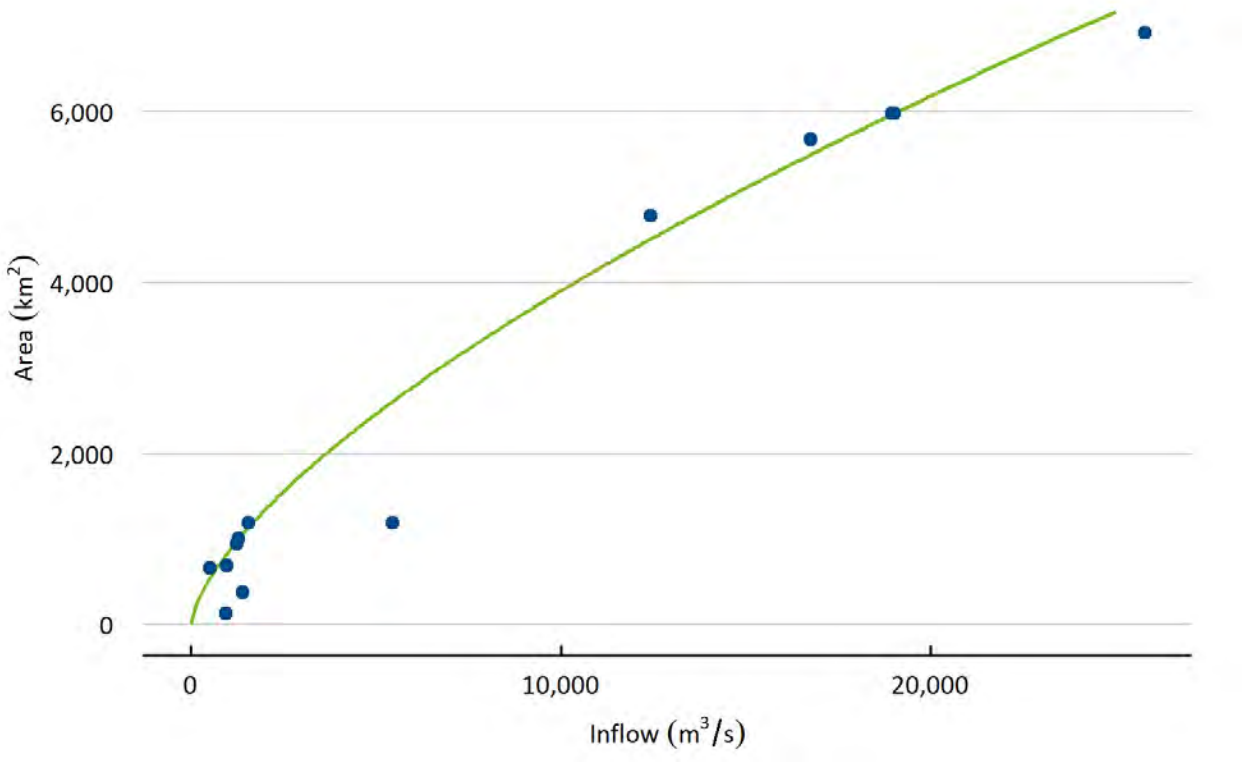

Figure 5-21 Relationship between flood discharge and inundation area for the Southern Gulf catchments

5.5.2 ESTIMATION OF INUNDATION AREA USING THE EMULATOR

The flood emulator was applied to time-series outputs from the river model for a range of scenarios. Figure 5-22 shows the distribution of annual maximum inundation area in the period 1890 to 2022 (133 years) for various climate and development scenarios. Scenario B (Water Harvesting) has little effect on maximum inundation area relative to Scenario A (Baseline), because this method relies on pumps to extract water from the river, which even with an assumed high capacity will be far lower than peak flows in most instances. The effects of dams on inundation are higher relative to water harvesting, because dams reduce and delay the peak by storing water during the high flows, depending upon the antecedent conditions. It is important to note that dam volumes, and thus their capacities to reduce peak flows, vary depending on the timing of the wet

season and how dry the catchment has been in the preceding years. The flooded area reductions are obvious under the Cdry and combined Cdry and dams scenarios, since inflows will be reduced. Scenario D (Cdry-Dam) for dry climate and the three instream dams has the lowest distribution of the flooded area estimates of all scenarios, essentially combining the effects of the dams and of lower streamflow (Table 5-4).

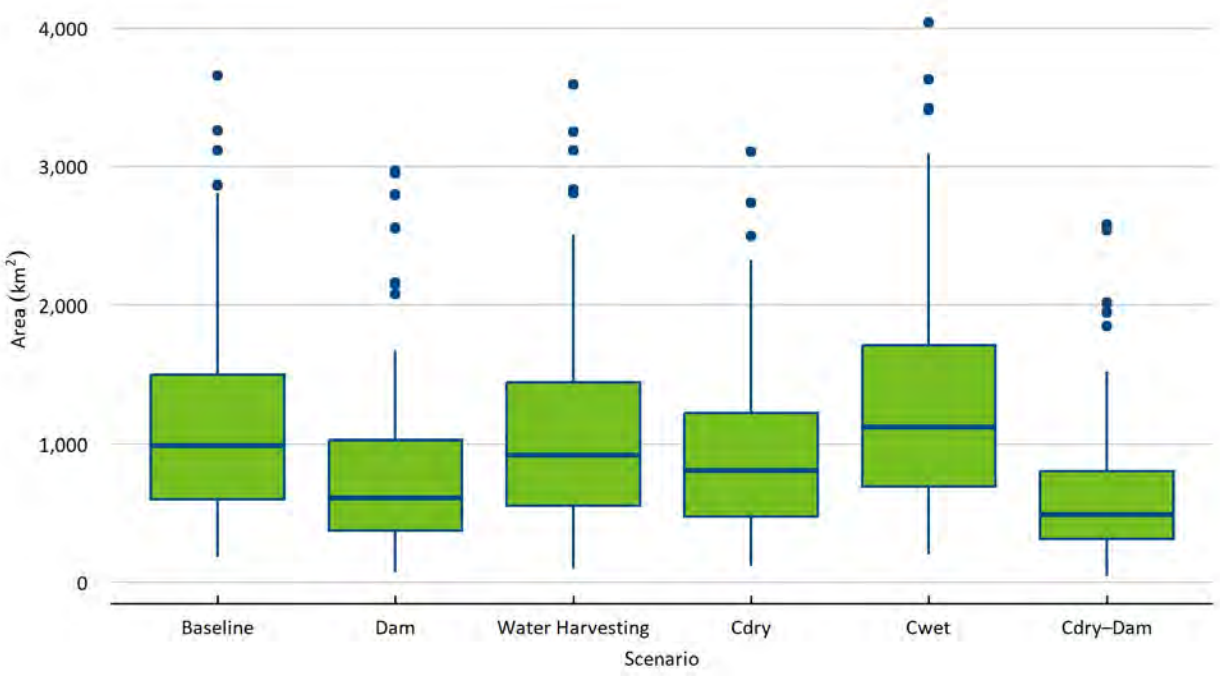

Figure 5-22 Estimated annual maximum flooded area for the various climate and development scenarios for the Southern Gulf catchments

Table 5-4 Emulator estimates of the flooded area for 133 years of simulation

Scenario	Mean annual maximum flooded area (km²)	Maximum flooded area (km²)
A (Baseline)	1132	3659
B (Dam)	785	2968
B (Water Harvesting)	1086	3589
Cdry (Dry Climate)	911	3108
Cwet (Wet Climate)	1286	4041
D (Cdry-Dam)	615	2578

6 Summary

This part of the Assessment had two major components: calibration of a two-dimensional flexible-mesh hydrodynamic model (MIKE 21 FM), followed by scenario modelling under projected dry and wet future climates (Cdry and Cwet) and hypothetical developments (three instream dams and Water Harvesting). The outputs from the hydrodynamic modelling were used to:

- identify areas susceptible to seasonal flooding under the historical climate and current development
- predict changes in inundation across the floodplains under future dry and wet climate scenarios
- predict how dam storages and water harvesting would alter the inundation dynamics across the floodplain
- assess the combined effects of future climate and development scenarios (Dams and Water Harvesting) on inundation extent and depth.

Observed discharge and stage height data were obtained from the Water Monitoring Information portal of the Queensland Government, and tide data were obtained from the Bureau of Meteorology. A flexible-mesh floodplain hydrodynamic model was configured for the middle and lower reaches of the Nicholson, Gregory and Leichhardt rivers and their tributaries. Sacramento rainfall-runoff simulations and discharge data from AWRA-R simulations were used as input at the hydrodynamic model boundaries. Flood inundation maps for individual flood events were produced using satellite (Landsat, MODIS, Sentinel-1 and Sentinel-2) imagery. Composite flood maps were also produced by combining all images to delineate the maximum flood extent in the catchment. These maps and the observed water level at Floraville on the Leichhardt River were used to calibrate the Southern Gulf hydrodynamic model. The calibrated hydrodynamic model was used to simulate the impacts of future climate and future developments on inundation extent, frequency and depth.

The hydrodynamic model was calibrated for the 2005 (AEP of 1 in 2), 2016 (AEP of 1 in 3), 2018 (AEP of 1 in 5), 2019 (AEP of 1 in 10) and 2023 (AEP of 1 in 38) flood events, and two of these flood events (2016 and 2023) were used for scenario modelling. The model was calibrated primarily by adjusting the roughness coefficient and the infiltration rate. While a good match was attained for the flood peaks, there were differences in the rising and falling limbs of the flood hydrograph. In general, model predictions were found to be more accurate for large floods.

Comparison with the Landsat, MODIS and Sentinel inundation maps revealed that the hydrodynamic model captured overall inundation patterns along the Nicholson, Gregory, Leichhardt and Albert rivers. However, the detection statistics showed that the cell-to-cell matching against observed satellite data was poor, largely due to the inability of MODIS to detect inundation of narrow floodplains. The model overpredicted inundation area, especially during a receding flood. Locations of poor fit generally coincided with complex anabranching, for example along the Gregory River and Beames Brook. Closer inspection of satellite imagery in these locations revealed that it often does not display flooding of these anabranches. The inability of MODIS to capture inundation in narrow floodplains has been reported in the Fitzroy catchment in

WA (Karim et al., 2011) and in other catchments in northern Australia (Ticehurst et al., 2013). Furthermore, MODIS regularly falsely identifies cloud shadow as inundation, which is particularly an issue when using imagery with high (up to 80%) cloud cover. The hydrodynamic model has some limitations, and lack of good-quality satellite images restricts rigorous calibration of the model results. Moreover, there are uncertainties in the river model simulations for inflow boundaries and locally generated runoff.

Future climate scenario modelling showed marked changes in inundation areas relative to those under Scenario A, with the major differences being observed under scenarios Cdry and Cwet. For example, under the Cdry scenario, the maximum inundation area decreased by 31.0% and 20.6% for the 2016 (AEP of 1 in 3) and 2023 (AEP of 1 in 38) events, respectively. For the Cwet scenario, the maximum inundation extent increased by 18.8% and 14.8% for the 2016 and 2023 events, respectively.

The reduction in modelled maximum inundation extent under Scenario B (Dam) is significant. The reductions in maximum inundation area were 33.8% and 5.9% for the 2016 and 2023 events, respectively. However, under the Water Harvesting scenario, the changes were very small relative to other scenarios. Under Scenario B (Water Harvesting), the reduction in maximum inundation extent for the 2016 event (AEP of 1 in 3) was 5.4%, and it was only 0.9% for the 2023 event (AEP of 1 in 38). The reductions were much higher for the combined Dry Climate and Development scenarios. For example, the reductions were 62.4% and 32.1% for the 2016 event for Cdry-Dam and Cdry-Water Harvesting, respectively. The Development scenario modelling demonstrated that these reductions in maximum inundation extent were largely dependent on the timing of the events and the water storage capacity of the dams. It is important to note that dam volumes, and thus their capturing capacities, vary depending on the timing of the wet season and how dry the catchment has been in the preceding years.

A flood inundation emulator was developed by investigating the relationship between the hydrodynamic model–simulated inundation area and the flood discharge. The emulator produced a good estimate of the hydrodynamic model–simulated inundation area, except for a few outliers. The flood emulator was applied to time-series outputs from the river model for various climate and development scenarios. Under Scenario B Water Harvesting, there was little change in the maximum inundation area relative to Scenario A, because even very high pump capacities would be small relative to the rates of streamflow during floods. The effect of dams on inundation was higher relative to Water Harvesting, because the dams reduce and delay the flood peak by storing water during the peak flow. The reductions were much higher under the Cdry and the combined Cdry and Dam scenarios.

References

Arcement GJ and Schneider VR (1989) Guide for selecting Manning's roughness coefficients for natural channels and floodplain. US Geological Survey, Virginia.

Arnell NW and Gosling SN (2016) The impacts of climate change on river flood risk at the global scale. Climatic Change 134(3), 387–401. DOI: 10.1007/s10584-014-1084-5.

Arthington AH, Godfrey PC, Pearson RG, Karim F and Wallace J (2015) Biodiversity values of remnant freshwater floodplain lagoons in agricultural catchments: evidence for fish of the Wet Tropics bioregion, northern Australia. Aquatic Conservation: Marine and Freshwater Ecosystems 25(3), 336–352. DOI: 10.1071/MF12251.

Australian Academy of Science (2021) The risks to Australia of a 3°C warmer world. Australian Academy of Science. Available online: <https://www.science.org.au/files/userfiles/support/reports-and-plans/2021/risks-australia-three-deg-warmer-world-report.pdf

Bayley PB (1991) The flood pulse advantage and the restoration of river–floodplain systems. Regulated Rivers: Research and Management 6, 75–86. DOI: 10.1002/rrr.3450060203.

Bayley PB (1995) Understanding large river floodplain ecosystems. Bioscience 45(3), 153–158. DOI: 10.2307/1312554.

Beighley RE, Eggert KG, Dunne T, He Y, Gummadi V and Verdin KL (2009) Simulating hydrologic and hydraulic processes throughout the Amazon River Basin. Hydrological Processes 23(8), 1221–1235. DOI: 10.1002/hyp.7252.

Bomers A, Schielen RMJ and Hulscher SJMH (2019) The influence of grid shape and grid size on hydraulic river modelling performance. Environmental Fluid Mechanics 19(5), 1273–1294. DOI: 10.1007/s10652-019-09670-4.

Budget Strategy and Outlook (2024) Budget 2024-25. A future made in Australia. Viewed 11 September 2024, https://budget.gov.au/content/factsheets/download/factsheet-fmia.pdf.

Bulti DT and Abebe BG (2020) A review of flood modeling methods for urban pluvial flood application. Modeling Earth Systems and Environment 6(3), 1293–1302. DOI: 10.1007/s40808-020-00803-z.

Bunn SE, Thoms MC, Hamilton SK and Capon SJ (2006) Flow variability in dryland rivers: boom, bust and the bits in between. River Research and Applications 22(2), 179–186. DOI: 10.1002/rra.904.

Charles S, Petheram C, Berthet A, Browning G, Hodgson G, Wheeler M, Yang A, Gallant S, Marshall A, Hendon H, Kuleshov Y, Dowdy A, Reid P, Read A, Feikema P, Hapuarachchi P, Smith T, Gregory P and Shi L (2016) Climate data and their characterisation for hydrological and agricultural scenario modelling across the Fitzroy, Darwin and Mitchell catchments. A technical report from the CSIRO Northern Australia Water Resource Assessment to the Government of Australia. CSIRO, Australia

Chiew FHS, Teng J, Vaze J, Post DA, Perraud JM, Kirono DGC and Viney NR (2009) Estimating climate change impact on runoff across southeast Australia: method, results, and implications of the modeling method. Water Resources Research 45. DOI: 10.1029/2008wr007338.

Chormanski J, Miroslaw-Swiatek D and Michalowski R (2009) A hydrodynamic model coupled with GIS for flood characteristics analysis in the Biebrza riparian wetland. Oceanological and Hydrobiological Studies 38(1), 65–73. DOI: 10.2478/v10009-009-0004-x.

Chow VT (1959) Open channel hydraulics. McGraw-Hill International Edition, Singapore.

Department of State Development, Manufacturing, Infrastructure and Planning (2019) North west Queensland economic diversification strategy 2019. Viewed 12 September 2024, https://www.statedevelopment.qld.gov.au/regions/regional-priorities/a-strong-and-prosperous-north-west-queensland/north-west-queensland-economic-diversification-strategy.

DHI (2012) MIKE 21 Flow Model: scientific documentation. Danish Hydraulic Institute, Denmark.

DHI (2016) MIKE 21 flow model FM, Hydrodynamic Module, User Guide. Danish Hydraulic Institute Water and Environment Pty Ltd, Hörsholm, Denmark. <https://manuals.mikepoweredbydhi.help/2017/Coast_and_Sea/MIKE_FM_HD_2D.pdf>.

Dhu T, Dunn B, Lewis B, Lymburner L, Mueller N, Telfer E, Lewis A, McIntyre A, Minchin S and Phillips C (2017) Digital earth Australia – unlocking new value from Earth observation data. Big Earth Data, 1(1–2), 64–74. DOI: 10.1080/20964471.2017.1402490.

Doble RC, Crosbie RS, Smerdon BD, Peeters L and Cook FJ (2012) Groundwater recharge from overbank floods. Water Resources Research 48(9). DOI: 10.1029/2011wr011441.

Dottori F, Szewczyk W, Ciscar JC, Zhao F, Alfieri L, Hirabayashi Y, Bianchi A, Mongelli I, Frieler K, Betts RA and Feyen L (2018) Increased human and economic losses from river flooding with anthropogenic warming. Nature Climate Change 8(9), 781–786. DOI: 10.1038/s41558-018-0257-z.

Ebert EE, Janowiak JE and Kidd C (2007) Comparison of near-real-time precipitation estimates from satellite observations and numerical models. Bulletin of the American Meteorological Society 88(1), 47–68. DOI: 10.1175/BAMS-88-1-47.

Engeny (2020) Burketown flood risk management study. A report to Burke Shire Council from Engeny Water Management. Burke Shire Council, Brisbane. https://www.burke.qld.gov.au/downloads/file/514/burke-shire-planning-scheme-2020-pdf.

Frazier P and Page K (2009) A reach-scale remote sensing technique to relate wetland inundation to river flow. River Research and Applications 25, 836–849. DOI: 10.1002/rra.1183.

Frazier P, Page K, Louis J, Briggs S and Robertson AI (2003) Relating wetland inundation to river flow using Landsat TM data. International Journal of Remote Sensing 24(19), 3755–3770. DOI: 10.1080/0143116021000023916.

Gallant J (2019) Merging lidar with coarser DEMs for hydrodynamic modelling over large areas. In: 23rd International Congress on Modelling and Simulation. Modelling and Simulation Society of Australia and New Zealand, 1161–1166.

Gallant J, Wilson N, Dowling T, Read A and Inskeep C (2011) SRTM-derived 1 second Digital Elevation Models Version 1.0 dataset. Geoscience Australia, Canberra. https://data.gov.au/dataset/ds-ga-aac46307-fce8-449d-e044-00144fdd4fa6/details?q=>.

Gallardo B, Gascon S, Gonzalez-Sanchis M, Cabezas A and Comin FA (2009) Modelling the response of floodplain aquatic assemblages across the lateral hydrological connectivity gradient. Marine and Freshwater Research 60(9), 924–935. DOI: 10.1071/mf08277.

Gibbs M, Hughes J and Yang A (2024a) River model calibration for the Southern Gulf catchments. A technical report from the CSIRO Southern Gulf Water Resource Assessment for the National Water Grid. CSIRO, Australia.

Gibbs M, Hughes J, Yang A, Wang B, Marvanek S and Petheram C (2024b) River model scenario analysis for the Southern Gulf catchments. A technical report from the CSIRO Southern Gulf Water Resource Assessment for the National Water Grid. CSIRO, Australia.

Gladkova I, Grossberg MD, Shahriar F, Bonev G and Romanov P (2012) Quantitative Restoration for MODIS Band 6 on Aqua. IEEE Transactions on Geoscience and Remote Sensing 50(6), 2409–2416. DOI: 10.1109/Tgrs.2011.2173499.

Guerschman JP, Warren G, Byrne G, Lymburner L, Mueller N and Van-Dijk A (2011) MODIS-based standing water detection for flood and large reservoir mapping: algorithm development and applications for the Australian continent. CSIRO Water for a Healthy Country National Research Flagship Report, Canberra.

Hawker L, Uhe P, Paulo L, Sosa J, Savage J, Sampson C and Neal J (2022) A 30 m global map of elevation with forests and buildings removed. Environmental Research Letters 17(2) 024016. DOI: 10.1088/1748-9326/ac4d4f.

Heiler G, Hein T and Schiemer F (1995) Hydrological connectivity and flood pulses as the central aspects for the integrity of a river–floodplain system. Regulated Rivers: Research and Management 11, 351–361. DOI: 10.1002/rrr.3450110309.

Horritt MS and Bates PD (2002) Evaluation of 1D and 2D numerical models for predicting river flood inundation. Journal of Hydrology 268(1–4), 87–99.

IPCC (2022) Climate Change 2022: Impacts, adaptation, and vulnerability. Contribution of Working Group II to the Sixth Assessment Report of the Intergovernmental Panel on Climate Change. [Pörtner HO, Roberts DC, Tignor M, Poloczanska ES, Mintenbeck K, Alegría A, Craig M, Langsdorf S, Löschke S, Möller V, Okem A and Rama B (eds)] Cambridge University Press, Cambridge, UK and New York, NY, USA. https://report.ipcc.ch/ar6/wg2/IPCC_AR6_WGII_FullReport.pdf.

Junk WJ, Bayley PB and Sparks RE (1989) The flood pulse concept in river–floodplain systems. In: Proceedings of the International Large River Symposium. Canadian Special Publications of Fisheries and Aquatic Sciences 106, 110–127. https://publications.gc.ca/site/eng/9.816457/publication.html

Karim F, Dutta D, Marvanek S, Petheram C, Ticehurst C, Lerata J, Kim S and Yang A (2015) Assessing the impacts of climate change and dams on floodplain inundation and wetland connectivity in the wet–dry tropics of northern Australia. Journal of Hydrology 522, 80–94. DOI: 10.1016/j.jhydrol.2014.12.005.

Karim F, Kinsey-Henderson A, Wallace J, Arthington AH and Pearson RG (2012) Modelling wetland connectivity during overbank flooding in a tropical floodplain in north Queensland, Australia. Hydrological Processes 26, 2710–2723. DOI: 10.1002/hyp.8364.

Karim F, Petheram C, Marvanek S, Ticehurst C, Wallace J and Gouweleeuw B (2011) The use of hydrodynamic modelling and remote sensing to estimate floodplain inundation and flood discharge in a large tropical catchment. In: Chan F, Marinova D and Anderssen RS (eds), 19th International Congress on Modelling and Simulation. Modelling and Simulation Society of Australia and New Zealand, Perth.

Kim B, Sanders BF, Schubert JE and Famiglietti JS (2014) Mesh type tradeoffs in 2D hydrodynamic modeling of flooding with a Godunov-based flow solver. Advances in Water Resources 68, 42–61. DOI: 10.1016/j.advwatres.2014.02.013.

Kron W (2015) Flood disasters – a global perspective. Water Policy 17(S1), 6–24. DOI: 10.2166/wp.2015.001.

Kumar V, Sharma KV, Caloiero T, Mehta DJ and Singh K (2023) Comprehensive overview of flood modeling approaches: a review of recent advances. Hydrology 10(7), 141. DOI: 10.3390/hydrology10070141.

Kvocka D, Falconer RA and Bray M (2015) Appropriate model use for predicting elevations and inundation extent for extreme flood events. Natural Hazards 79(3), 1791–1808. DOI: 10.1007/s11069-015-1926-0.

Liu Q, Qin Y, Zhang Y and Li ZW (2015) A coupled 1D–2D hydrodynamic model for flood simulation in flood detention basin. Natural Hazards 75(2), 1303–1325. DOI: 10.1007/s11069-014-1373-3.

LWA (2009) An Australian handbook of stream roughness coefficients. Land and Water Australia, Canberra.

Mackay C, Suter S, Albert N, Morton S and Yamagata K (2015) Large scale flexible mesh 2D modelling of the Lower Namoi Valley. In: Floodplain Management Association National Conference. Floodplain Management Australia, 1–14.

McJannet D, Yang A and Seo L (2023) Climate data characterisation for hydrological and agricultural scenario modelling across the Victoria, Roper and Southern Gulf catchments. A technical report from the CSIRO Victoria River and Southern Gulf Water Resource Assessments for the National Water Grid. CSIRO, Australia.

Meadows M, Jones S and Reinke K (2024) Vertical accuracy assessment of freely available global DEMs (FABDEM, Copernicus DEM, NASADEM, AW3D30 and SRTM) in flood-prone environments. International Journal of Digital Earth 17(1). DOI: 10.1080/17538947.2024.2308734.

Middleton BA (2002) The flood pulse concept in wetland restoration. In: Middleton BA (ed.) Flood pulsing in wetlands: restoring the natural hydrological balance. John Wiley & Sons, Inc, USA.

Neal J, Villanueva I, Wright N, Willis T, Fewtrell T and Bates P (2012) How much physical complexity is needed to model flood inundation? Hydrological Processes 26(15), 2264–2282. DOI: 10.1002/hyp.8339.

Nicholas AP and Mitchell CA (2003) Numerical simulation of overbank processes in topographically complex floodplain environments. Hydrological Processes 17(4), 727–746. DOI: 10.1002/hyp.1162.

Nobre AD, Cuartas LA, Hodnett M, Rennó CD, Rodrigues G, Silveira A, Waterloo M and Saleska S (2011) Height Above the Nearest Drainage – a hydrologically relevant new terrain model. Journal of Hydrology 404(1–2), 13–29. DOI: 10.1016/j.jhydrol.2011.03.051.

NT Government (2023) Territory Water Plan. A plan to deliver water security for all Territorians, now and into the future. Viewed 6 September 2024, https://watersecurity.nt.gov.au/__data/assets/pdf_file/0003/1247520/territory-water-plan.pdf.

Ogden R and Thoms M (2002) The importance of inundation to floodplain soil fertility in a large semi-arid river. International Association of Theoretical and Applied Limnology, SIL Proceedings, 28(2), 744–749. DOI: 10.1080/03680770.2001.11901813.

Opperman JJ, Galloway GE, Fargione J, Mount JF, Richter BD and Secchi S (2009) Land use. Sustainable floodplains through large-scale reconnection to rivers. Science 326(5959), 1487–1488. DOI: 10.1126/science.1178256.

Overton IC (2005) Modelling floodplain inundation on a regulated river: integrating GIS, remote sensing and hydrological models. River Research and Applications 21(9), 991–1001. DOI: 10.1002/Rra.867.

Owers CJ, Lucas RM, Clewley D, Planque C, Punalekar S, Tissott B, Chua SMT, Bunting P, Mueller N and Metternicht G (2021) Implementing national standardised land cover classification systems for Earth Observation in support of sustainable development. Big Earth Data 5(3), 368–390. DOI: 10.1080/20964471.2021.1948179.

Peake P, Fitzsimons J, Frood D, Mitchell M, Withers N, White M and Webster R (2011) A new approach to determining environmental flow requirements: sustaining the natural values of floodplains of the southern Murray–Darling Basin. Ecological Management & Restoration 12(2), 128–137. DOI: 10.1111/j.1442-8903.2011.00581.x.

Phelps QE, Tripp SJ, Herzog DP and Garvey JE (2015) Temporary connectivity: the relative benefits of large river floodplain inundation in the lower Mississippi River. Restoration Ecology 23(1), 53–56. DOI: 10.1111/rec.12119.

Pinos J and Timbe L (2019) Performance assessment of two-dimensional hydraulic models for generation of flood inundation maps in mountain river basins. Water Science and Engineering 12(1), 11–18. DOI: 10.1016/j.wse.2019.03.001.

Queensland Government (2023) Queensland Water Strategy. Water. Our life resource. Viewed 11 September 2024, https://www.rdmw.qld.gov.au/qld-water-strategy/strategic-direction.

Queensland Reconstruction Authority (2012) Report on flood investigation for Gregory Downs. Department of Natural Resources and Mines, Queensland Government, Brisbane.

Queensland Reconstruction Authority (2013) Doomadgee flood mapping study. Department of Natural Resources and Mines, Queensland Government, Brisbane.

https://www.data.qld.gov.au/dataset/queensland-flood-mapping-program-2013-series/resource/9e35a262-a9b2-4a4c-89cc-7393b7bb6372.

Rice M, Hughes L, Steffen W, Bradshaw S, Bambrick H, Hutley N, Arndt D, Dean A and Morgan W (2022) A supercharged climate: rain bombs, flash flooding and destruction. Canberra. https://www.climatecouncil.org.au/wp-content/uploads/2022/03/Final_Embargoed-Copy_Flooding-A-Supercharged-Climate_Climate-Council_ILedit_220310.pdf.

Sanders BF (2007) Evaluation of on-line DEMs for flood inundation modeling. Advances in Water Resources 30(8), 1831–1843. DOI: 10.1016/j.advwatres.2007.02.005.

Schumann G, Bates PD, Horritt MS, Matgen P and Pappenberger F (2009) Progress in integration of remote sensing–derived flood extent and stage data and hydraulic models. Reviews of Geophysics 47(4). DOI: 10.1029/2008rg000274.

Shaikh M, Green D and Cross H (2001) A remote sensing approach to determine environmental flows for wetlands of the Lower Darling River, New South Wales, Australia. International Journal of Remote Sensing 22(9), 1737–1751. DOI: 10.1080/01431160118063.

Sims N, Anstee J, Barron O, Botha E, Lehmann E, Li L, McVicar T, Paget M, Ticehurst C, Van-Niel T and Warren G (2016) Earth observation remote sensing: a technical report to the Australian Government from the CSIRO Northern Australia Water Resource Assessment. CSIRO, Canberra.

Symonds AM, Vijverberg T, Post S, van der Spek B, Henrotte J and Sokolewicz M (2016) Comparison between Mike 21 FM, Delft3D and Delft3D FM flow models of Western Port Bay, Australia. Lynett P (ed.) Proceedings of the 35th International Conference on Coastal Engineering. ICCE, Turkey.

Tabari H (2020) Climate change impact on flood and extreme precipitation increases with water availability. Scientific Reports 10(1), 13,768. DOI: 10.1038/s41598-020-70816-2.

Teng J, Jakeman AJ, Vaze J, Croke BFW, Dutta D and Kim S (2017) Flood inundation modelling: a review of methods, recent advances and uncertainty analysis. Environmental Modelling & Software 90, 201–216. DOI: 10.1016/j.envsoft.2017.01.006.

Thomas M, Philip S, Zund P, Stockmann U, Hill J, Gregory L, Watson I and Thomas E (2024) Soils and land suitability for the Southern Gulf catchments. A technical report from the CSIRO Southern Gulf Water Resource Assessment for the National Water Grid. CSIRO, Australia.

Thoms MC (2003) Floodplain–river ecosystems: lateral connections and the implications of human interference. Geomorphology 56(3–4), 335–349. DOI: 10.1016/S0169-555x(03)00160-0.

Ticehurst C, Dutta D, Karim F, Petheram C and Guerschman JP (2015) Improving the accuracy of daily MODIS OWL flood inundation mapping using hydrodynamic modelling. Natural Hazards 78(2), 803–820. DOI: 10.1007/s11069-015-1743-5.

Ticehurst CJ, Chen Y, Karim F, Dutta D and Gouweleeuw B (2013) Using MODIS for mapping flood events for use in hydrological and hydrodynamic models: experiences so far. In: International Congress on Modelling and Simulation. Modelling and Simulation Society of Australia and New Zealand, 1721–1727.

Tockner K, Bunn SE, Quinn G, Naiman R, Stanford JA and Gordon C (2008) Floodplains: critically threatened ecosystems. In: Polunin NC (ed.) Aquatic ecosystems. Cambridge University Press, Cambridge, UK, 45–61.

Tockner K, Lorang MS and Stanford JA (2010) River flood plains are model ecosystems to test general hydrogeomorphic and ecological concepts. River Research and Applications 26(1), 76–86. DOI: 10.1002/rra.1328.

Townsend PA and Walsh SJ (1998) Modeling floodplain inundation using an integrated GIS with radar and optical remote sensing. Geomorphology 21(3–4), 295–312.

Tuteja NK and Shaikh M (2009) Hydraulic modelling of the spatio-temporal flood inundation patterns of the Koondrook Perricoota Forest Wetlands – The Living Murray. In: 18th World IMACS, MODSIM Congress. Modelling and Simulation Society of Australia and New Zealand, 4248–4254.

Ulubasoglu MA, Rahman MH, Onder YK, Chen Y and Rajabifard A (2019) Floods, bushfires and sectoral economic output in Australia, 1978–2014. Economic Record 95(308), 58–80. DOI: 10.1111/1475-4932.12446.

Wang ZC and Gao ZQ (2022) Dynamic monitoring of flood disaster based on remote sensing data cube. Natural Hazards 114(3), 3123–3138. DOI: 10.1007/s11069-022-05508-3.

Xu HQ (2006) Modification of normalised difference water index (NDWI) to enhance open water features in remotely sensed imagery. International Journal of Remote Sensing 27(14), 3025–3033. DOI: 10.1080/01431160600589179.

Yang A, Petheram C, Marvanek S, Baynes F, Rogers L, Ponce-Reyes R, Zund P, Seo L, Hughes J, Gibbs M, Wilson P, Philip S and Barber M (2024) Assessment of surface water storage options in the Victoria and Southern Gulf catchment. A technical report from the CSIRO Victoria River and Southern Gulf Water Resource Assessments for the National Water Grid. CSIRO, Australia.

Yu Q, Wang YY and Li N (2022) Extreme flood disasters: comprehensive impact and assessment. Water 14(8), 1211. DOI: 10.3390/w14081211.

As Australia's national science agency and innovation catalyst, CSIRO is solving the greatest challenges through innovative science and technology.

CSIRO. Unlocking a better future for everyone.

Contact us

1300 363 400
+61 3 9545 2176
csiroenquiries@csiro.au
csiro.au

For further information

Environment
Dr Chris Chilcott
+61 8 8944 8422
chris.chilcott@csiro.au

Environment
Dr Cuan Petheram
+61 467 816 558
cuan.petheram@csiro.au

Agriculture and Food
Dr Ian Watson
+61 7 4753 8606
Ian.watson@csiro.au